# ANALYSIS OF ECCENTRICALLY BRACED FRAMES WITH SHEAR LINKS

## A DISSERTATION

***Submitted in the partial fulfilment of the requirements for the award of the degree of***

**MASTER OF TECHNOLOGY**

**in**

**EARTHQUAKE ENGINEERING**

**(With specialization in Seismic Vulnerability and Risk Assessment)**

***by***

**ZEESHAN MUSHTAQ**

**(17553010)**


**DEPARTMENT OF EARTHQUAKE ENGINEERING**
**INDIAN INSTITUTE OF TECHNOLOGY ROORKEE**
**ROORKEE-247667 (INDIA)**
**JUNE, 2019**

# CANDIDATE'S DECLARATION

I hereby, declare that the work which is being presented in this dissertation entitled, **"Analysis of Eccentrically Braced Frames with Shear Links"**, being submitted in partial fulfilment of the requirements for the award of degree of "**Master of Technology**" in "**Earthquake Engineering**" with specialization in Seismic Vulnerability and Risk Assessment, to the Department of Earthquake Engineering, Indian Institute of Technology Roorkee, under the supervision of **Dr. P.C. Ashwin Kumar**, Assistant Professor, Department of Earthquake Engineering, Indian Institute of Technology Roorkee, is an authentic record of my own work carried out during the period of April 2018 to June 2019.

I declare that I have not submitted the material embodied in this dissertation for the award of any other degree or diploma.

Place: Roorkee
Date: June 14, 2019

**Zeeshan Mushtaq**
Enrollment no. 17553010

# CERTIFICATE

This is to certify that the above statement made by the candidate is correct to the best of my knowledge and belief.

Place: Roorkee
Date: June 14, 2019

**Dr. P.C. Ashwin Kumar**
Assistant Professor
Department of Earthquake Engineering
Indian Institute of Technology Roorkee

# ACKNOWLEDGEMENTS

I would like to express my heartfelt gratitude to my supervisor Dr. P.C. Ashwin for his sheer guidance. I immensely appreciate the freedom he gave me in all aspects of the project work. His comments were extremely fruitful and always helped me to overcome the problems that I faced during this work.

I would like to acknowledge the extremely good computer facilities provided by the department without which this work would not have been possible. The scholarship given by Ministry of Human Resources and Development, Government of India is highly appreciated for this dissertation work.

I would also like to thank my colleagues especially Tamil Selvan and V. Avanish for lending their help whenever I needed it.

I must reserve the deepest gratitude to my family. I will forever be indebted to my parents for making countless sacrifices to provide me excellent education. Thank you for everything you have given me throughout my life.

# ABSTRACT

The application of eccentrically braced frames (EBFs) as lateral load resisting system has become increasingly popular due to its high stiffness and excellent ductility. This thesis presents the seismic assessment of a suite of EBF systems designed in accordance with AISC 341-16. Results from the analysis demonstrate the concentration of deformations and energy dissipation within few storeys even exceeding the codified values. The scatter of these parameters with the height of the frames was targeted using Performance Based Plastic Design (PBPD) Procedure. The performance of EBFs designed using latter was found to be comparatively much better than that of conventionally designed EBFs.

De-coupling the link segment from the rest of frame members by providing replaceable type link facilitates control of strength, ductility and stiffness of EBFs independently. Moreover, it ensures quick and convenient post-damage repair by removal and replacement of the distorted link sections without hindering the operational use of the building. This thesis presents the analysis of EBF systems with replaceable shear links composed of lower grade steel connected through bolted end-plate connections to the floor beam. Results demonstrate that the performance of latter is similar to that of conventional EBFs in which the link section is continuous with the floor beam despite the flexibility of the link to beam connections.

# TABLE OF CONTENTS


CANDIDATE'S DECLARATION ..... i
CERTIFICATE ..... i
ACKNOWLEDGEMENTS ..... iii
ABSTRACT ..... v
TABLE OF CONTENTS ..... vii
LIST OF FIGURES ..... xi
LIST OF TABLES ..... xv
1. INTRODUCTION ..... 1
2. BEHAVIOR AND DETAILING OF LINKS ..... 5
2.1 Yield Behavior of Links ..... 5
2.2 Detailing of Links ..... 7
3. DESIGN PHILOSOPHY OF EBF SYSTEMS ..... 9
3.1 Design Philosophy ..... 9
3.1.1 Design of Dissipative Links ..... 10
3.1.2 Design of Non-Dissipative Members ..... 11
3.2 Design Example ..... 12
3.2.1 Building Information ..... 12
3.2.2 Design Frame Sections ..... 14
3.2.3 Verification of Results ..... 16
4. NON-LINEAR MODELLING OF EBFS ..... 19
4.1 Modelling of Links ..... 19
4.1.1 Back-bone Curve Depictions ..... 20
4.1.2 Acceptance Criteria ..... 20
4.1.3 Calculation of Link Yield Rotation Angle ..... 20
4.2 Modelling of other Frame Members ..... 21
4.3 Validation of Non-linear Modelling ..... 21
4.3.1 Building Information ..... 22

4.3.2 Comparison of Results ..... 23
5. DESIGN OF EBFS WITH SHEAR LINKS ..... 25
5.1 Building Information ..... 25
5.2 Structural Design Loads ..... 27
5.3 Structure Modelling ..... 28
5.4 Design of Archetypes ..... 29
6. ASSESSMENT OF EBFS WITH SHEAR LINKS ..... 31
6.1 Non-linear Static Analysis ..... 31
6.1.1 Yield Pattern ..... 31
6.1.2 Pushover Curves ..... 33
6.2 Non-linear Dynamic Analysis ..... 33
6.2.1 Selection of Ground Motions ..... 34
6.2.2 Seismic Response of the Archetypes ..... 36
6.3 3D Modelling and Analysis of Archetypes ..... 48
6.3.1 Design and Modelling of the Archetypes ..... 48
6.3.2 Non-linear Static Analysis ..... 49
6.3.3 Non-linear Dynamic Analysis at DBE Level ..... 51
6.3.4 Non-linear Dynamic Analysis at MCE Level ..... 52
7. PERFORMANCE BASED DESIGN OF EBFS ..... 57
7.1 Design Procedure ..... 57
7.1.1 Desired Yield Mechanism ..... 57
7.1.2 Design Lateral Forces ..... 58
7.1.3 Design Base Shear ..... 58
7.1.4 Design of Yielding Members ..... 60
7.2 Performance Based Design of 6 and 14 Storey EBFs ..... 61
7.2.1 Distribution of Design Lateral Loads ..... 62
7.2.2 Distribution of Design Lateral Strength ..... 63
7.3 Non-linear Analysis of Archetypes ..... 64

7.3.1 Non-linear Static Analysis ..... 64
7.3.2 Non-linear Dynamic Analysis ..... 66
7.3.3 Energy Dissipation Results from PERFORM 3D ..... 68
8. EBFS WITH REPLACEABLE SHEAR LINKS ..... 71
8.1 Replaceable Link to Beam Connections ..... 72
8.1.1 Replaceable Link with End-plate Connection ..... 72
8.1.2 Replaceable Link with Web-bolted Connection ..... 73
8.2 Design and Analysis of EBFs with Replaceable Shear Links ..... 74
8.2.1 Replaceable Link to Beam Connections ..... 75
8.2.2 Modelling and Design of Archetypes ..... 76
8.2.3 Results of Non-linear Static Analysis ..... 78
8.2.4 Results of Non-linear Dynamic Analysis ..... 81
8.2.5 Overall Performance of the Replaceable Link Type EBFs ..... 87
9. CONCLUSIONS ..... 89
REFERENCES ..... 91
APPENDICES ..... 93
APPENDIX A: Sample Design (S14) ..... 93
Calculation of Base Shear ..... 93
Design of 14-storey EBF ..... 94
Check on Inter-storey Drift and Link Rotation Angle ..... 97
Check on Stability of the Frame ..... 98
APPENDIX B: Scaled and Unscaled Response Spectra of Selected Ground Motions ..... 100
APPENDIX C: Design Frame Sections ..... 105
Design Frame Sections for Conventional Archetypes ..... 105
Design Frame Sections for Replaceable Link Type EBFs ..... 106

# LIST OF FIGURES

Fig 1.1 EBF configurations and corresponding plastic mechanisms (adapted from popov et al. 1987) ..... 2
Fig 2.1 Inelastic link rotation (adapted from T. Okazaki 2004) ..... 6
Fig 3.1 Simplified free body diagram of K-braced frame (adapted from Popov et al. 1987) ..... 10
Fig 3.2 Elevation of the building frame considered for design ..... 13
Fig 3.3 Simplified half-frame model ..... 16
Fig 4.1 Back-bone curve to simulate the post-yield behavior ..... 19
Fig 4.2 Elevation of the frame Ricles and Popov (1987) ..... 22
Fig 4.3 Comparison of inter-storey drift and inelastic link rotation envelopes ..... 23
Fig 4.4 Comparison of axial forces in beams ..... 24
Fig 5.1 (a) Plan and (b) Elevation of a typical archetype building ..... 26
Fig 5.2 Equivalent lateral force distribution of the archetypes ..... 30
Fig 6.1 Yield pattern exhibited by the archetypes corresponding to first collapse of any component ..... 32
Fig 6.2 Normalized pushover curves of the archetypes ..... 33
Fig 6.3 Spectral accelerations of the selected ground motions ..... 35
Fig 6.4 Maximum normalized shear envelopes in links for (a) S3 and S6 and (b) S10 and S14 ..... 38
Fig 6.5 Inter-storey drift and inelastic link rotation envelopes for (a) S3 (b) S6 (c) S10 and (d) S14 ..... 40
Fig 6.6 Comparison of axial forces in columns for (a) S3 and S6 and (b) S10 and S14 42
Fig 6.7 Comparison of time history analysis deformations with predicted deformations for (a) S3 (b) S6 (c) S10 and (d) S14 ..... 45
Fig 6.8 Rigid-plastic collapse mechanism for K-braced EBFs ..... 45
Fig 6.9 Relation between peak inter-storey drift and inelastic link rotation for S14 ..... 46
Fig 6.10 Axial force time history of the ground storey link of S6 subjected to El Centro earthquake ..... 47
Fig 6.11 Isometric view of 14 storey model M14 ..... 48
Fig 6.12 Yield pattern of M14 frame corresponding to the first collapse of any component ..... 50
Fig 6.13 Comparison of pushover curves of M14 and S14 ..... 50

Fig 6.14 Inter-storey drift and inelastic link rotation envelopes for (a) 6 story and (b) 14 story archetypes ..... 52
Fig 6.15 Design target and average response spectra at DBE and MCE levels ..... 53
Fig 6.16 Inter-storey drift and inelastic link rotation envelopes for (a) 6 story and (b) 14 story archetypes ..... 54
Fig 7.1 Equivalence of energy to evaluate design lateral force (adapted from Chao et al. 2005) ..... 59
Fig 7.2 Yield mechanism for calculating the required shear strength of links (adapted form Chao et al. 2005) ..... 61
Fig 7.3 Comparison of design lateral forces between ELF and PBPD procedures ..... 63
Fig 7.4 Yield mechanism corresponding to the first collapse of any component for (a) P6 (b) Q6 and (c) S6 ..... 65
Fig 7.5 Normalized pushover curves for six story frames ..... 66
Fig 7.6 Comparison of peak inelastic link rotation and inter-storey drift envelopes for (a) 6 and (b) 14 storey archetypes ..... 68
Fig 7.7 Distribution of energy dissipated by links along the height of archetypes ..... 69
Fig 8.1 Replaceable links in EBF systems (adapted from Mansour et al. 2011) ..... 71
Fig 8.2 Replaceable link with bolted end-plate connection and (a) Floor beam deeper than the link section and (b) Floor beam and link section of the same depth (adapted from Dubina et al. 2008) ..... 73
Fig 8.3 Replaceable link with web-bolted connection (adapted from Mansour et al. 2011) ..... 74
Fig 8.4 Deformation of conventional link (adapted from Dubina et al. 2008) ..... 75
Fig 8.5 Deformation of replaceable link bolted to end-plates (adapted from Dubina et al. 2008) ..... 76
Fig 8.6 Yield pattern exhibited by the archetypes corresponding to first collapse of any component ..... 79
Fig 8.7 Comparison of pushover curves of replaceable link type EBFs with conventional EBFs for (a) 3 and 6 story and (b) 10 and 14 storey archetypes ..... 80
Fig 8.8 Comparison of maximum normalized shear envelopes in replaceable type and conventional links for (a) 3 and 6 storey and (b) 10 and 14 storey archetypes ..... 82

Fig 8.9 Comparison of peak inter-storey drift and inelastic link rotation envelopes of replaceable type and conventional links for (a) 3 (b) 6 (c) 10 and (d) 14 storey archetypes ..... 85
Fig 8.10 Relation between peak inter-storey drift and inelastic link rotation for R14 ... 87
Fig B.1 Unscaled response spectra of the ground motions ..... 100
Fig B.2 Scaled response spectra of the ground motions ..... 101
Fig B.3 Unscaled and scaled response spectra of the individual ground motions ..... 104

# LIST OF TABLES

Table 3-1 Vertical distribution of base shear ..... 13
Table 3-2 Design shear for the frame ..... 13
Table 3-3 Comparison of shear in the links ..... 14
Table 3-4 Link sections used and their shear capacities ..... 15
Table 3-5 Comparison of axial forces and moments ..... 16
Table 3-6 Comparison of inter-storey drift ..... 17
Table 5-1 Assembly Weights ..... 27
Table 5-2 Dead load on the exterior walls ..... 28
Table 5-3 Layout of archetypes ..... 29
Table 5-4 Design base shear of the archetypes ..... 29
Table 6-1 Summary of the selected ground motions ..... 35
Table 6-2 Maximum deviation of the average response spectrum from design target spectrum ..... 36
Table 6-3 Shear capacity to demand ratio of links ..... 41
Table 6-4 Design gravity resisting frame sections ..... 49
Table 7-1 Distribution of design lateral strength and design link sections for P6 and Q6 ..... 63
Table 7-2 Distribution of design lateral strength and design link sections for P14 and Q14 ..... 64
Table 8-1 Comparison of frame weights for the conventional and replaceable link type EBFs ..... 77
Table 8-2 Comparison of the shear capacity to demand ratio of replaceable type and conventional links ..... 83
Table A.1 Calculation of the floor weights ..... 94
Table A.2 Equivalent Lateral Force distribution and link design shear ..... 95
Table A.3 Link sections provided and their shear capacities ..... 96
Table A.4 Column and brace sections provided ..... 96
Table A.5 Inter-storey drift and link rotation angle from elastic analysis of the frame . 98
Table A.6 Calculation of stability coefficient ..... 99
Table C.1 Design frame sections of S3 and S6 ..... 105
Table C.2 Design frame sections of S10 and S14 ..... 105
Table C.3 Design frame sections of R3 ..... 106

Table C.4 Design frame sections of R6.....106
Table C.5 Design frame sections of R10.....106
Table C.6 Design frame sections of R14.....107

# 1. INTRODUCTION

A lateral load resisting system should have sufficient ductility as well as stiffness for seismic applications. It should have high elastic stiffness to limit drift. At the same time, it should have good ductility to dissipate the seismic (or wind) input energy without undergoing structural or non-structural collapse. Concentrically Braced Frames (CBFs) are used as lateral load resisting systems due to high stiffness but they lack sufficient ductility and energy dissipation characteristics as the failure occurs due to buckling of the braces characterized by pinched hysteretic behavior. On the contrary, Moment Resisting Frames (MRFs) exhibit very good ductility and energy dissipation characteristics due to the formation of plastic hinges at the base of columns and at the ends of the beams but they have low stiffness resulting in excessive drift.

Eccentrically Braced Frames (EBFs) are a hybrid between MRFs and CBFs. EBFs combine the advantages of both these lateral load resisting systems while minimizing their disadvantages. EBFs exhibit high stiffness due to the presence of the diagonal braces connected at some eccentricity to the columns which could be arranged in various configurations as shown in Fig 1.1. The lateral load from an earthquake induces axial forces in the braces. These axial forces are transferred to the adjacent columns and braces through shear and flexural actions in a small beam segment known as the link.

In EBFs, yielding is concentrated primarily within the link segments though limited yielding in the beams outside the links is not detrimental to the global frame behavior. All the members of the frame are designed to remain elastic regardless of the magnitude of the earthquake (or wind). Thus the links act as structural fuses which dissipate the seismic energy through controlled inelastic deformations resulting in excellent ductility and energy dissipation characteristics. This characteristic of the EBFs is mainly due to two factors. Firstly, yielding is concentrated in the links which are designed to resist extensive plastic deformations without any significant loss of strength. Secondly, braces do not buckle as the capacity design principle makes sure that the link is the weakest part of the EBF system. The buckling of the braces is the reason for the poor ductility and energy dissipation in CBFs. Consequently, the preclusion of buckling of braces ensures controlled hysteresis in EBFs.

Eccentrically braced frames in various configurations along with corresponding plastic mechanisms are shown in Fig 1.1.

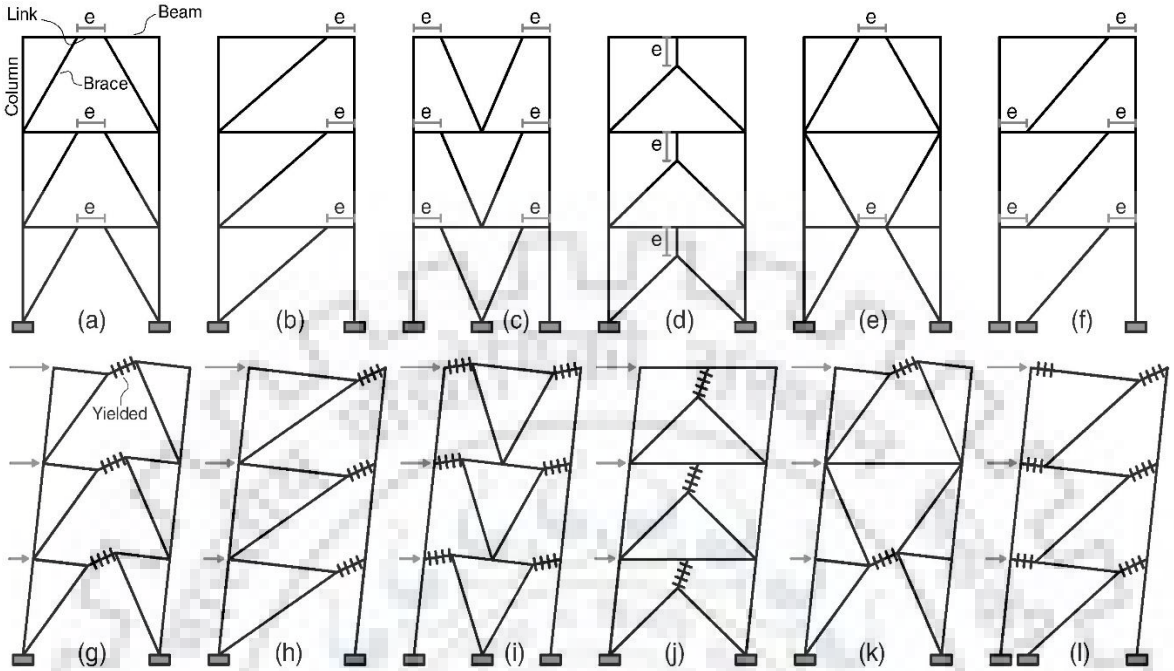


Fig 1.1 EBF configurations and corresponding plastic mechanisms (adapted from popov et al. 1987)

EBFs also provide greater flexibility in architectural design as the offset braces provide sufficient clearance for windows, doors and other openings.

In the conventional EBFs, the link is continuous with the beam. The link is primarily designed for shear while the beam outside of link is designed to resist high axial force and high moment induced due to strain-hardened link. Striking a balance between these two requirements is an iterative procedure often resulting in oversized link sections and hence increasing the cost of entire structure in purview of the capacity design. The design of links is the critical factor in the context of optimizing the design of EBF systems. De-coupling the link segment from the rest of frame members by providing replaceable type links provides a viable solution to control the strength, ductility and stiffness of EBFs independently. The inelastic deformations in the replaceable type link can be isolated by providing links of lower yield strength. Conversely, this objective can be achieved by providing links of conventional steel and the rest of the members, that are supposed to be non-dissipative, of High Strength Steel (HSS).

This thesis presents the assessment of EBF systems with short shear links and braces in chevron arrangement designed in accordance with AISC-341-16 [1]. Non-linear dynamic

analysis was performed at Design Basis Earthquake (DBE) and Maximum Considered Earthquake (MCE) levels for far-field ground motions. The analysis was done on 2D as well as 3D models to determine the contribution of the interior gravity frames in resisting the lateral forces. Furthermore, the EBF systems in which link segments are replaceable type made of conventional steel while the rest of the members are made of High Strength Steel (HSS) were also analyzed and their performance compared to that of conventional EBFs. To improve upon the seismic performance of the EBF systems, the frames were also designed using Performance Based Plastic Design (PBPD) procedure in which the target level of performance was based on two key parameters; a desirable yield mechanism and maximum target deformation.

# 2. BEHAVIOR AND DETAILING OF LINKS

This chapter presents a brief description of the yield behavior of links and the shear capacity of short links. A summary of link rotation and effect of axial force on the performance of links is presented. Further, the compactness requirements that the link sections have to satisfy are discussed.

## 2.1 Yield Behavior of Links

The length of link, $e$, is the most important parameter that controls the strength, stiffness, ductility and hence the overall behavior of the EBF system. The links are classified on the basis of link length ratio, $\rho$, which is defined as follows:

$$\rho = \frac{e}{\frac{M_P}{V_P}} \tag{2.1}$$

where, $V_p$ and $M_p$ are plastic shear and moment capacities of the link section respectively. Links with $\rho < 1.6$ are classified as short links. Shear yielding controls the behavior of these links and hence they are also referred to as shear links. Links with $\rho > 2.6$ are classified as long links. These links yield primarily in flexure and hence these links are also referred to as long links. Links with $\rho$ values between 1.6 and 2.6 are classified as intermediate links. These links do not exhibit a distinct shear or flexure yielding behavior, rather it is the combination of the two. The effect of the moment-shear interaction is therefore significant in latter type of links.

The nominal shear capacity, $V_n$, of the link is taken as lesser of the values given by shear and moment dominant behavior as follows:

$$V_n = \min\left\{V_P, \frac{2M_P}{e}\right\} \tag{2.2}$$

The estimation of maximum shear forces that could be induced in links, $V_{\max}$, is important for the capacity design. The links develop shear significantly larger than their nominal shear capacities due to strain hardening. As such, the frame members have to resist the forces developed by the fully yielded and strain hardened links. If $V_{\max}$ is underestimated, other frame members could undergo yielding which is very undesirable. The overstrength concept is used to get a reliable estimate of $V_{\max}$ as follows:

$$V_{max} = R_y \Omega V_n \tag{2.3}$$

where, $R_y$ is the ratio of expected to nominal yield stress and $\Omega$ is the overstrength factor which includes the effect of strain hardening and is taken as 1.5 as per AISC 341-16 [1].

Fig 2.1 shows the expected plastic mechanism of the EBFs with different bracing arrangements. The angle which the link intercepts with the beam outside of the link is referred to as the link rotation angle. Initially this rotation is due to elastic action which is generally less than 0.01 radians. The inelastic part of rotation is called as inelastic link rotation angle, $\gamma_p$. The inelastic rotation capacity of links is defined as the maximum inelastic rotation angle which the links can sustain when subjected to at least one full cycle of loading without its shear resistance falling below a defined limit. This limit can is usually set at 80% of the maximum shear induced in the links ($0.8V_{max}$) during the cyclic loading.

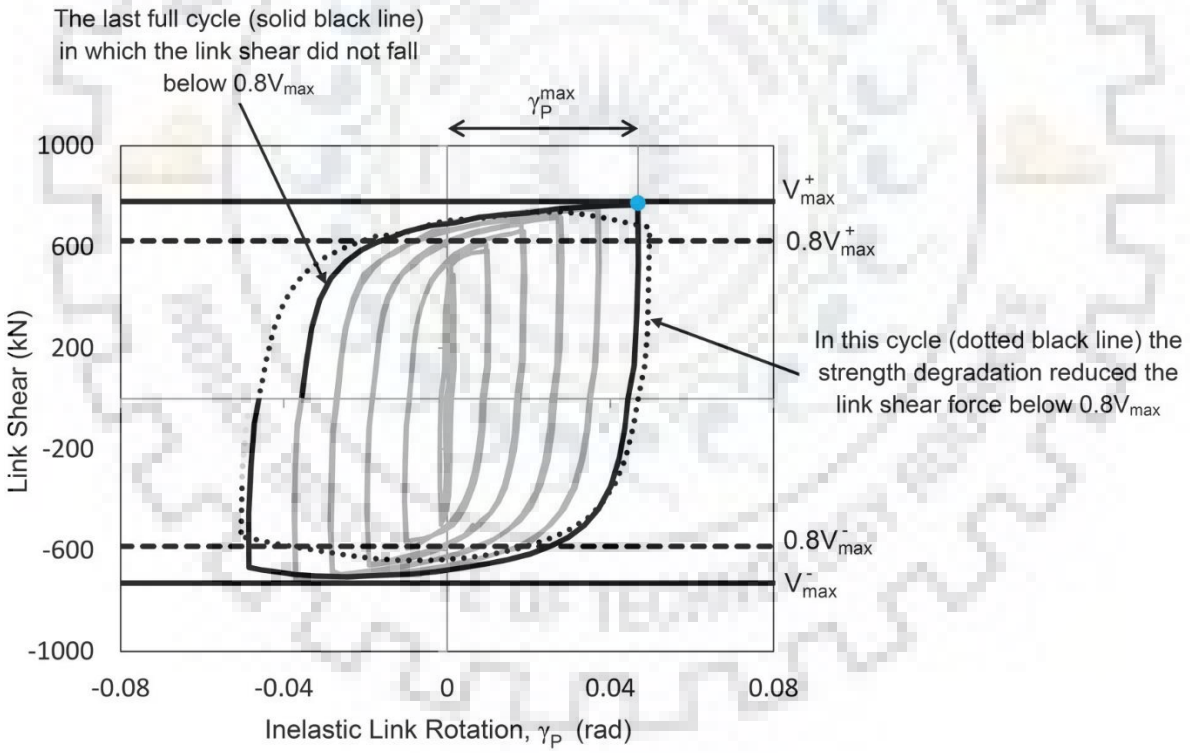


Fig 2.1 Inelastic link rotation (adapted from T. Okazaki 2004)

AISC 341-16 limits the link rotation capacity of the short links to 0.02 radians and that of the long links to 0.02 radians. The capacity of the intermediate links can be estimated by linear interpolation.

The adjacent members can restrain the link axially and hence induce axial force in it. The axial force can have detrimental effect on the behavior of links as experiments have

shown that it reduces the plastic strength as well as the rotation capacity of links. The EBFs in the chevron configuration have the advantage of not inducing axial forces in links. This is the primary reason that chevron EBFs have been chosen for this study, the secondary reason being the absence of the link to column connections which can be very problematic.

## 2.2 Detailing of Links

The link sections are required to satisfy certain compactness requirements to avoid web buckling under shear or flange buckling under link end moments to ensure good ductility and energy dissipation of the EBF systems. The performance of links is satisfactory only when the web is stiffened using vertical stiffeners and they satisfy the ductility requirement for highly ductile sections although moderately ductile sections suffice for short links.

The web slenderness ratio is limited to prevent the web from buckling under shear and is set at $0.64\sqrt{\frac{E}{F_y}}$ according to AISC 341-16; where $E$ is the elastic modulus and $F_y$ is the yield strength of material.

The flange slenderness ratio is limited to prevent the flange from buckling which results in strength degradation under intense loading. This ratio is limited to $0.3\frac{E}{F_y}$.

The stiffening of links by end and intermediate stiffeners is a pre-requisite for achieving stable controlled hysteresis by avoiding premature buckling of the web and flanges. These stiffeners are usually full-depth located on both sides of the web and are provided for all link lengths. The end stiffeners also provide stability at the brace-beam-link connection panel.

# 3. DESIGN PHILOSOPHY OF EBF SYSTEMS

The first thing to decide in the design of EBFs is the selection of a suitable bracing configuration from the various configurations shown in Fig 1.1. The arrangement of Fig 1.1 (a) is symmetric and avoids link-to-column connections as the links are not adjacent to columns. The arrangement of Fig 1.1 (b) is particularly suitable if the bays are narrow. It is preferable to choose a bracing arrangement in which the brace to beam angles are larger than 40 degrees because smaller brace to beam angles induce large axial forces in beams adjoining the links, causing in them strength and stability problems. The bracing configurations that do not induce significant axial force in the links should be preferred for better performance.

The chevron configuration as shown in Fig 1.1 (a) is chosen for this study as this configuration does not induce large axial forces in the links and also avoids beam to column connections which could be problematic.

## 3.1 Design Philosophy

Strength and ductility are two basic requirements of lateral load resisting systems. In an EBF system, these parameters depend directly on the characteristics of link sections. Hence the design of EBFs is centered around the design of links. The capacity design approach is used which can be described in two steps:

(a) Size the links to provide the required frame strength; detail the links to provide adequate ductility.

(b) Design rest of the members such that the link is weakest part of the system, fully developing the strength and ductility of links and therefore of the entire frame.

Using this approach, the links are designed for specified hazard level forces while other members are designed for the forces generated by fully yielded and strain-hardened links. These represent the maximum forces that could be induced in these members irrespective of the magnitude of earthquake. The strength and ductility of the EBFs can be optimized by concentrating the yielding in links. This approach is analogous to that used in the design of Moment Resisting Frames wherein yielding is restricted to the beam ends by ensuring that the columns are stronger than beams (strong column weak beam approach). The plastic design procedure is used to size the members in accordance with this design philosophy.

### 3.1.1 Design of Dissipative Links

Links are the first members to be sized. The design of links is the most critical part of the procedure as the design of all the remaining members depends on the link sections provided. Smaller link sections will result in under-designing of the frame members. On the contrary, heavier link sections will result in stockier frame members and increase the cost of the frame unnecessarily.

A simple relationship exists between the lateral forces on the frame and the shear forces that are developed in the links for every configuration. A simplified free body diagram for a portion of an EBF in chevron configuration is illustrated in Fig 3.1. In this figure, $V_{cum}$ is the accumulated story shear from the top of the structure upto the level under

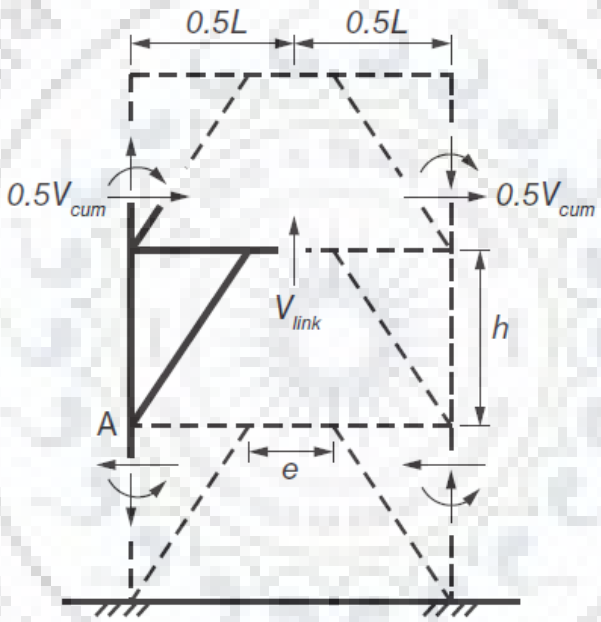


Fig 3.1 Simplified free body diagram of K-braced frame (adapted from Popov et al. 1987)

consideration and $V_{link}$ is the shear force induced in the link. The shear induced in links due to the gravity loads is insignificant and hence neglected in the design for sizing the links.

Equating the summation of the moments about point A gives the following simple relationship between above two parameters:

$$V_{link} = \frac{h}{L} V_{cum} \tag{3.1}$$

where, $h$ is the story height and $L$ is the bay width.

Having calculated the shear in links, a suitable section is selected to supply the required shear strength. All other members are designed for the forces generated by the fully yielded and strain hardened links. This necessitates the use of overstrength concept to estimate the ultimate shear and end moments developed in link sections. The ultimate shear that the link can develop, $V_{ult}$, is taken as follows:

$$V_{ult} = 1.5V_P \tag{3.2}$$

For the chevron configuration, the ultimate link end moments at the two ends, $M_a$ and $M_b$, are taken as follows:

$$M_a = M_b = \frac{V_{ult}e}{2} \tag{3.3}$$

### 3.1.2 Design of Non-Dissipative Members

Beams adjoining the links are subjected to large axial forces and moments and are therefore designed as beam-column elements. The large axial forces could potentially reduce the plastic moment capacity of section to the extent that it will be unable to resist the ultimate link moments and consequently yield. Designing these beams is problematic, so it is desirable to reduce the axial force and moment demands in these beams by providing large brace to beam angles and providing shorter links respectively. Further, providing fully restrained brace to beam connections will transfer some fraction of the link end moments into braces thus reducing the moment demand in beams.

AISC 341-16 recommends an overstrength factor of 1.1 for designing beams adjacent to links which is 88% of the factor (1.25) used for brace design. The justification for this reduction is that limited yielding in the beams will not deteriorate overall behavior of the frame. Also, any overstrength that is available in the link sections will also be present in beams outside the links since both of these are a single continuous section. The contribution of composite slab in resisting the axial forces and moments is also generally neglected. Beams have to satisfy the compactness requirements for moderately ductile sections.

Braces are designed as beam-column elements. AISC 341-16 recommends an overstrength factor of 1.25 for I-shaped sections. Experimental tests on I-shaped sections have shown that an overstrength factor of 1.5 can be reached. But a lower value of 1.25 is used in brace design for better economy. The justification for this is that material overstrength of the brace is not considered in design, rather a resistance factor of 0.9 is

used. When both the afore-mentioned factors are considered, the effective overstrength factor would be $(1.1/0.9)\times 1.25$ which matches well with the AISC recommended overstrength factor of 1.5.

Braces in an EBF system are designed not to buckle. Hence many of the provisions for braces that are required for stable cyclic buckling in Concentrically Braced Frames are not required here. Nevertheless, braces have to satisfy the section compactness requirements for moderately ductile sections.

Columns are designed to remain elastic under the combined demand of ultimate link forces and gravity loads. The design procedure is based on assumption that all the links will yield simultaneously and reach their maximum strengths which is not supported by the tests on various multi-story EBFs. For this reason, AISC 341-16 recommends to design the columns for a reduced overstrength factor of 88% of 1.25 except for the columns in the upper three stories in which case overstrength factor of 1.25 is used. Columns are required to satisfy the compactness requirements for highly ductile members.

Once all the members are designed, the frame is checked for drift and link rotation angle demands. AISC 341-16 recommends to limit the inter-storey drift of EBFs at 2%. The link rotation is limited at 0.08 rad and 0.02 rad for short and long links respectively.

## 3.2 Design Example

This section presents the design of a six storey eccentrically braced frame building using computer package SAP 2000 [4]. This design procedure was followed throughout the thesis. The building designed is the same as presented in seismic design manual of International Building Code 2012 [5]. The use of this building facilitated the comparison of results and the verification of design procedure followed in this thesis.

### 3.2.1 Building Information

The building is 120-foot × 150-foot in plan with a story height of 12 feet. The building has two frames oriented in each direction for a total of four frames to resist the lateral loads. The elevation of the frame considered for design is shown in Fig 3.2.

The building is located in site class D. The design spectral response acceleration parameters for short period, $S_{DS}$, and 1-sec period, $S_{D1}$, are 1 and 0.60 in g units respectively. The building was designed to resist dead load of 75 psf (pounds per square foot) and live load of 65 psf for floors while the roof was designed for dead load of 36

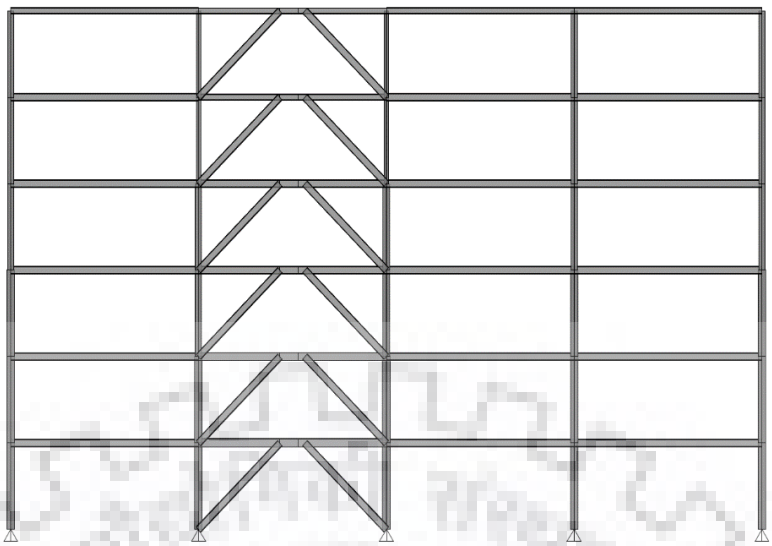

Fig 3.2 Elevation of the building frame considered for design

psf and live load of 20 psf. The building has an effective seismic weight of 7231 kips. The lateral seismic coefficient as computed in accordance with ASCE 7-16 [6] was 0.072 giving a base shear of 521 kips. The vertical distribution of base shear was accomplished using equivalent lateral procedure and is shown in Table 3.1.

Table 3-1 Vertical distribution of base shear

| Storey | 1 | 2 | 3 | 4 | 5 | 6 |
|---|---|---|---|---|---|---|
| Equivalent lateral force (kips) | 20 | 49 | 81 | 117 | 156 | 98 |

The equivalent lateral forces are resisted by two EBFs. The design shear for a frame after accounting for 5% accidental eccentricity is tabulated in Table 3.2.

Table 3-2 Design shear for the frame

| Storey | 1 | 2 | 3 | 4 | 5 | 6 |
|---|---|---|---|---|---|---|
| Design Shear (kips) | 10 | 26 | 42 | 61 | 81 | 51 |

The frame was designed for the following load combinations:

(a) $1.4D + 0.5L + 1.0Q_E$

(b) $0.7D + 1.0Q_E$

where, $D$, $L$ and $Q_E$ represent the dead, live and lateral seismic load effects respectively. The frame was modelled in SAP2000 with the same assumptions as used in IBC (2012) These are enlisted below:

(a) The beam to column connections were moment resisting.

(b) The brace to beam connection was fully restrained while at the other end, the attachment of brace was idealized as pinned with bolted connection.

(c) The ground storey columns were pinned to the foundation using bolted base plates.

(d) All the lateral forces were assumed to be resisted by EBFs.

(e) The links were not composite with the slab.

### 3.2.2 Design Frame Sections

From the model of the frame hereby designated as HFM-6, the shear forces induced in the links were calculated and compared with the IBC (2012) values (which were calculated analytically) as shown in Table 3.3.

Table 3-3 Comparison of shear in the links

| Shear in links (kips), $V_L$ | HFM-6 | IBC (2012) |
|---|---|---|
| 1 | 110.7 | 108.0 |
| 2 | 106.3 | 104.0 |
| 3 | 96.1 | 94.0 |
| 4 | 78.9 | 77.2 |
| 5 | 54.2 | 52.8 |
| 6 | 21.0 | 20.4 |

Short shear links were provided with a link length ratio of 1.3 approximately. The links were designed for shear forces tabulated in Table 3.3. The nominal shear capacity of the link sections, $V_P$, is calculated with the following expression:

$$V_P = 0.6 F_y A_w \tag{3.4}$$

where, $F_y$ is the yield strength of material and $A_w$ is the area of web of the link section. In accordance with the capacity design approach used in EBFs, all the members except links are intended to remain elastic and are therefore designed for forces induced by fully yielded and strain hardened links. The shear strength of links is amplified with overstrength factor of 1.25 which includes the effects of material overstrength and strain hardening. This amplified shear strength, $V_m$, of links is calculated as follows:

$$V_m = R_y \Omega V_P \tag{3.5}$$

where, $R_y$ is the ratio of expected yield stress to specified minimum yield stress. $R_y$ depends upon the grade of steel and is taken as 1.1 for ASTM A992 Grade 50 steel which was used in this design example. It has a yield strength of 50 ksi (kips per square inch) and ultimate strength, $F_u$, of 65 ksi. The link sections provided along with their shear

capacities are shown in Table 3.4. All member sections provided were the same as in IBC (2012) to facilitate the comparison of results.

Table 3-4 Link sections used and their shear capacities

| Storey | Shear in links, $V_L$ (kips) | Section | Plastic shear capacity, $V_P$ (kips) | Adjusted shear capacity, $V_m$ (kips) |
|---|---|---|---|---|
| 1 | 110.7 | W10×68 | 125 | 172 |
| 2 | 106.3 | W10×68 | 125 | 172 |
| 3 | 96.1 | W10×68 | 125 | 172 |
| 4 | 78.9 | [1]BU13×53 | 88 | 121 |
| 5 | 54.2 | BU9×34 | 60 | 82.5 |
| 6 | 21.0 | BU9×34 | 60 | 82.5 |

Having selected the link sections, rest of the members were designed. In this thesis, the design forces in the frame members were computed from a simplified half-frame model in which the frame is dissected into two symmetrical halves with a cut through the center of link sections. The lateral loads in accordance with equivalent lateral distribution were not applied on the model. Instead, the shear that the provided link sections can develop, amplified for overstrength, $V_m$ was applied at the end of dissected link sections as shown in Fig 3.3. This is justified since the lateral loads acting on the frame are, in effect, translated into high shear forces in links. The column joints were restrained against translational degree of freedom in horizontal direction to ensure the stability of half-frame model. The gravity loads tributary to the frame were also applied on the half-frame model and the design forces in columns, beams and braces were computed using the load combinations afore-mentioned. The most economical section based on weight satisfying the demand was assigned to the frame members.

[1] BU represents the built-up sections used in IBC (2012).

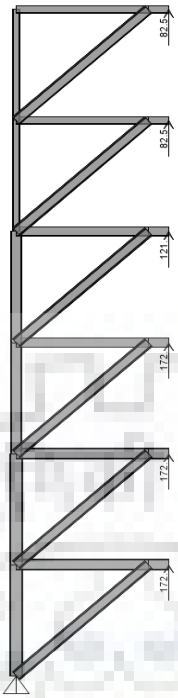


Fig 3.3 Simplified half-frame model

### 3.2.3 Verification of Results

The design forces for ground storey column, brace and beam adjacent to the link obtained from half-frame model are compared against the IBC (2012) values as shown in Table 3.5.

Table 3-5 Comparison of axial forces and moments

| Member | Axial force (kips) | | Moment (kip-ft) | |
|---|---|---|---|---|
| | IBC (2012) | HFM-6 | IBC (2012) | HFM-6 |
| Column | 980 | 1001 | 57.4 | 53 |
| Brace | 327 | 333 | 178 | 183 |
| Beam | 204 | 201 | 190 | 198 |

The fundamental time period of the model was found to be 1.16 sec which is approximately the same as IBC (2012) value of 1.19 sec. The comparison of inter-storey drift is shown in Table 3.6.

Table 3-6 Comparison of inter-storey drift

| Storey | Inter-storey Drift Ratio (%) | |
|---|---|---|
| | IBC (2012) | HFM-6 |
| 1 | 0.96 | 0.89 |
| 2 | 1.11 | 1.06 |
| 3 | 1.15 | 1.13 |
| 4 | 1.30 | 1.34 |
| 5 | 1.15 | 1.19 |
| 6 | 0.72 | 0.80 |

The design forces obtained from half-frame model and fundamental time period and inter-storey drift from full-frame model match very well with IBC (2012) results.

# 4. NON-LINEAR MODELLING OF EBFS

This chapter presents the modelling features of shear-critical links and the rest of frame members designed as beam column elements. The validity of the modelling features was verified by modelling an EBF that was designed and analyzed by previous researchers and comparing the results thereby.

## 4.1 Modelling of Links

This thesis deals with the EBFs employing short links which are predominantly designed for shear action. This shear behavior was modelled by two plastic shear hinges lumped at either end of the elastic link element. The elastic action occurs within the elastic beam element while the deformations post the elastic limit occur in the lumped plasticity hinges. Strain-hardening bilinear curves with some residual strength were assigned to these lumped plastic hinges and some suitable ultimate deformation was assumed. The inelastic response of link was obtained through the integration of plastic strain occurring over the length of the hinge. The shear hinges were based on the backbone curve as shown in Fig 4.1 recommended by FEMA-356 [7] to simulate the post-yield behavior. The isotropic hysteretic model was employed. Post-yield stiffness equal to 4% of the initial elastic stiffness was used subject to a maximum overstrength of 30% above the yield strength. The link was assumed not to be composite with the slab. The moment-shear interaction is not significant in case of short links and was hence not considered. The axial deformation of link elements was also neglected. This is justified since the axial force induced in link elements in the EBFs having chevron bracing arrangement is insignificant.

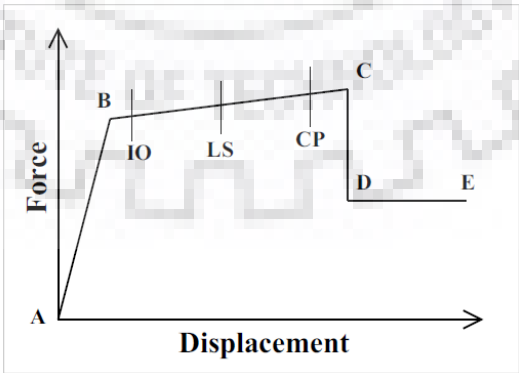


Fig 4.1 Back-bone curve to simulate the post-yield behavior

### 4.1.1 Back-bone Curve Depictions

Linear response is exhibited between point A which represents unloaded component to effective yield point B depicted on the back-bone curve (Fig 4.1). Point C depicts the ultimate strength of the component and the deformation at which severe strength degradation occurs (along line CD). Within the deformation range corresponding to points D and E, the component exhibits residual strength which for short shear links is about 80% of the yield strength. The strength is effectively zero at deformations beyond point E.

### 4.1.2 Acceptance Criteria

The acceptance criteria for performance of the building is generally evaluated at three discrete levels as mentioned below:

a. Immediate Occupancy (IO) level: At this level, the structure retains its pre-earthquake strength and stiffness and it is safe to reoccupy the structure after earthquake.
b. Life Safety (LS) level: At this level, the building may experience extensive damage to its structural as well as non-structural components but it retains some margin against onset of total or partial collapse. It is deemed necessary to do some repairs before reoccupying.
c. Collapse Prevention (CP) level: At this damage level, the building may pose severe hazard to life safety due to collapse of non-structural components though the global failure does not occur and hence the loss of life can be avoided.

These three performance levels lie between the points B and C on the backbone curve as shown in Fig 4.1. All the abscissae and ordinates except the yield deformation of the backbone curve were directly taken from the Table 5-6 of FEMA-356. The performance of the EBFs was evaluated with reference to inelastic link rotations of 0.11 rad and 0.14 rad at Immediate Occupancy Level and Collapse Prevention Level respectively.

### 4.1.3 Calculation of Link Yield Rotation Angle

The yield rotation angle, $\gamma_y$, is calculated in accordance with FEMA-356 as follows:

$$\gamma_y = \frac{Q_{CE}}{K_e e} \tag{4.1}$$

where, $Q_{CE}$ is the expected strength of link beam and $K_e$ is the elastic stiffness of link beam computed as the combination of shear stiffness, $K_s$, and flexural stiffness, $K_b$, as follows:

$$K_e = \frac{K_s K_b}{K_s + K_b} \tag{4.2}$$

$$K_s = \frac{GA_w}{e} \tag{4.3}$$

$$K_b = \frac{12EI}{e^3} \tag{4.4}$$

where, $G$ is the shear modulus, $E$ is the modulus of elasticity, $A_w$ is the area of link web and $I$ is the moment of inertia of link beam. The expected strength, $Q_{CE}$, for short shear links is calculated as follows:

$$Q_{CE} = 0.6F_y A_w \tag{4.5}$$

## 4.2 Modelling of other Frame Members

All the frame members except links were modelled by means of elastic beam-column elements with axial force - bending moment interaction (P-M) hinges lumped at either ends as they are subjected to significant axial force and bending moment. The expected strength of these members was evaluated based on the following interaction surface:

$$Q_{CE} = 1.18F_y Z\left\{1 - \frac{P}{P_y}\right\} \leq ZF_y \tag{4.6}$$

where, $Z$ = plastic section modulus

$P$ = axial force in the member at the instant of computation of non-linear analysis

$P_y$ = expected axial yield force of the member

## 4.3 Validation of Non-linear Modelling

The non-linear modelling procedure mentioned in the afore-mentioned sections was used to analyze a six story EBF (modelled in SAP2000) that was previously designed and analyzed by Ricles and Popov [7] and their results were compared to validate the modelling procedure.

### 4.3.1 Building Information

The building has two EBFs oriented in either direction to resist the lateral loads. Each EBF had bracings in chevron configuration in upper three stories while in the bottom three stories, the braces were provided in the eccentric D-configuration as shown in Fig 4.2. Short shear links of length 26 inches and 30 inches were provided respectively in the bottom three and top three stories. The beams were fabricated from A36 steel, the columns from A572 grade 50 steel, and the braces from A441 structural tubing. The member sections provided were the same as Ricles and Popov (1987).

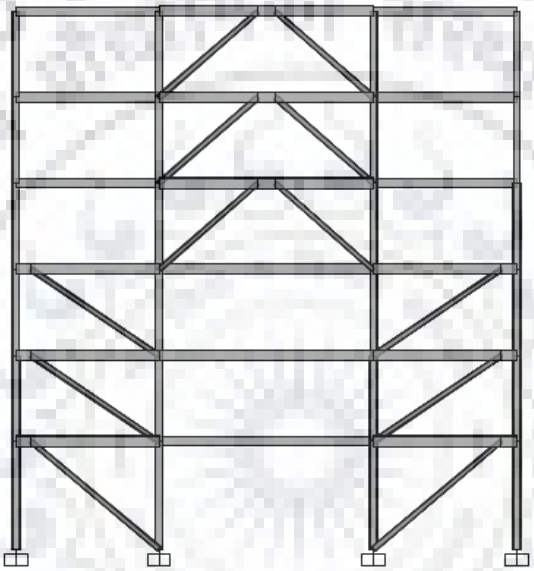

Fig 4.2 Elevation of the frame Ricles and Popov (1987)

All connections in the frame were moment resisting. Center to center dimensions between the members were used. The total mass of building was divided equally among the two EBFs. The mass associated with each floor was lumped at the column nodes on the basis of tributary width of floor beams. All the components of frame except the links were assumed to be force-controlled for axial and flexural actions. Ricles and Popov (1987) had assigned non-proportional damping, with only mass-related viscous damping assigned to links and Rayleigh damping based on 5% of critical for the first and fourth modes assigned to rest of members. However, Rayleigh damping equal to 5% of critical was assigned to all the frame members of the EBF hereby designated as MV-6. Identical modelling features were implemented for MV-6 and Ricles and Popov (except damping which is not a potential parameter to alter the results significantly) to facilitate the comparison of results.

The model was analyzed for first 15 seconds of 1966 Parkfield earthquake having a peak ground acceleration of 0.49 g.

### 4.3.2 Comparison of Results

Both the models MV-6 and Ricles and Popov (1987) exhibited similar yielding pattern. Ricles and Popov (1987) predicted yielding mostly concentrated in the link elements while beams adjacent to links also yielded at some floors. The top storey link did not predict any shear yielding for both the models. The only difference in the context of yielding pattern existed for the ground storey beam of unbraced panel which yielded under flexure for Ricles and Popov (1987) while it did not exhibit any yielding for MV-6 model.

The comparison of inter-storey drift and inelastic link rotation envelopes is shown in Fig 4.3 respectively.

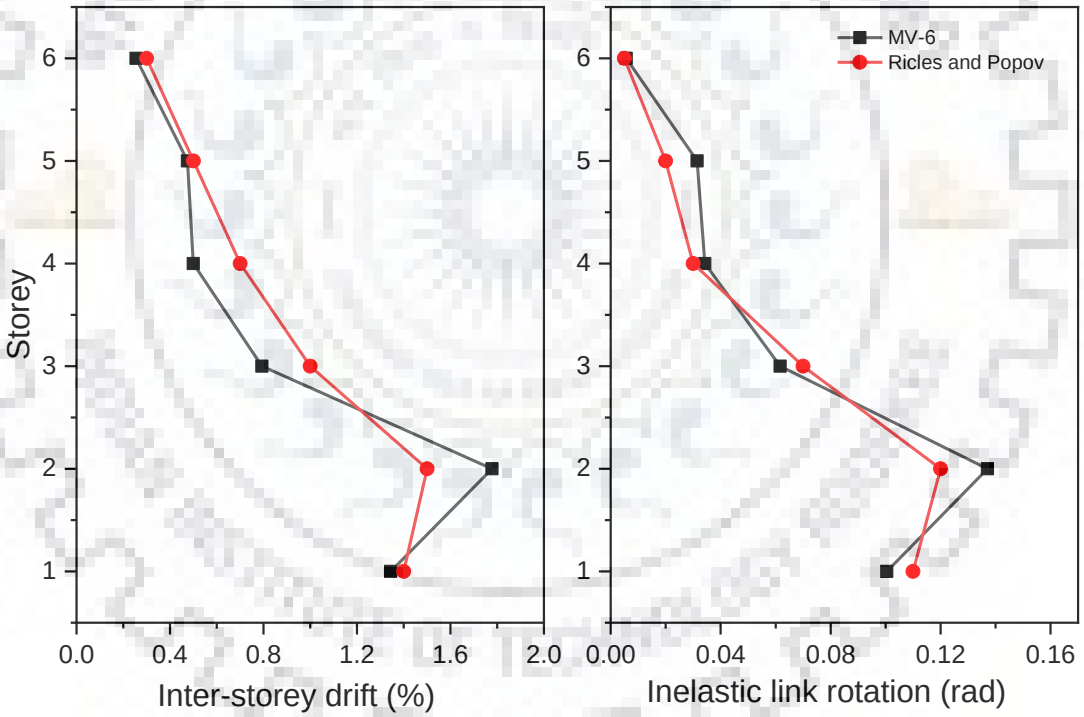


Fig 4.3 Comparison of inter-storey drift and inelastic link rotation envelopes

The comparison of axial forces in beams adjacent to links is shown in Fig 4.4.

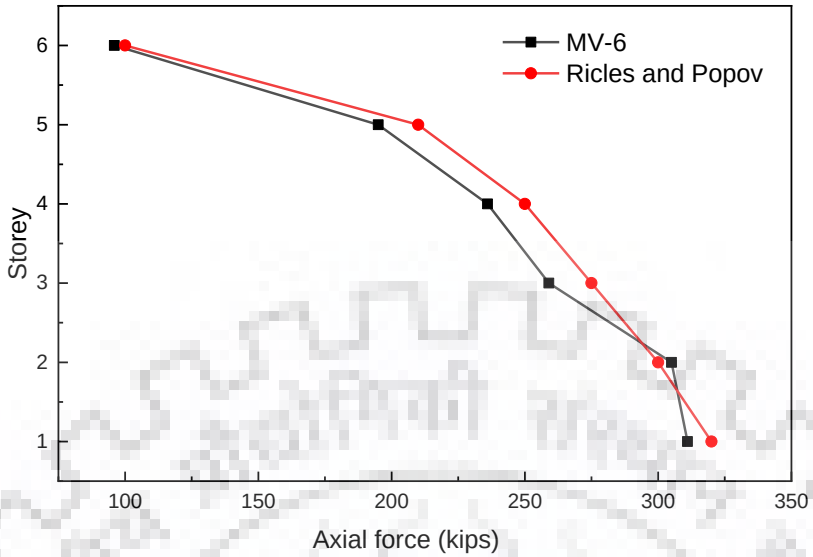


Fig 4.4 Comparison of axial forces in beams

The maximum percentage difference in the values of inter-storey drift and link rotation angles were found to be 15% and 12% respectively which occurred at the second storey level. For the maximum axial forces developed in beams adjacent to links, this difference was less than 6%. Hence the results from the two models are in good agreement with each other.

# 5. DESIGN OF EBFS WITH SHEAR LINKS

This chapter presents the design of EBFs of various heights employing short shear links. A suite of 3, 6, 10 and 14 storey EBFs with chevron bracing arrangement were designed in accordance with ASCE 341-16 and later examined for non-linear static and dynamic response.

## 5.1 Building Information

The buildings are located in San Francisco (California) which is a high seismicity zone. The resistance to lateral loads is facilitated by two EBFs oriented in either direction located along the perimeter of the building. All the buildings are rectangular in plan with 30-foot bays in either direction. The story height is kept uniform at 12 feet. The buildings are 120-foot × 150-foot (based on centerline dimensions) in plan. The edge of the deck is 1.5 feet to the exterior of the gridline. The plan and elevation for a typical archetype building is shown in Fig 5.1.

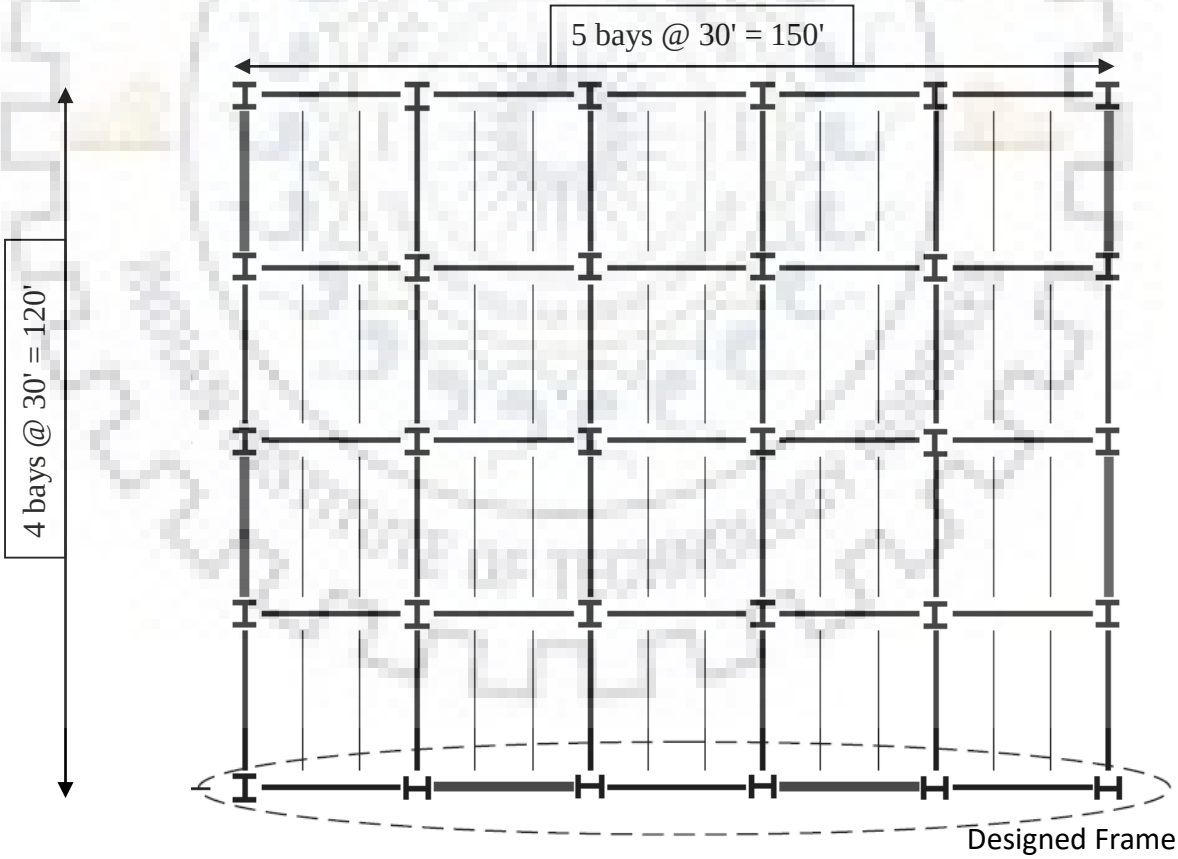


(a)

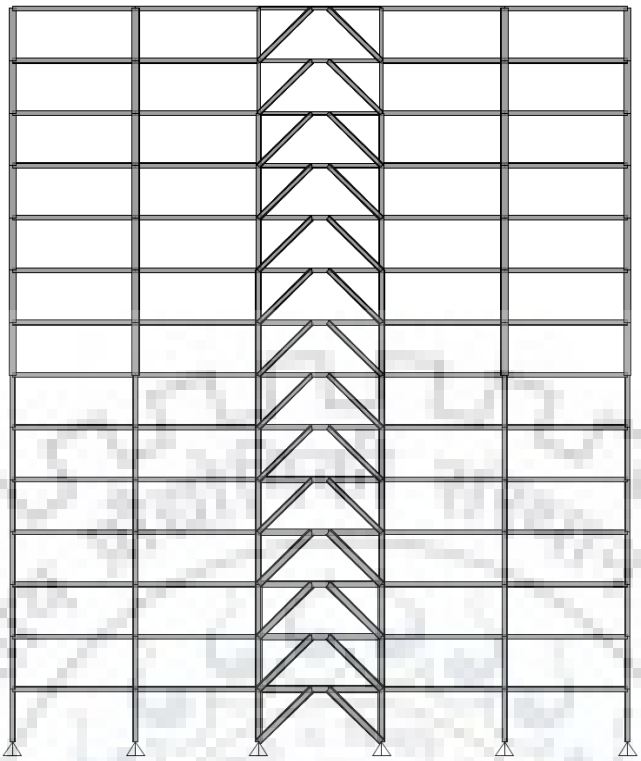

(b)

Fig 5.1 (a) Plan and (b) Elevation of a typical archetype building

The models for 3, 6, 10 and 14 storey EBFs are designated as S3, S6, S10 and S14 respectively.

The buildings do not have any horizontal or vertical irregularity either on the basis of their geometry or configuration. Horizontal irregularity Type 1 and vertical irregularity Types 1 and 5 are subject to post design analysis verification. The buildings are meant for office occupancy and are classified as Risk Category II structures. An importance factor of unity was taken. Response Reduction Factor, $R$, Overstrength factor, $\Omega$, and Displacement Amplification Factor, $C_d$, were taken in accordance with AISC 341-16 as follows:

$$R = 8.0 \qquad \Omega = 2.0 \qquad C_d = 4.0$$

All the members used were rolled wide-flange sections of ASTM A992 Grade 50 steel having specified minimum yield strength, $F_y$, and ultimate strength, $F_u$, as follows:

$$F_y = 50\ ksi \qquad F_u = 65\ ksi$$

The ratio of expected yield stress to specified minimum yield stress, $R_y$, was taken as 1.1.

The modulus of elasticity, $E$, and shear modulus, $G$, were taken as follows:

$$E = 29{,}000\ ksi \qquad G = 11{,}200\ ksi$$

## 5.2 Structural Design Loads

The archetype buildings were designed for following load combinations in accordance with ASCE 7-16 [6]:

1. $1.4D$
2. $1.2D + 1.6L$
3. $1.2D + L + Q_E$
4. $1.2D + L - Q_E$
5. $0.9D + Q_E$
6. $0.9D - Q_E$

where, $D$, $L$ and $Q_E$ represent the dead, live and seismic load effects respectively. Snow and wind loads were not taken into design consideration. The seismic load effects outweigh the significance of wind loads in low and mid-rise buildings especially in high seismicity site classes as considered for the archetype buildings.

The assembly weights were taken in accordance with ASCE 7-16 [8] as shown in Table 5.1.

Table 5-1 Assembly Weights

| Dead Loads | | | |
|---|---|---|---|
| Floor | | Roof | |
| Description | Magnitude | Description | Magnitude |
| Floor finish | 5 psf | Built-up roof | 6 psf |
| 2-in, 18 ga. deck | 3 psf | Insulation | 2 psf |
| 3.25-in light weight concrete fill | 39 psf | Metal roof deck | 4 psf |
| Steel framing | 10 psf | Steel framing | 8 psf |
| Mechanical/Plumbing/Electrical | 4 psf | Mechanical/Plumbing/Electrical | 4 psf |
| Ceiling | 4 psf | Ceiling | 4 psf |
| Partitions | 10 psf | Partitions | 5 psf |
| Miscellaneous | 3 psf | Miscellaneous | 3 psf |
| Total Dead Load | 78 psf | Total Dead Load | 36 psf |
| Live Loads | | | |
| Description | Magnitude | Description | Magnitude |
| Offices | 50psf | Ordinary Flat Roof | 20 psf |
| Partitions | 15 psf | | |
| Total Live Loads | 65 psf | | |

The assembly weights on the exterior wall are given in Table 5.2.

Table 5-2 Dead load on the exterior walls

| Description | Magnitude |
|---|---|
| Cladding | 7 psf |
| Metal studs | 2 psf |
| Insulation | 2 psf |
| $\frac{5}{8}$-in gypsum board | 3 psf |
| Miscellaneous | 5 psf |
| Total Dead Load | 19 psf |

The buildings are located in Seismic Design Category D having short period spectral acceleration, $S_{DS}$, of 1.0g and 1-sec spectral acceleration, $S_{D1}$, of 0.60g. The long-period transition period was taken as 12 seconds. The base shear was calculated in accordance with ASCE 7-16. The vertical distribution of calculated base shear was done using the Equivalent Lateral Force (ELF) procedure. The vertical seismic loads were not considered for design. The center of stiffness was assumed to be at an eccentricity of 5% from the center of mass to account for accidental torsional moments. However, no eccentricity was considered in the analysis of drift which was computed at the center of mass of each storey. Since the buildings were regular and symmetric, the center of mass coincided with the center of stiffness. The effective seismic weight of the building, $W$, was calculated in accordance with ASCE 7-16.

## 5.3 Structure Modelling

The archetypes were modelled in SAP2000. The features used to model links as well as beam, column and brace components in these archetypes were kept the same as that of MV-6 discussed in chapter 4.

Rayleigh damping of 5% was assigned for such number of modes corresponding to which the modal mass participation was at least 90%.

The global P-Δ effects (due to the non-LFRS framings that are not directly tributary to the EBFs) were simulated by modelling the fictitious leaning columns. The leaning column line was located one bay-width away from EBFs. These leaning columns were modelled as elastic elements pinned at every connection in order to avoid the induction of significant bending moments. They had large effective cross-sectional areas to simulate the aggregate effect of all the gravity columns. The leaning columns were connected

through pinned attachments to the EBFs by rigid truss elements at floor levels. The gravity load tributary to the EBFs was applied directly while rest of the gravity load ($1.0D + 0.5L$) was applied on the leaning columns.

## 5.4 Design of Archetypes

The archetypes were designed using the half-frame model concept mentioned in chapter 3 implemented for the design of HF-6. The design procedure for these archetypes is not repeated here for brevity. The distribution of lateral forces, design of frame members and subsequent verification of inter-storey drift, link rotation angle and global stability for a sample model (S14) are explained in Appendix A. The same design and verification procedure was followed for all the archetypes.

The layout of EBFs is summarized in Table 5.3.

Table 5-3 Layout of archetypes

| Storeys | Model ID | No. of bays | Bay-width (feet) | Link length (inches) | Average link length ratio |
|---|---|---|---|---|---|
| 3 | S3 | 1 | 30 | 48 | 1.43 |
| 6 | S6 | 1 | 30 | 48 | 1.36 |
| 10 | S10 | 1 | 30 | 42 | 1.35 |
| 14 | S14 | 1 | 30 | 42 | 1.15 |

The summary of design base shear calculations for the archetypes is tabulated in Table 5.4.

Table 5-4 Design base shear of the archetypes

| Model | S3 | S6 | S10 | S14 |
|---|---|---|---|---|
| Maximum Fundamental Time Period, $T_{max}$ (sec) | 0.62 | 1.04 | 1.52 | 1.96 |
| Fundamental Time period, $T$ (sec) | 0.70 | 1.31 | 1.79 | 2.24 |
| Effective Seismic Weight of Building, $W$ (kips) | 3950 | 8720 | 15080 | 21440 |
| Seismic Response Coefficient, $C_s$ | 0.120 | 0.072 | 0.050 | 0.044 |
| Total Base Shear (kips) | 474 | 628 | 754 | 944 |
| Design Base Shear for EBF, $V$ (kips) | 246 | 327 | 392 | 491 |

The Equivalent Lateral Force (ELF) distribution along the height of the archetypes is shown in Fig 5.2.

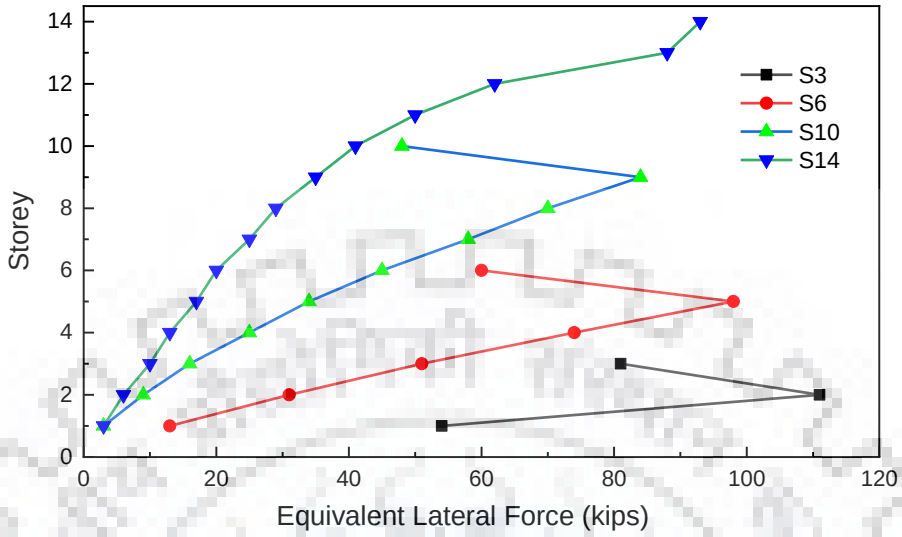


Fig 5.2 Equivalent lateral force distribution of the archetypes

The design frame sections of the archetypes are shown in Appendix C. The seismic strength requirements governed the design of link sections for all the archetypes. Capacity design requirements in addition to the section compactness limitations governed the size of braces and columns for S3 and S6. Link rotation angle and drift limitations governed the size of columns and braces for S10 and S14. The frame sections limiting the Inter-storey Drift Ratio to 2% could not limit the link rotation angle to 0.08 rad in S10 and S14 implying that the link rotation limitation governed the design primarily.

# 6. ASSESSMENT OF EBFS WITH SHEAR LINKS

A suite of eccentrically braced frame archetypes of different heights were designed in chapter 5. This chapter presents the analysis of these archetypes. The frames were analyzed using both non-linear static and dynamic analyses. The analyses focused on yield pattern of frames, force and deformation demands, concentration of deformations at some storey levels and inter-relations between various parameters.

## 6.1 Non-linear Static Analysis

The non-linear static analysis (commonly known as pushover analysis) presents a direct evaluation of the global structural response in terms of plastic hinging mechanism, global strength and ductility whilst also allowing for the evaluation of individual components. The structure is subjected to gravity loading followed by monotonic lateral loading which continuously increases through elastic and inelastic response until a pre-determined ultimate condition is reached.

The non-linear static analysis was carried out in two steps. In the first step, the gravitational loads were applied on the models. Thereafter, the lateral loads were applied. Since the magnitude of gravitational loads were known a-priori, they were applied through force control procedure while displacement control procedure was used for application of lateral loads in purview of high ductility of the EBF systems. The lateral displacements were distributed in accordance with the first mode of vibration even though the modal participation of fundamental mode was less than 90% for S10 and S14 models. This lateral displacement was applied at the corner of top storey also known as control node, starting with small displacement and monotonically increasing until the target level of displacement was reached. A lateral displacement equal to 4% of height of the archetypes was targeted, though this limit is significantly larger than the maximum displacement likely to be experienced during the design earthquake. The goal here is to determine the progressive yielding and collapse of the links and to study the concentration or scatter of the inelastic action with respect to the height of archetypes.

The results of non-linear static analysis are presented in the following sections.

### 6.1.1 Yield Pattern

The primary aim for the non-linear static analysis of archetypes was to predict the pattern of yielding. The pattern of yielding for the archetypes is depicted with reference to the

displacement level corresponding to collapse of any component as shown in Fig 6.1. The ground storey links were the first components to collapse except for S3 model in which case no component underwent collapse. The links at the top storey/storeys did not yield. Moreover, the links exhibited different levels of yielding along the height of the archetypes indicated by color-coded designations, extensive yielding being mostly concentrated in the lower levels. The non-dissipative zones were not involved in yielding as expected from the design philosophy of the EBFs.

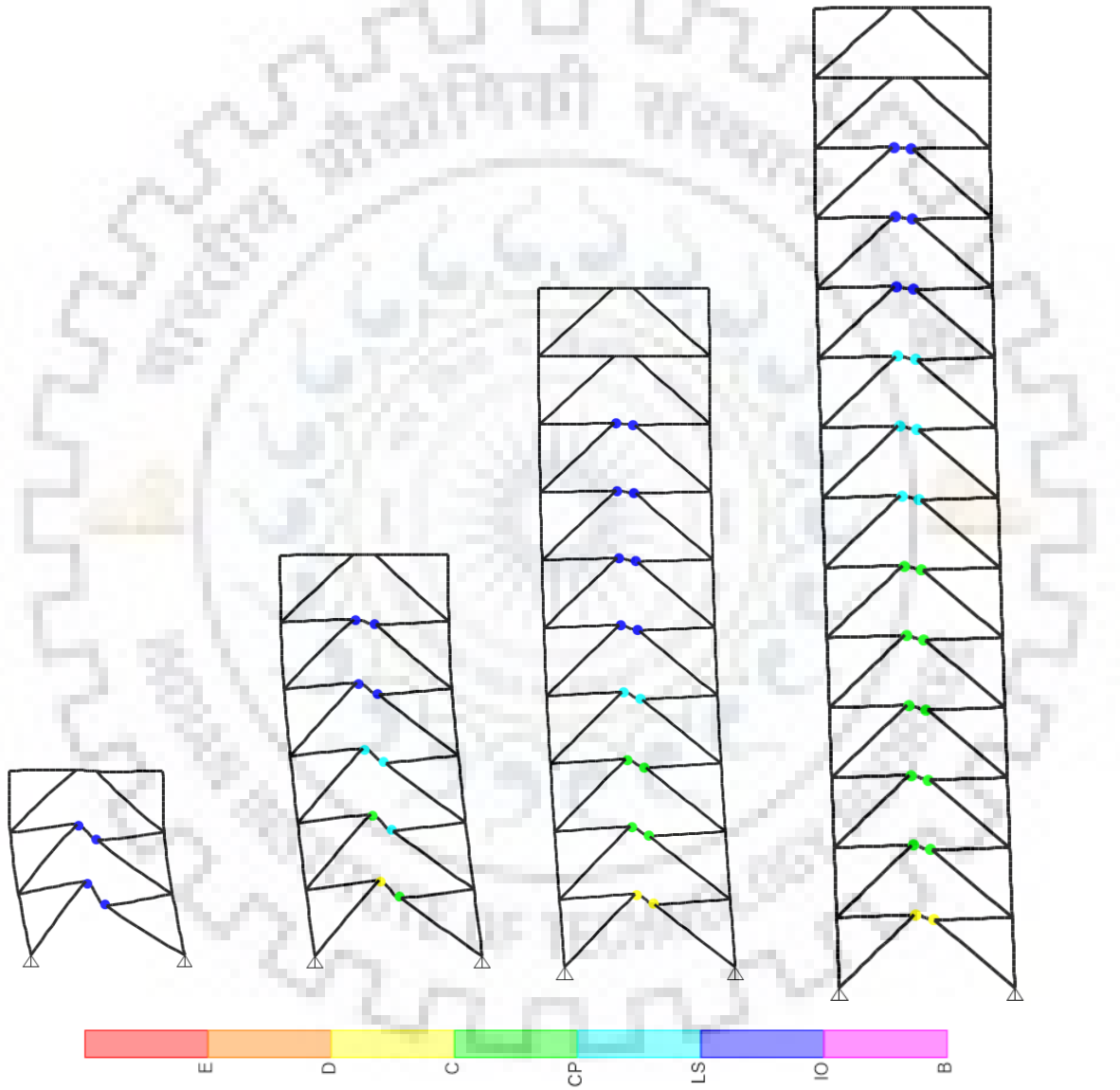


Fig 6.1 Yield pattern exhibited by the archetypes corresponding to first collapse of any component

The extent of yielding of the members as well as the acceptance criteria IO (Immediate Occupancy), LS (Life Safety) and CP (Collapse Prevention) in the above figure is designated by color-coding. B, C, D and E are the points defining the various coordinates

on the backbone curve as depicted in Fig 4.1. This representation of member-yielding is followed throughout this thesis.

### 6.1.2 Pushover Curves

The pushover curves are plotted in terms of base shear normalized to the design seismic horizontal shear, $\alpha$, versus the control node displacement expressed in percentage of height of the structures, $\delta$, as shown in Fig 6.2. The curves indicate very good strength as well as ductility characteristic of the archetypes. The sudden drop in lateral strength is characterized by the collapse of dissipative link elements starting from lower storeys and progressing towards upper ones with the monotonic increase in the control node displacement.

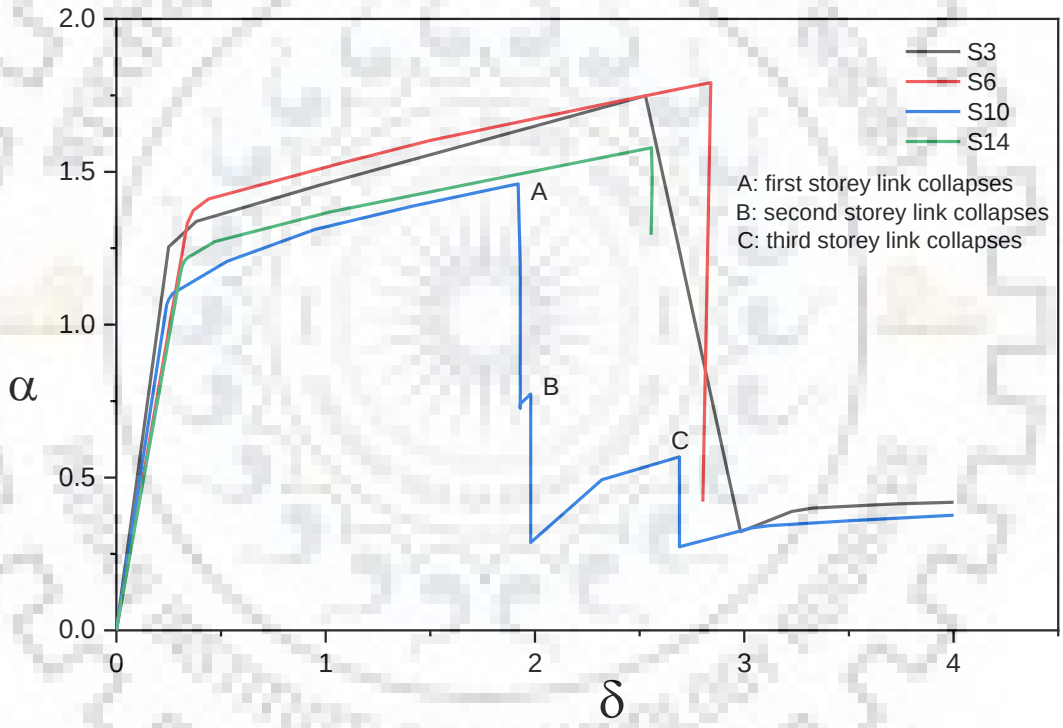


Fig 6.2 Normalized pushover curves of the archetypes

## 6.2 Non-linear Dynamic Analysis

The non-linear dynamic analysis is the most complete form of analysis since it models the inelastic response of the structures while considering the dynamic effects. Thus it overcomes the inherent shortcoming of non-linear static analysis of not fully capturing the dynamic response especially for higher modes of vibration.

The analysis was initiated by the application of gravity loads with the inclusion of 50% live loads. Geometric stiffness was calculated based on this application and added to the

elastic stiffness of the model and the modified stiffness was used for subsequent dynamic analysis. The incremental equations of motion were solved using implicit Hilber-Hughes-Taylor method $(\alpha = 0, \beta = 0.25, \gamma = 0.50)$ which is essentially based on direct integration technique.

The non-linear dynamic response of the archetypes was recorded for variable number of integration steps (1500-15000) having a variable step-size (0.01-0.005 sec) translating into variable run times (25-75 sec) for the different acceleration records. No sensitivity analysis for the variation in the time steps was done. However, the step-sizes used were sufficiently small to ensure the stability of solutions.

### 6.2.1 Selection of Ground Motions

The non-linear dynamic analysis was carried for an ensemble of eleven ground motions. The source to site distance of the seismic events was characterized by Joyner and Boore distance, $R_{jb}$, which is defined as the shortest distance from site to the surface projection of fault measured horizontally. The source to site distance was greater than 10 km for all selected ground motions and hence these qualify as far-field ground motions. The acceleration records for a particular recording station in orthogonal horizontal directions were evaluated and the component having higher Peak Ground Acceleration (PGA) value corresponding to the fundamental time period, $T$, of the archetypes was selected. Each ground motion was scaled to be compatible with the design target spectrum. Period range of $0.2T$ to $2T$ was targeted for scaling in accordance with ASCE 7. The ground motion records were scaled such that the average of response spectra of the selected ground motions closely matches the design target spectrum and does not fall below 90% of the latter within the specified period range as shown in Fig 6.3.

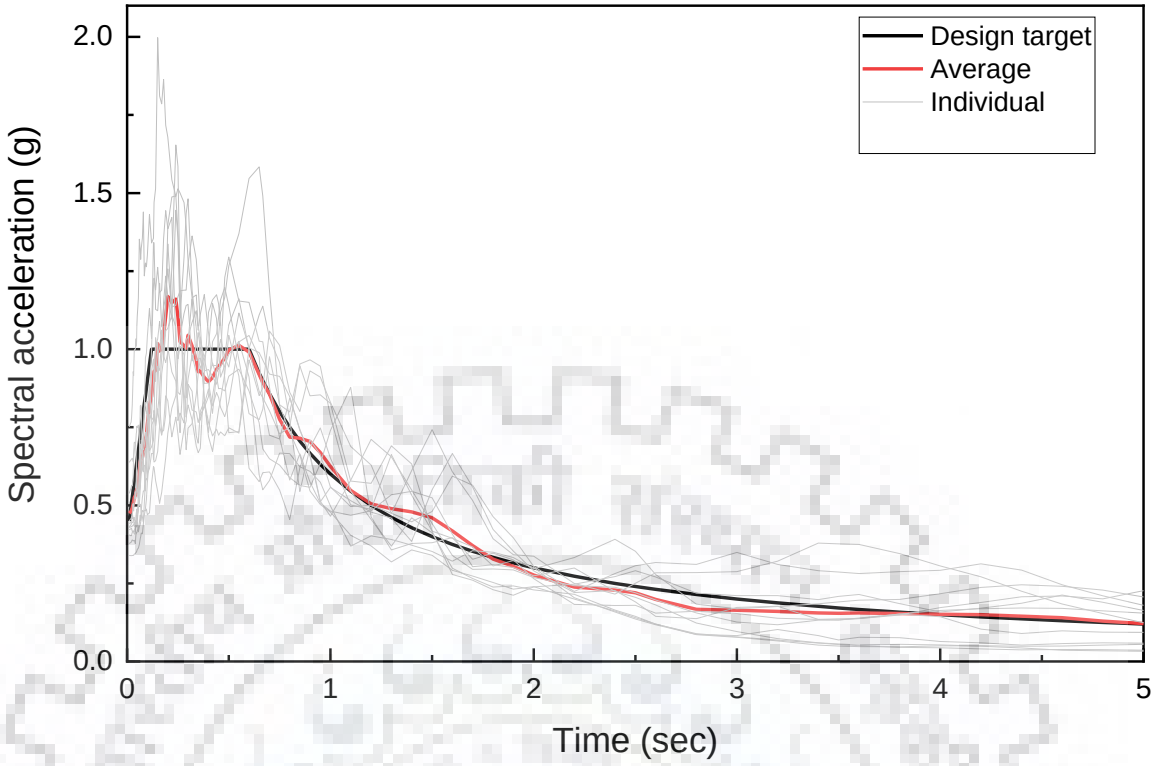


Fig 6.3 Spectral accelerations of the selected ground motions

The ground motions were taken from PEER NGA-West2 [9] ground motion database. Some information regarding the ground motions selected is presented in Table 6.1. The scaled and unscaled response spectra of the ground motions are presented in Appendix B.

Table 6-1 Summary of the selected ground motions

| Serial | Earthquake | Year | Scale Factor | Magnitude | Distance, $R_{jb}$ (km) | Fault Mechanism |
|---|---|---|---|---|---|---|
| 1 | Loma Prieta | 1989 | 1.3133 | 6.93 | 19.97 | Reverse Oblique |
| 2 | Northridge | 1994 | 0.8124 | 6.69 | 20.11 | Reverse |
| 3 | El Mayor Mexico | 2010 | 1.3913 | 7.2 | 19.12 | strike slip |
| 4 | Superstition Hills | 1987 | 1.5025 | 6.54 | 18.2 | strike slip |
| 5 | Northridge | 1994 | 2.3256 | 6.69 | 12.92 | Reverse |
| 6 | Kobe Japan | 1995 | 2.6259 | 6.9 | 28.08 | strike slip |
| 7 | Hector Mine | 1999 | 2.394 | 7.13 | 41.81 | strike slip |
| 8 | Taiwan | 1986 | 2.3764 | 7.3 | 56.16 | Reverse |
| 9 | Chuetsu Japan | 2007 | 1.3246 | 6.8 | 15.89 | Reverse |
| 10 | El Mayor Mexico | 2010 | 1.8094 | 7.2 | 18.21 | strike slip |
| 11 | Darfield New Zealand | 2010 | 1.5929 | 7 | 11.86 | strike slip |

The deviation of average response spectrum from the design target spectrum within period range of interest $(0.2T - 2T)$ is shown in Table 6.2. The maximum deviation observed is 19% which occurs at time period of around 1.5 seconds. This deviation is positive with respect to the target spectrum implying that the results derived from the analyses could be expected to lie on the conservative end for some archetypes for which the fundamental time period is close to 1.5 seconds (S6 and S10).

Table 6-2 Maximum deviation of the average response spectrum from design target spectrum

| Model ID | Period range of interest in sec $(0.2T - 2T)$ | Maximum deviation (%) |
|---|---|---|
| S3 | 0.29-2.9 | 19 |
| S6 | 0.26-2.6 | 19 |
| S10 | 0.36-3.6 | 19 |
| S14 | 0.48-4.8 | 19 |

The archetypes were analyzed for both global and component level responses. The progression and scatter of yielding, drift and link rotation angle demands and forces in the members were evaluated. Correlations between various parameters were established. The results predicted from linear assessment procedures were compared against the non-linear dynamic results to verify the suitability of various factors like displacement amplification factor and overstrength factor recommended by AISC 341-16 for design. The results of the response parameters were evaluated in terms of peak, median and 84 percentile values. The median results were used to evaluate the design parameters while 84 percentile results were used to illustrate dispersion and sensitivity of the response parameters to the ground motion characteristics.

### 6.2.2 Seismic Response of the Archetypes

All the archetypes were characterized by scattered pattern of yielding. The links at all the floors yielded for all acceleration records except for the top storey links in which case yielding occurred for only some of the records. However, the degree of yielding was not uniform over the height of structures, extensive yielding being mostly concentrated in the lower levels as predicted by non-linear static analysis also. The links at various floor levels exhibited simultaneous yielding within the duration of same inelastic excursions for some ground motions. However, the underlying basis of this behaviour could not be established. The links performed satisfactorily except for the first storey link in S14 which collapsed under Hector ground motion record although this did not alter the overall

behaviour by causing soft-storey mechanism formation. The frame members in addition to link elements did not yield at any story level for any acceleration record as expected from the design philosophy. The results of some key performance parameters are presented in following sections.

#### 6.2.2.1 Shear Demand in links

The maximum shear, $V_{max}$ induced in links normalized by expected shear capacities $\left(R_y V_P\right)$ is plotted (Fig 6.4) and compared against the AISC-341 recommended value of 1.25 for design. The maximum shear induced is under-predicted for most links. However, the 84 percentile results exceeded 1.25 at few floor levels, mostly lower storeys and lower segment of the top storeys, while the median results were less than this value for all the archetypes. For the top storey links, the maximum normalized shear was comparatively lesser even reaching a value of unity in S10 and S14 indicating very insignificant overstrength. The values are highly scattered with frame height causing the deformations to concentrate within few storeys.

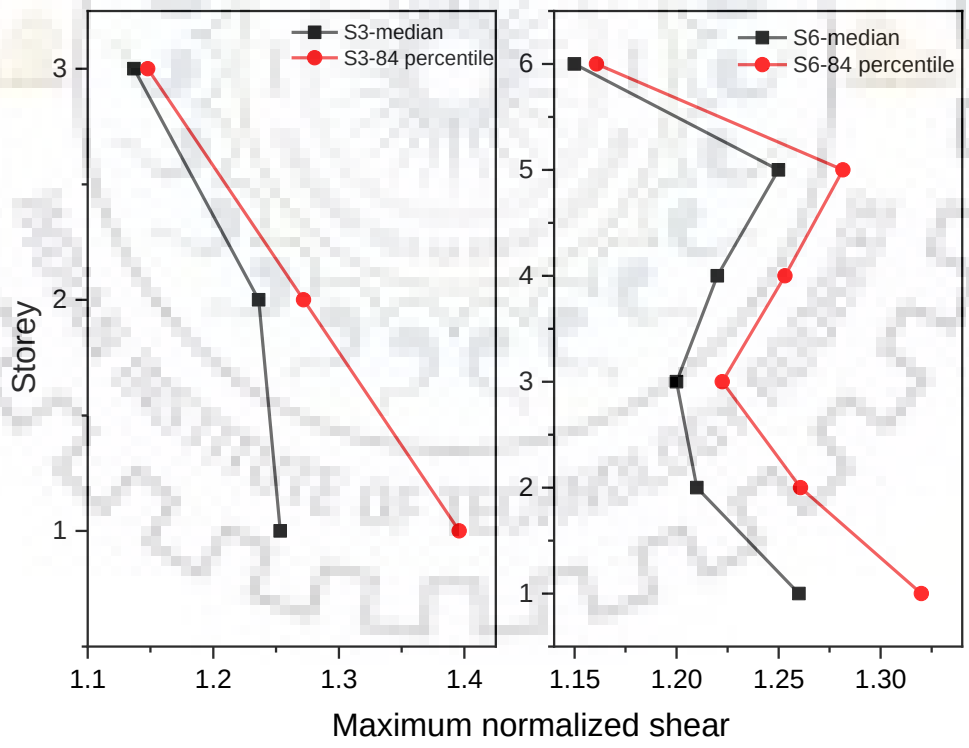


(a)

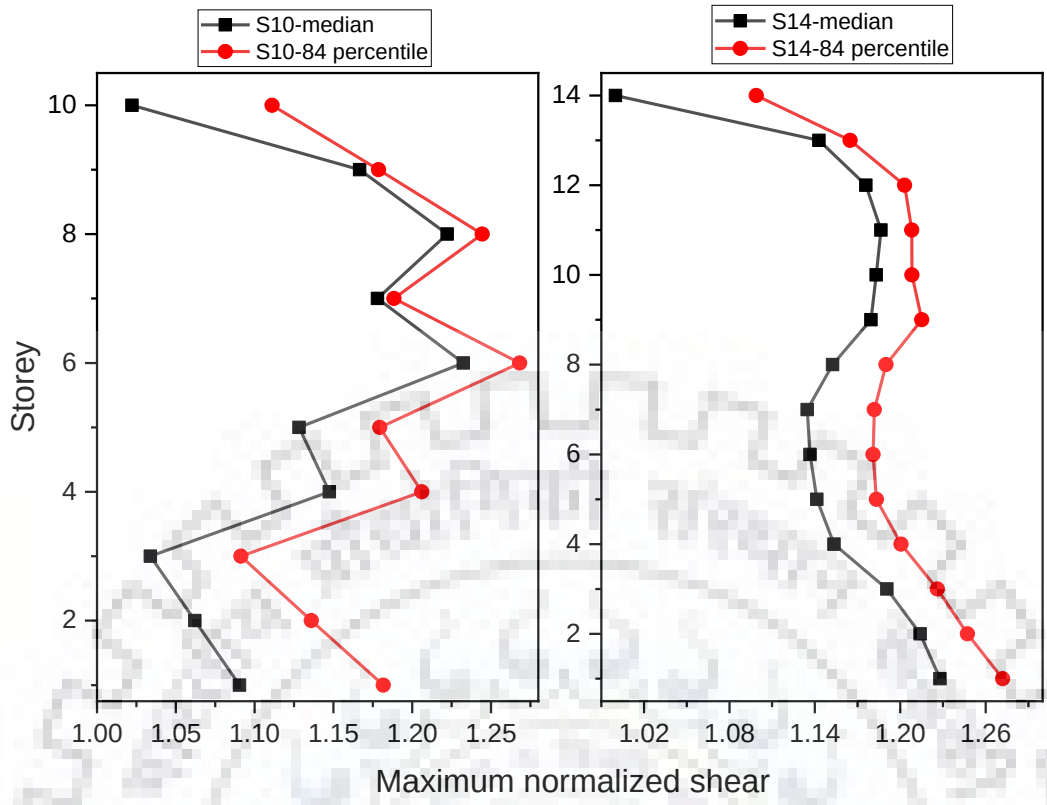


(b)

Fig 6.4 Maximum normalized shear envelopes in links for (a) S3 and S6 and (b) S10 and S14

### 6.2.2.2 Drift and Inelastic Link Rotation Demands

The distribution of inter-storey drift and inelastic link rotation with the height of archetypes is the same as that of normalized maximum shear in links (Fig 6.5). Inter-storey drift did not exceed the code limitation of 2%. However, the inelastic link rotation demand limitation of 0.08 radians was exceeded in lowermost storeys of all the archetypes as well as some upper storeys of S14. The 84 percentile rotations exceeded this limit significantly at some floor levels implying sensitivity to particular acceleration history in lieu of the shear forces. Maximum deformation demands were restricted to the lower storeys and the lower segment of upper storeys and thus uniform dissipation of energy cannot be anticipated. The significance of higher mode vibrations was evident in S10 and S14 models which exhibited concentration of deformations in upper storeys.

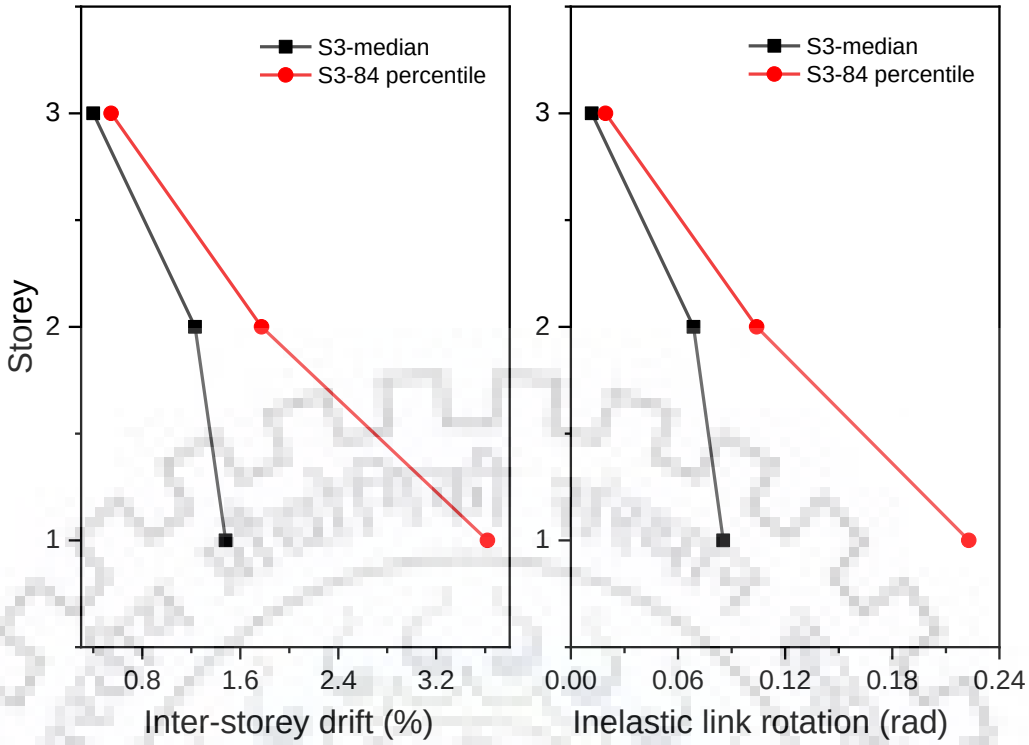
S3-median
S3-84 percentile
Storey
3
2
1
0.8
1.6
2.4
3.2
Inter-storey drift (%)
S3-median
S3-84 percentile
3
2
1
0.00
0.06
0.12
0.18
0.24
Inelastic link rotation (rad)

(a)

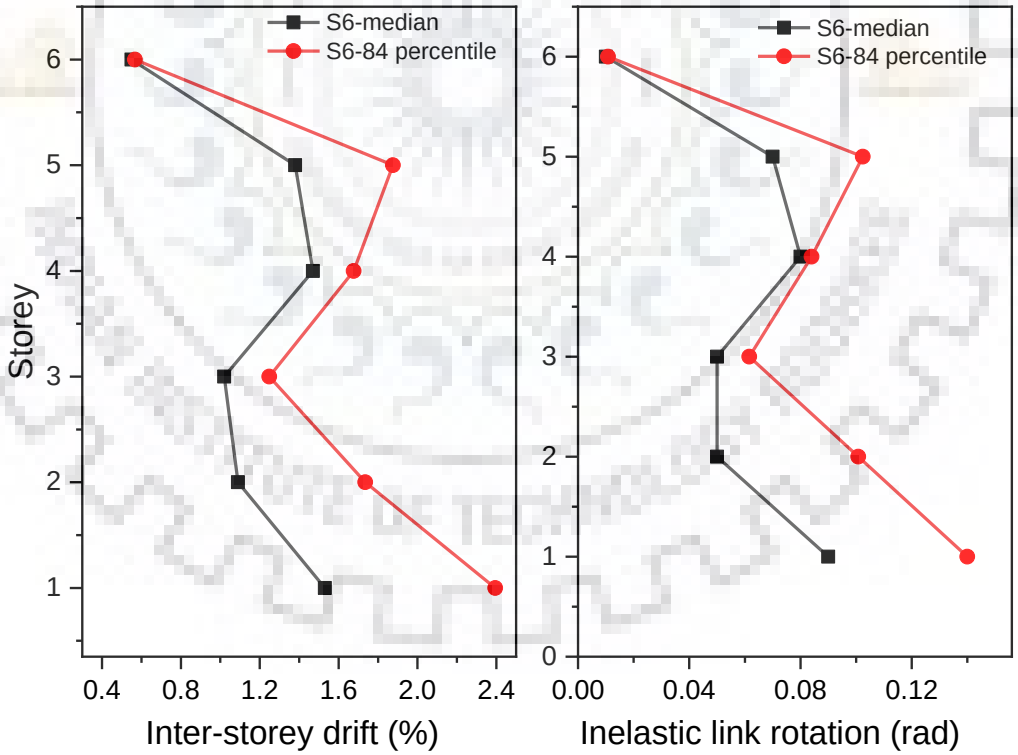
S6-median
S6-84 percentile
Storey
6
5
4
3
2
1
0.4
0.8
1.2
1.6
2.0
2.4
Inter-storey drift (%)
S6-median
S6-84 percentile
6
5
4
3
2
1
0
0.00
0.04
0.08
0.12
Inelastic link rotation (rad)

(b)

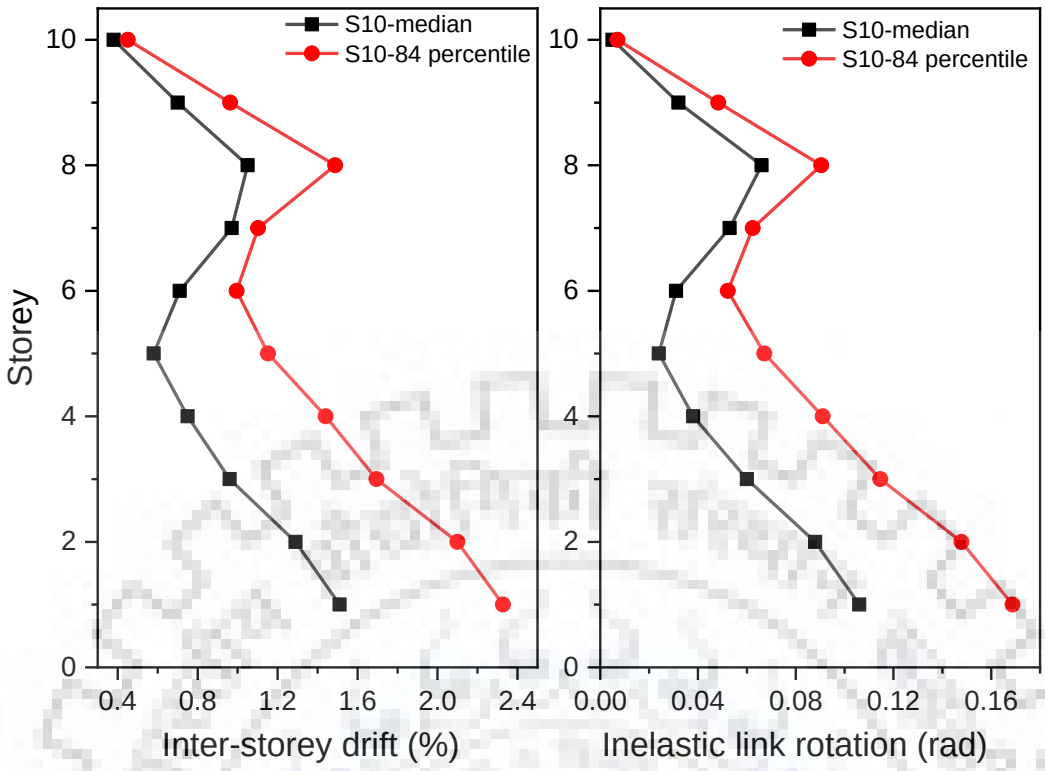


(c)

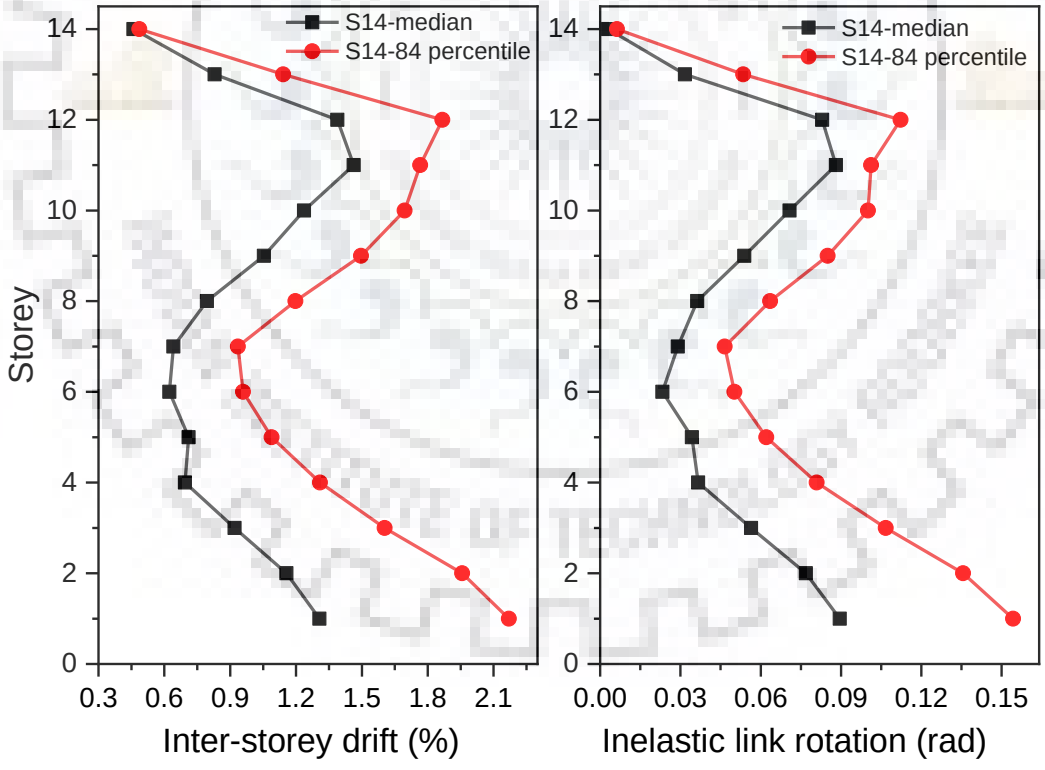


(d)

Fig 6.5 Inter-storey drift and inelastic link rotation envelopes for (a) S3 (b) S6 (c) S10 and (d) S14

The deformation demands were insignificant in top-most storeys owing to very high shear capacity to design shear demand ratios (Table 6.3) of the link beams. The capacity to demand ratio was kept uniform at all floor levels excluding the links in top storeys where the compactness requirements of links and limitation on link length ratio ($\rho < 1.6$ for short links) necessitated the use of stockier sections. Furthermore, significantly higher link rotations were required to achieve inter-storey drift of 2% implying that the link rotation angle limitation generally controlled the design when capacity design requirements did not. Capacity design requirements controlled the design for S3 and S6 archetypes (low-rise).

Table 6-3 Shear capacity to demand ratio of links

| Storey | Capacity to Demand ratio of links | | | |
|---|---|---|---|---|
| | S3 | S6 | S10 | S14 |
| 1 | 1.59 | 1.18 | 1.15 | 1.10 |
| 2 | 1.64 | 1.18 | 1.15 | 1.10 |
| 3 | 3.66 | 1.25 | 1.15 | 1.10 |
| 4 | | 1.19 | 1.14 | 1.12 |
| 5 | | 1.48 | 1.14 | 1.10 |
| 6 | | 3.61 | 1.17 | 1.14 |
| 7 | | | 1.15 | 1.12 |
| 8 | | | 1.26 | 1.10 |
| 9 | | | 2.34 | 1.10 |
| 10 | | | 4.21 | 1.11 |
| 11 | | | | 1.15 |
| 12 | | | | 1.19 |
| 13 | | | | 1.75 |
| 14 | | | | 4.54 |

#### 6.2.2.3 Axial Forces in Columns

The median of maximum axial forces induced in columns due to various ground motions are plotted against the design axial forces calculated from capacity design. The amplified axial forces using an overstrength factor of 2 for seismic effects are also plotted (Fig 6.6). The design axial forces show very good resemblance with median results but are comparatively greater by about 10-20%. The amplified axial forces are significantly larger than the median values and the use of amplified axial forces for design is rather redundant and highly un-conservative since the columns designed in accordance with

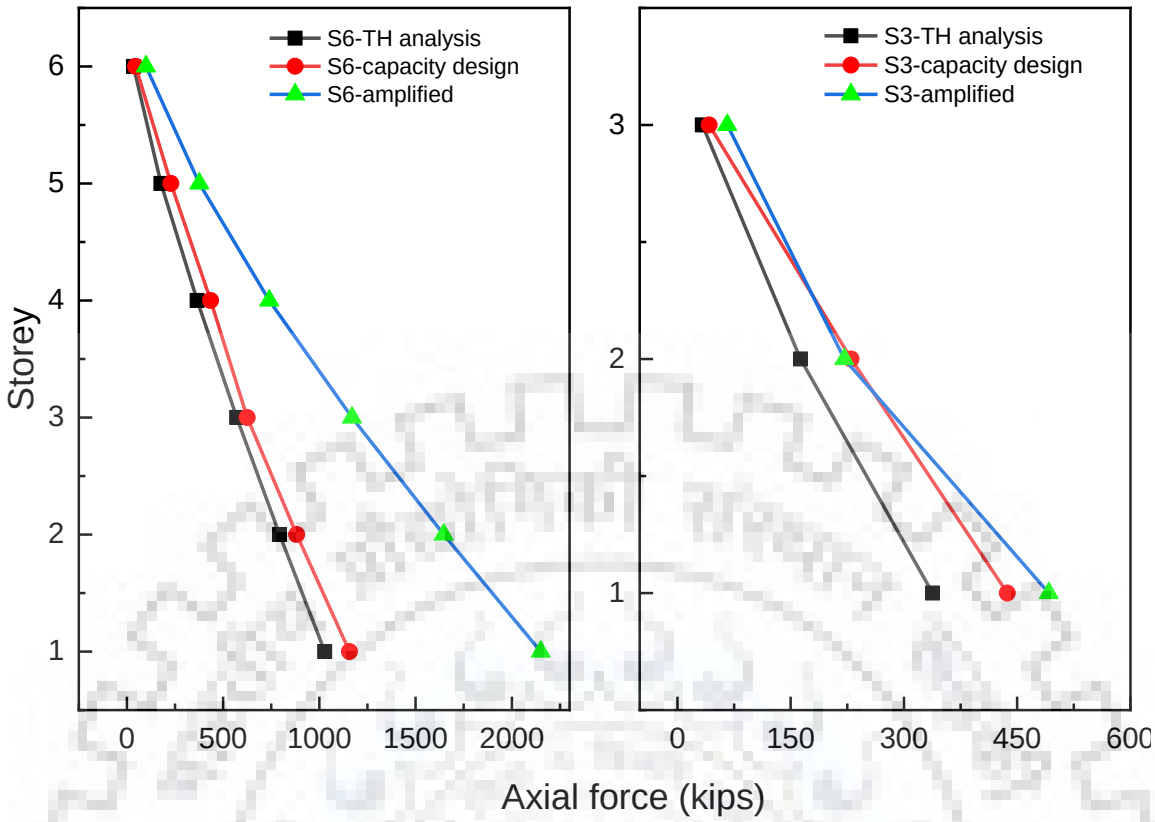


(a)

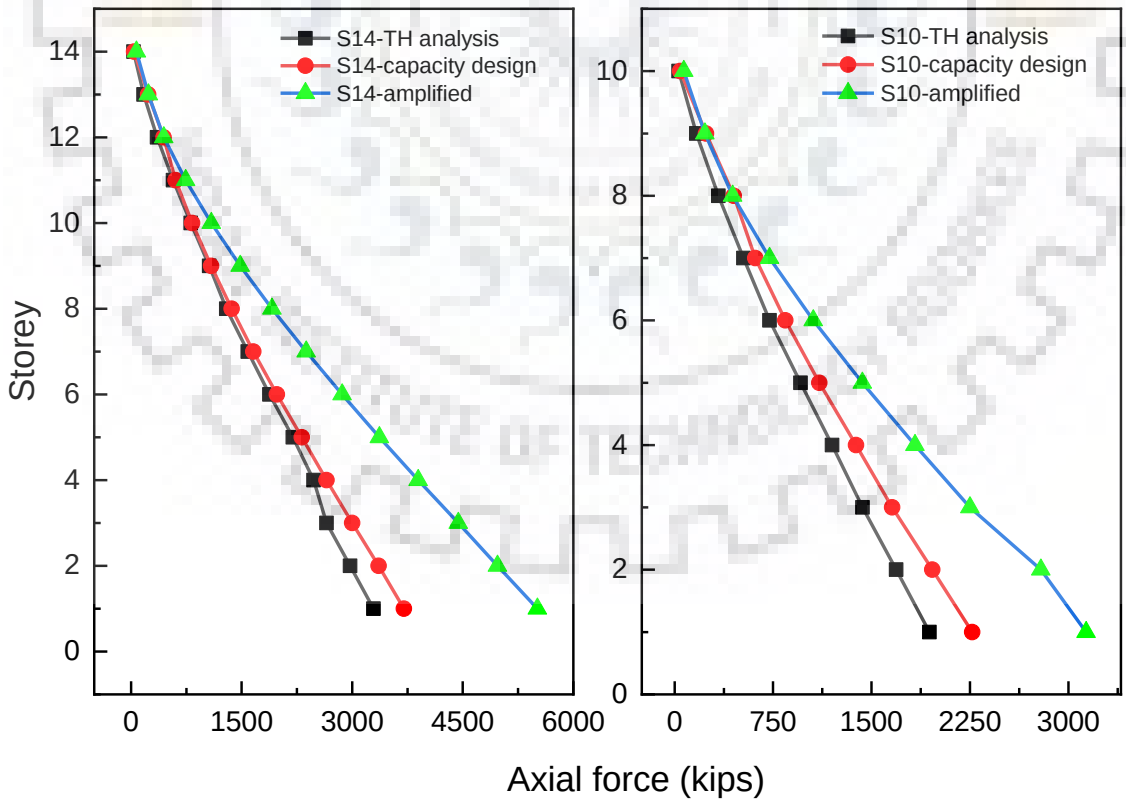


(b)

Fig 6.6 Comparison of axial forces in columns for (a) S3 and S6 and (b) S10 and S14

capacity design procedure performed satisfactorily in all the archetypes. The reduction in the overstrength factor of 1.25 by 12% for the design of columns as recommended by AISC-341 seems reasonable in purview of the improbable simultaneous yielding of links.

#### 6.2.2.4 Prediction of Deformations using Displacement Amplification Factor

AISC-341 recommends Displacement Amplification Factor of 4 to predict the inelastic deformation levels from elastic level. The predicted deformations (inter-storey drift and link rotations) are plotted against the median and 84 percentile values evaluated from time history analysis (Fig 6.7). The deformations predicted in design revealed extensive mismatch with the median results especially for taller archetypes. Displacement Amplification Factor of 4 seemed to underestimate the inelastic deformations in the lower storeys. Any underestimation or overestimation in the prediction of inelastic deformations at some floor levels has undesirable consequences resulting in concentration of yielding (and possibly soft-story mechanism) or unnecessarily heavier frame sections respectively since the deformation limitations control the design in mid and high-rise EBF systems. A more thorough assessment perhaps of the nature prescribed by FEMA P695 [10] is therefore required to evaluate the suitability of Displacement Amplification Factor.

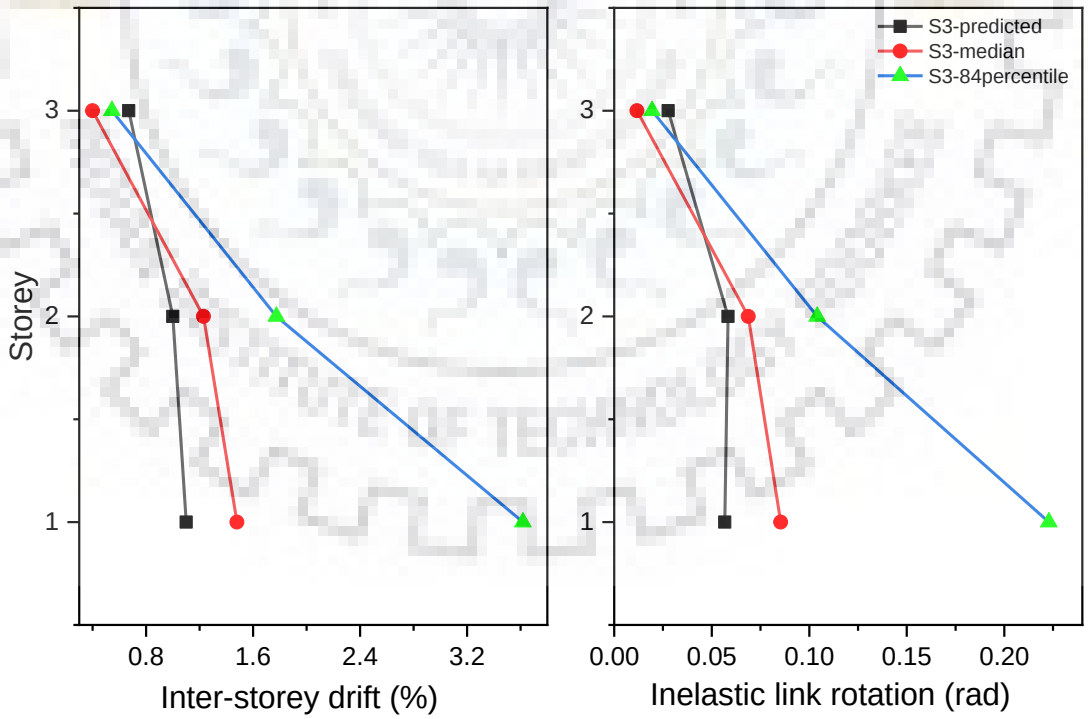


(a)

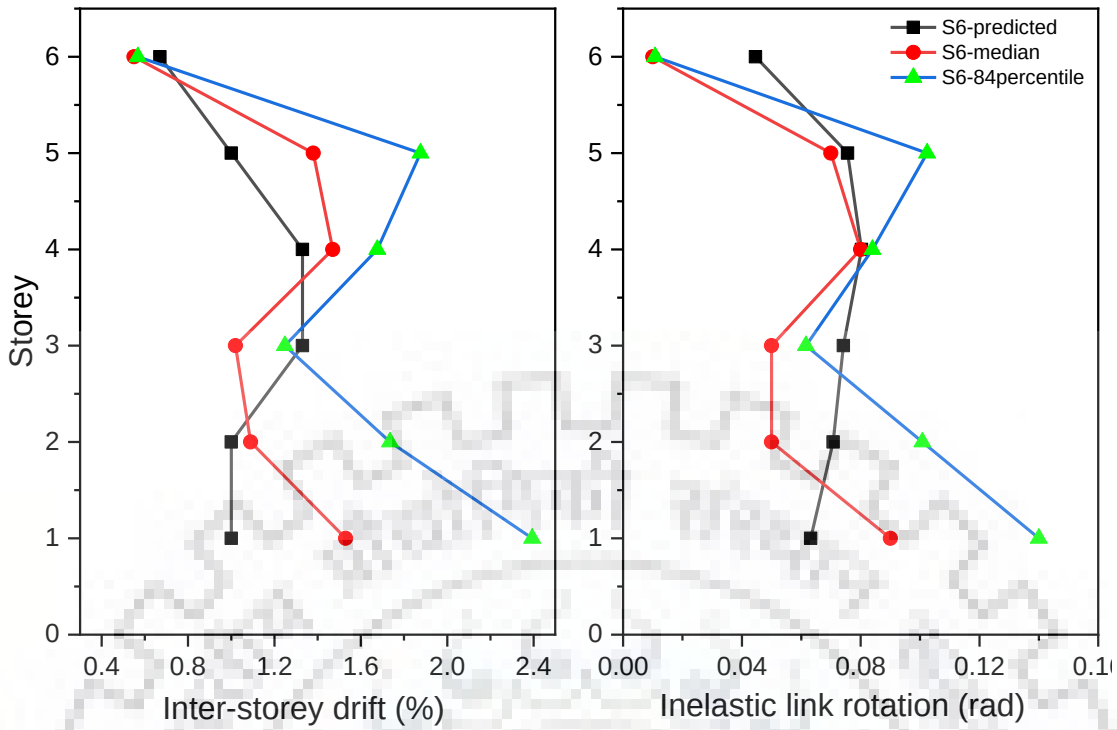
Storey
Inter-storey drift (%)
Inelastic link rotation (rad)
S6-predicted
S6-median
S6-84percentile

(b)

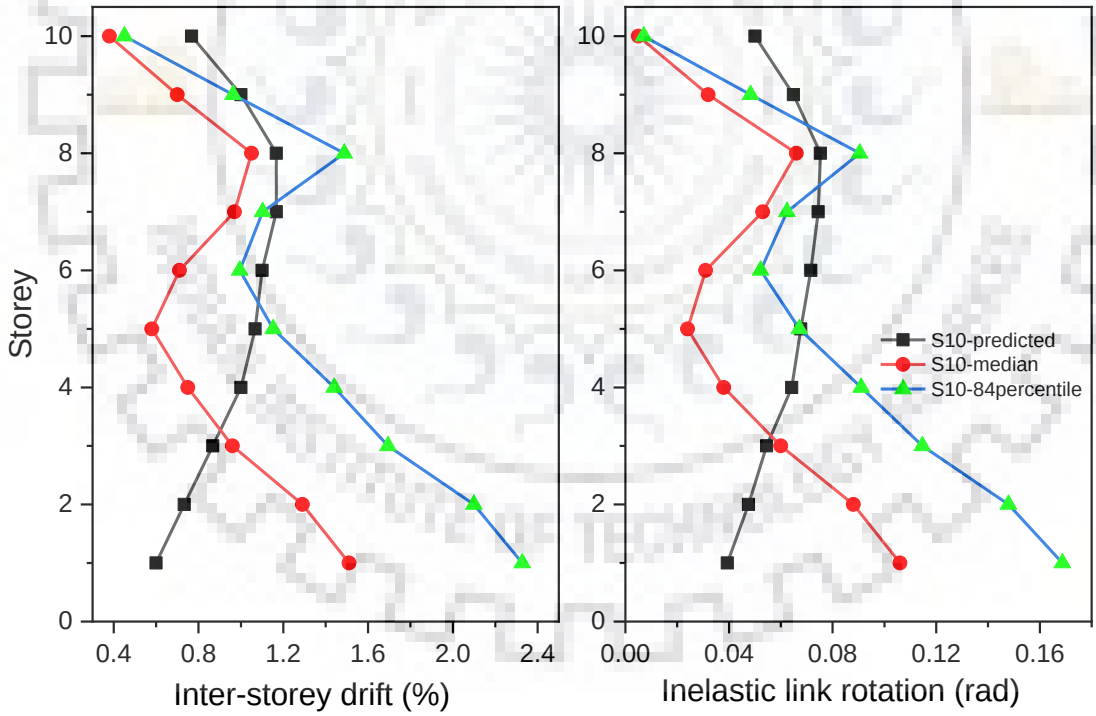
Storey
Inter-storey drift (%)
Inelastic link rotation (rad)
S10-predicted
S10-median
S10-84percentile

(c)

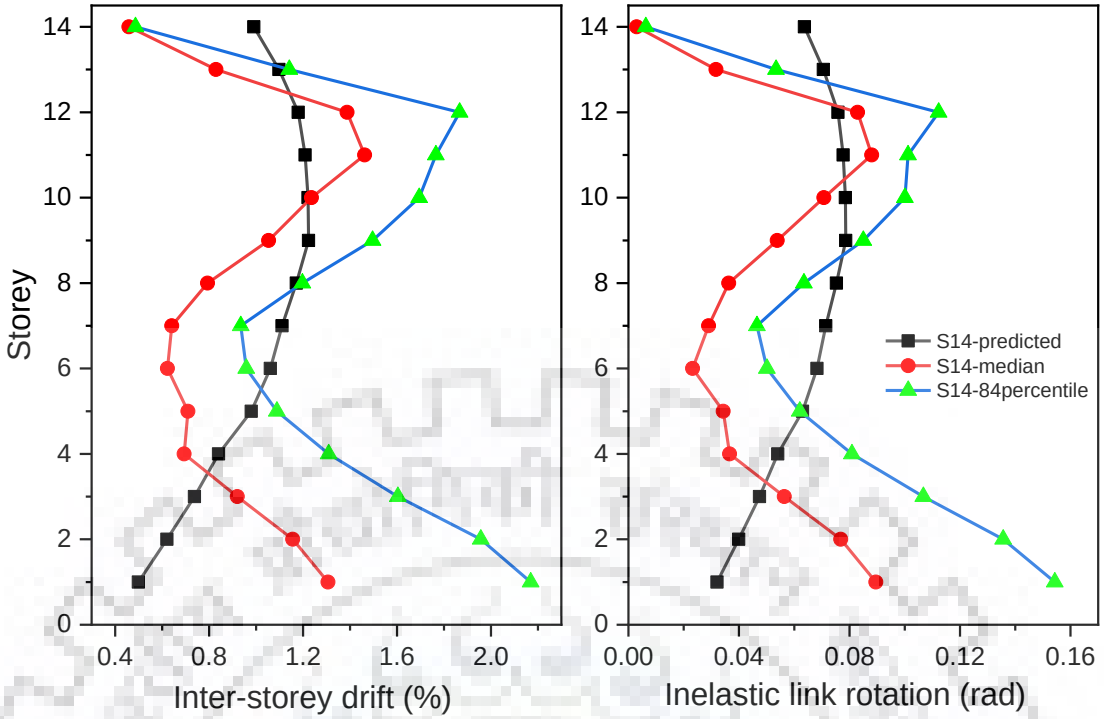


(d)

Fig 6.7 Comparison of time history analysis deformations with predicted deformations for (a) S3 (b) S6 (c) S10 and (d) S14

### 6.2.2.5 Relation Between Drift and Inelastic Link Rotation

The inelastic link rotations are estimated for design as a function of frame geometry and inelastic drifts, assuming the frame behavior to be rigid-plastic (Fig 6.8). The inelastic drifts are estimated from elastic drifts using Displacement Amplification Factor, the suitability of which is unreliable as mentioned in preceding sections. The goal here is to

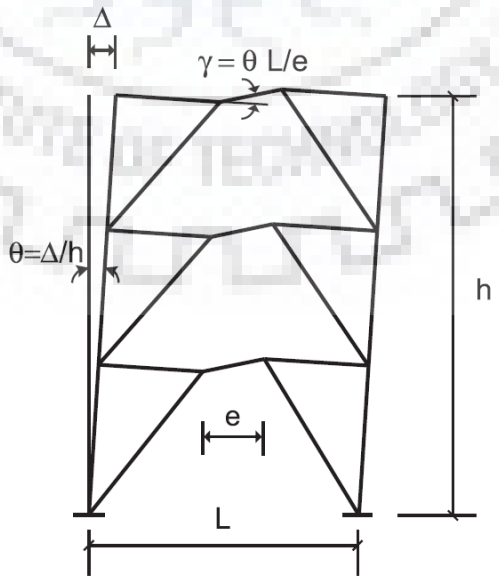


Fig 6.8 Rigid-plastic collapse mechanism for K-braced EBFs

evaluate the suitability of assumed relationship between inelastic drift and link rotation (in which the use of Displacement Amplification Factor is implicit) based on rigid plastic behavior when peak deformations are reached in non-linear dynamic analysis.

The peak drifts and link rotations were computed at every storey for each ground motion record and a strong correlation between the two parameters was achieved; the maximum values of these parameters occurred in the same space-time domain for every acceleration record hence confirming the physical relationship between them. The pairs of results were plotted and linear relationships were established using regression analysis for each archetype separately. Data points corresponding to top storey links were excluded in purview of very insignificant rotations. The plot is shown in Fig 6.9 for S14. The equation can be written as follows:

$$\frac{\delta}{h} = 0.129\gamma + 0.0029 \tag{5.1}$$

where $\delta$ is inter-storey drift, $h$ is the story height and $\gamma$ is inelastic link rotation. The intercept in the above equation is approximately equal to the ratio of link length, $e$, to the bay width, $L$, (0.133) and gives the following relation upon substitution.

$$\gamma = \frac{L}{e}\left\{\frac{\delta}{h} - 0.0029\right\} \tag{5.2}$$

The above equation predicts the relationship between the two parameters very precisely

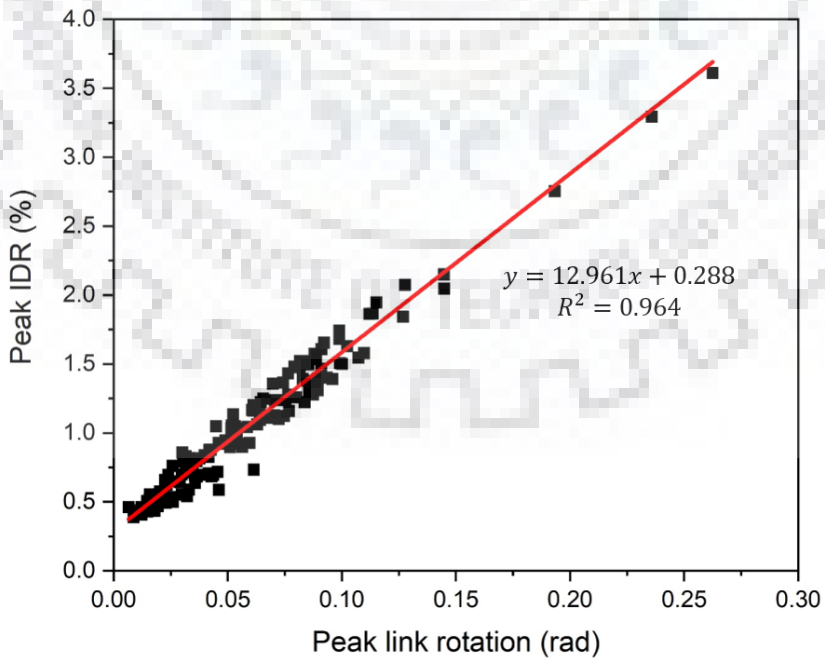


Fig 6.9 Relation between peak inter-storey drift and inelastic link rotation for S14

as can be seen from the plot and is consistent with the assumption of rigid plastic mechanism with inter-storey drift index at a yield of 0.29%. Similar relation was established for S6 and S10 archetypes with inter-storey drift index at yield of 0.32% and 0.29% respectively.

#### 6.2.2.6 Axial Forces in Links

The axial force induced in link segments can have detrimental effect on its behavior as experiments have shown that it reduces plastic strength as well as rotation capacity of links. The EBFs in chevron configuration have the advantage of not inducing significant axial forces in links. This was verified here by tracing the axial force time history of the ground storey link segment of S6 subjected to El Centro acceleration record (Fig 6.10). Similar results were found for rest of the links in all ground motions.

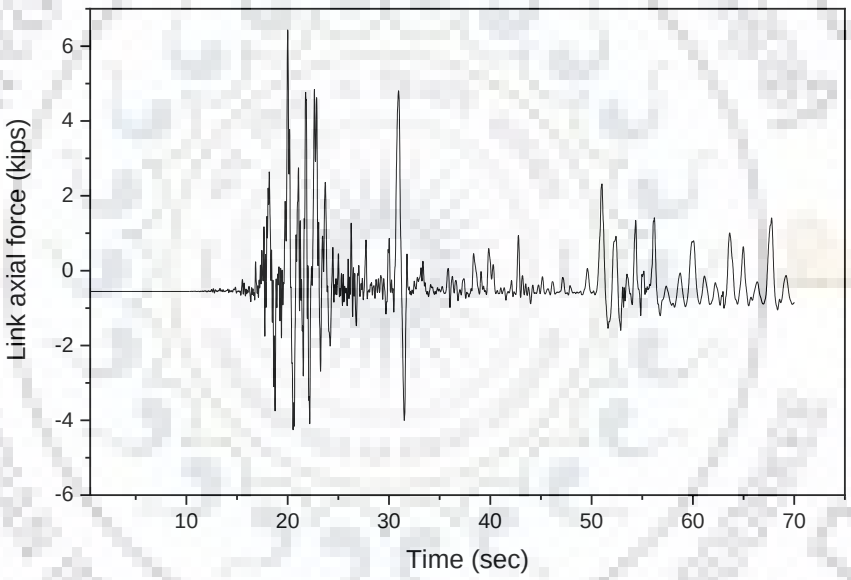


Fig 6.10 Axial force time history of the ground storey link of S6 subjected to El Centro earthquake

## 6.3 3D Modelling and Analysis of Archetypes

This section presents the design and analysis of 6 and 14 storey EBFs with short shear links. The same archetypes S6 and S14 were modelled in 3D and analyzed using non-linear static and dynamic analysis at both Design Basis Earthquake (DBE) and Maximum Considered Earthquake (MCE) levels. The DBE level ground motions were the same as used for 2D analysis. The 6 and 14 storey 3D models are designated as M6 and M14 respectively. The isometric view of M14 model is shown in Fig 6.11.

Fig 6.11 Isometric view of 14 storey model M14

### 6.3.1 Design and Modelling of the Archetypes

The building properties including plan, elevation, design loads and site conditions were the same as mentioned in preceding sections. The link design shear was approximately the same as calculated from 2D analysis. Therefore, same link sections were used (as used in S6 and S14) which caused the rest of frame sections to be the same in purview of capacity design approach. The gravity resisting frame members used in M6 and M14 are

enlisted in Table 6.4. Same beam sections were provided in all the floor levels except the roof. The column sections were also kept the same over several storeys.

Table 6-4 Design gravity resisting frame sections

| Storey | Columns | | Storey | Beams | |
|---|---|---|---|---|---|
| | M6 | M14 | | M6 | M14 |
| 1-3 | W14×132 | W14×233 | Floor | W12×72 | W14×61 |
| 3-6 | W12×96 | W14×233 | Roof | W10×45 | W10×45 |
| 7 | | W14×233 | | | |
| 7-14 | | W12×132 | | | |

The modelling features of link element as well as the rest of EBF members were kept the same as used in S6 and S14. The non-LFRS columns were modelled using elastic beam-column elements and P-M3 interaction hinges were lumped at either ends. The non-LFRS beams were primarily designed for flexure and non-linearity was modelled using M3 lumped plasticity hinges at both ends. The backbone curves of both M3 and P-M3 interacting hinges were based on AISC 41-13.

The slab was modelled using thin shell element of 100mm thickness with unit weight of 0.15 kips/ft$^3$. The compressive strength of slab was taken as 576 kips/ft$^2$. Each slab panel was divided into sub-panels by providing smaller meshes to facilitate uniform distribution of load. All these modelling features were kept same between the 2D and 3D models so that their results could be compared and the significance of certain parameters inherent to only one of the two models could be evaluated.

### 6.3.2 Non-linear Static Analysis

The non-linear analysis results of only the 14 storey archetype are presented here. The same procedure used in the analysis of S14 was used for M14. The pattern of yielding predicted by 2D and 3D analysis of archetypes was same. However, the non-LFRS beams started to yield once the links had collapsed under increased roof displacements. The yield pattern exhibited by M14 corresponding to displacement at which the first component collapsed is shown in Fig 6.12

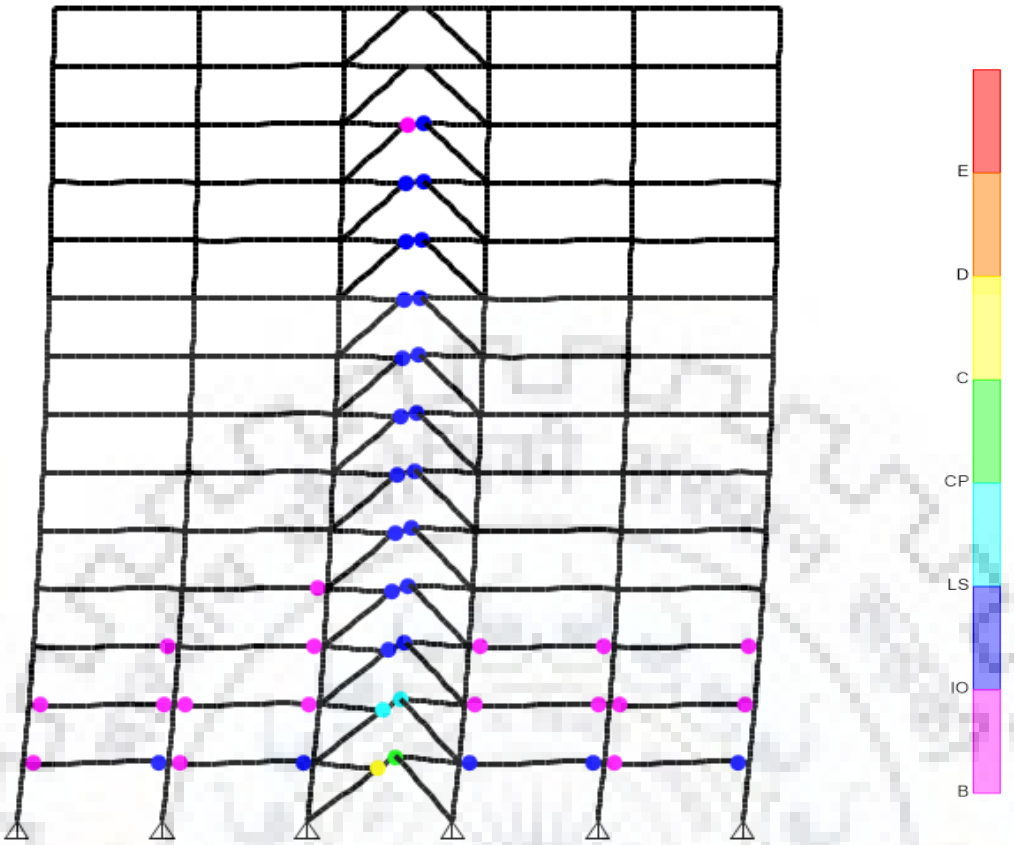


Fig 6.12 Yield pattern of M14 frame corresponding to the first collapse of any component

The $\alpha - \delta$ (pushover) curve for M14 is plotted (Fig 6.13) and compared against that of

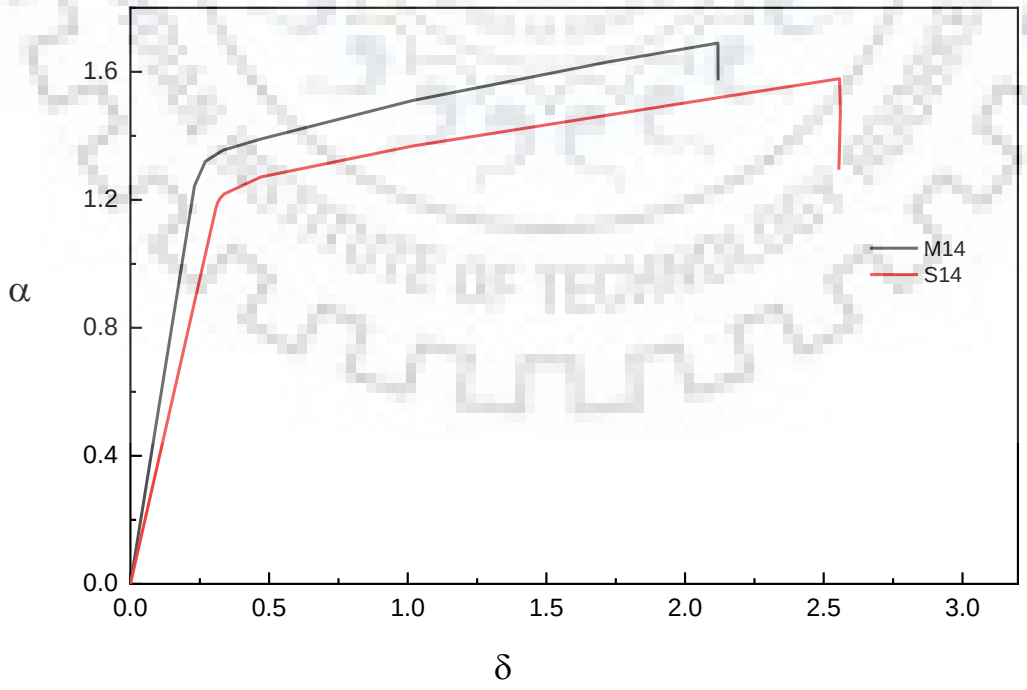


Fig 6.13 Comparison of pushover curves of M14 and S14

S14. The curve indicates slightly higher lateral strength and lesser ductility of M14 compared to that of S14.

### 6.3.3 Non-linear Dynamic Analysis at DBE Level

The same ground motion records used in the 2D analysis of archetypes were used at DBE level. The archetypes were characterized by scattered pattern of yielding. Links at all the floors yielded for all acceleration records except for the top storey links in which case yielding occurred only for few records. However, the degree of yielding was not uniform over the height of the structures, extensive yielding being mostly concentrated in the lower levels. For M6, the beams adjacent to links yielded at various floor levels for multiple ground motion records but this did not affect the overall frame behavior since the hinges did not rotate significantly on account of being spurious and hence did not partake in kinematics of collapse mechanism. The non-LFRS beams in lower storeys of M14 also yielded for a few ground motions.

The deformation demands computed for 3D models were comparatively lesser than that for 2D models, the difference being maximum at the lower segment of upper storeys (Fig 6.14). This implies that frames in addition to the EBFs contribute to lateral load resisting which was neglected in the design of 2D models. The median time history results at all the floor levels were within code-specified deformation limitations. However, the peak results for individual acceleration records did exceed these limitations.

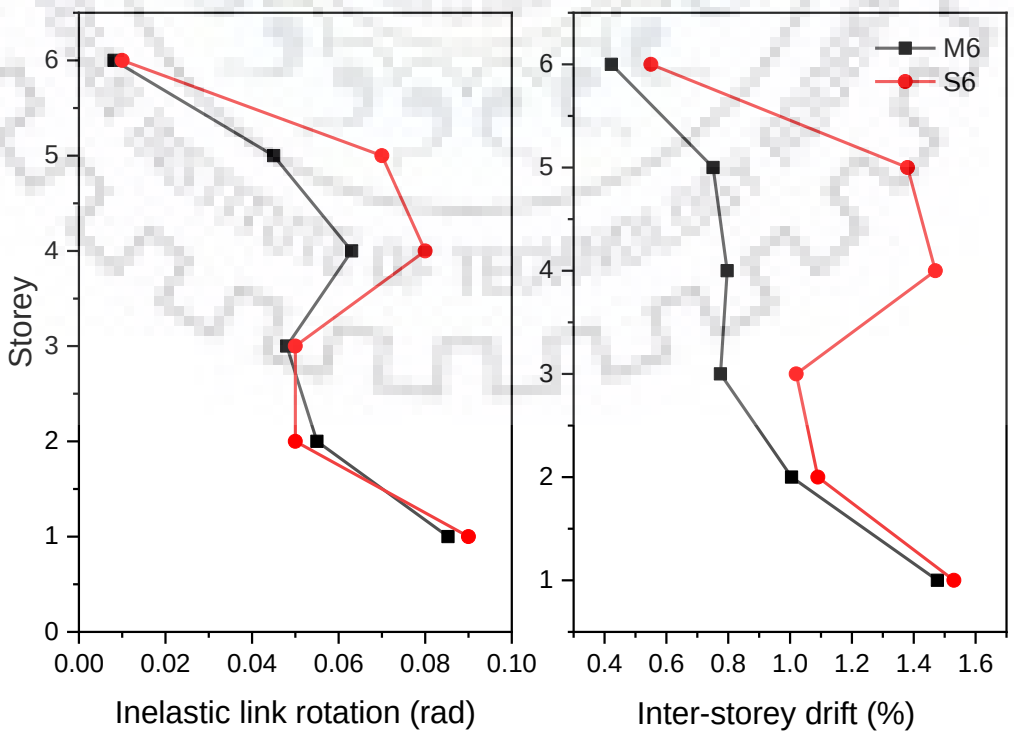

(a)

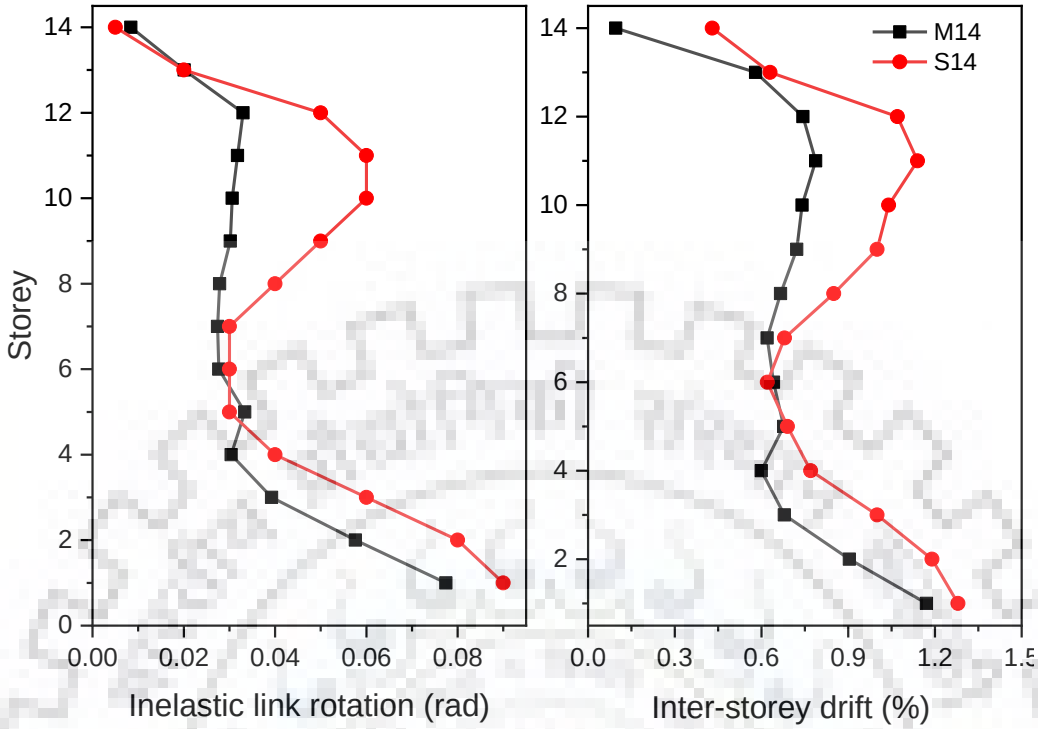


(b)

Fig 6.14 Inter-storey drift and inelastic link rotation envelopes for (a) 6 story and (b) 14 story archetypes

### 6.3.4 Non-linear Dynamic Analysis at MCE Level

For the analysis at MCE level, the ordinates of DBE level acceleration records used (refer Appendix B) were scaled up by a factor of 1.5 (Fig 6.15). The archetypes M6 and M14 analyzed for DBE level ground motions were evaluated at MCE level. The primary aim was to investigate the performance of the archetypes at MCE level and try to set acceptability criteria which have not been standardized for EBF systems. The connections were assumed to lose their integrity at inter-storey drift exceeding 5%. The links were assumed to collapse at link rotations of 0.15 radians. The results of the analysis are presented in following sections.

The links at all the storeys yielded. The top storey links however, did not exhibit any yielding for several acceleration records. The degree of yielding was extensive for lower storey links only. The beams adjacent to links also yielded at several floors for most of the records. The 1$^{st}$ and 3$^{rd}$ storey braces yielded in M6 for multiple records. Non-EBF beams also yielded especially at those floor levels at which the link yielding was very

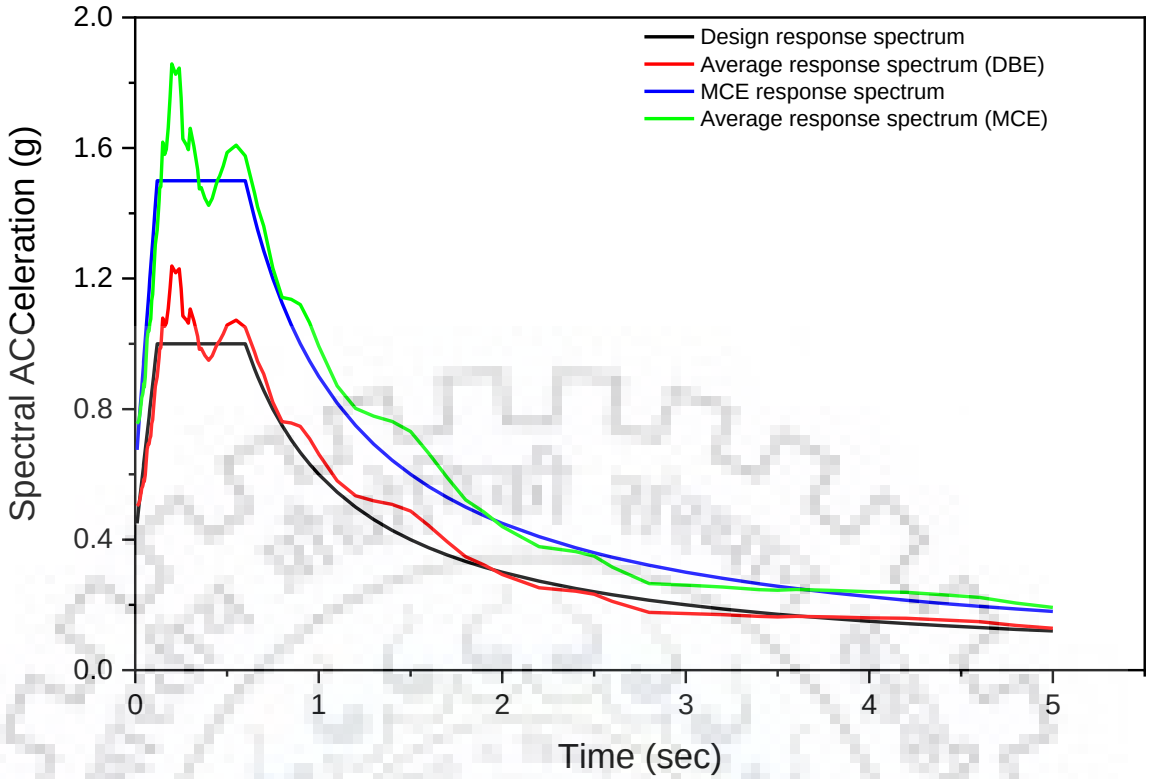


Fig 6.15 Design target and average response spectra at DBE and MCE levels

extensive. The 3rd storey non-EBF columns also yielded in M14 for few acceleration records.

The collapse of link at any particular floor level was followed by increased levels of yielding of the rest of members below this level. This could be explained by the drastic reduction in storey stiffness concentrating the deformations at that level potentially causing the collapse of frame members in addition to links. This was especially found to be dangerous if the yielding of columns occurred along with link yielding since it resulted in soft storey mechanism. The probability of yielding of columns at any storey level is maximum just before the collapse of links at or above the same level when the links develop full overstrength. Hence the collapse prevention of links could be a viable reference to avoid the global collapse of the structure and could be used as acceptability criterion for performance evaluation of EBF systems at MCE level.

The yielding of different members was characterized by an excellent hierarchy. The beams adjacent to the links yielded only once the links had yielded. Whenever braces or columns exhibited some yielding, they did so only after the links and beams adjacent to links had yielded.

The inter-storey drift was much smaller than 5% limit at which connections were assumed to lose their integrity (Fig 6.16). This limit was exceeded only in the lower storeys of M14

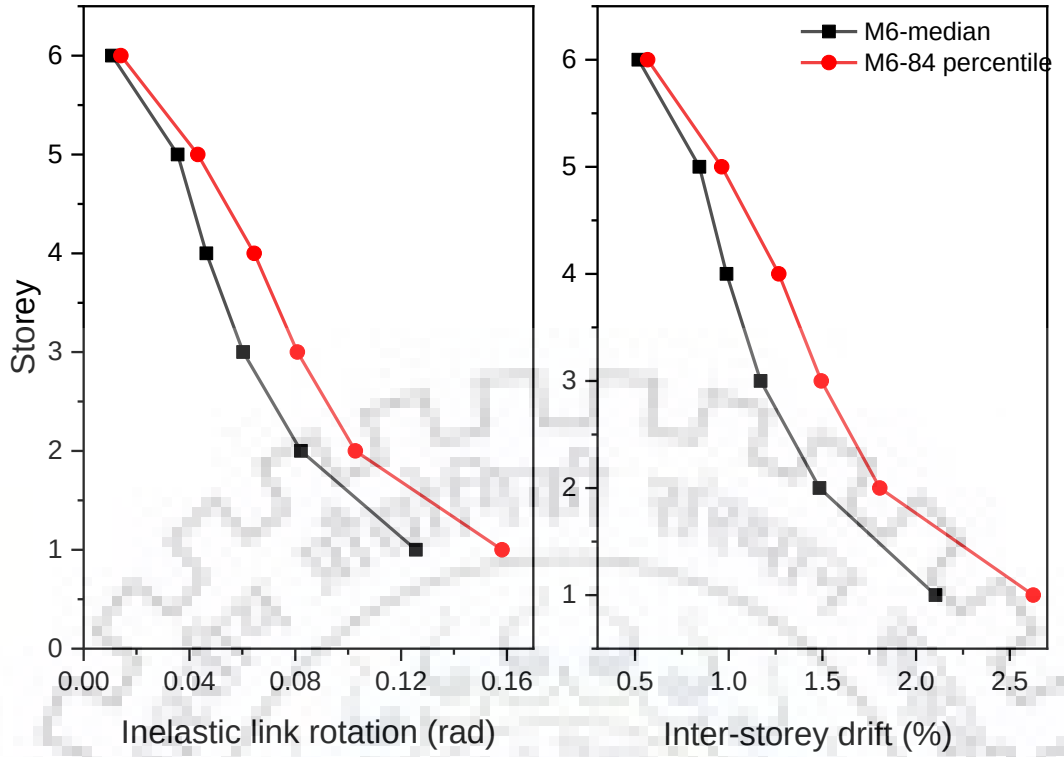


(a)

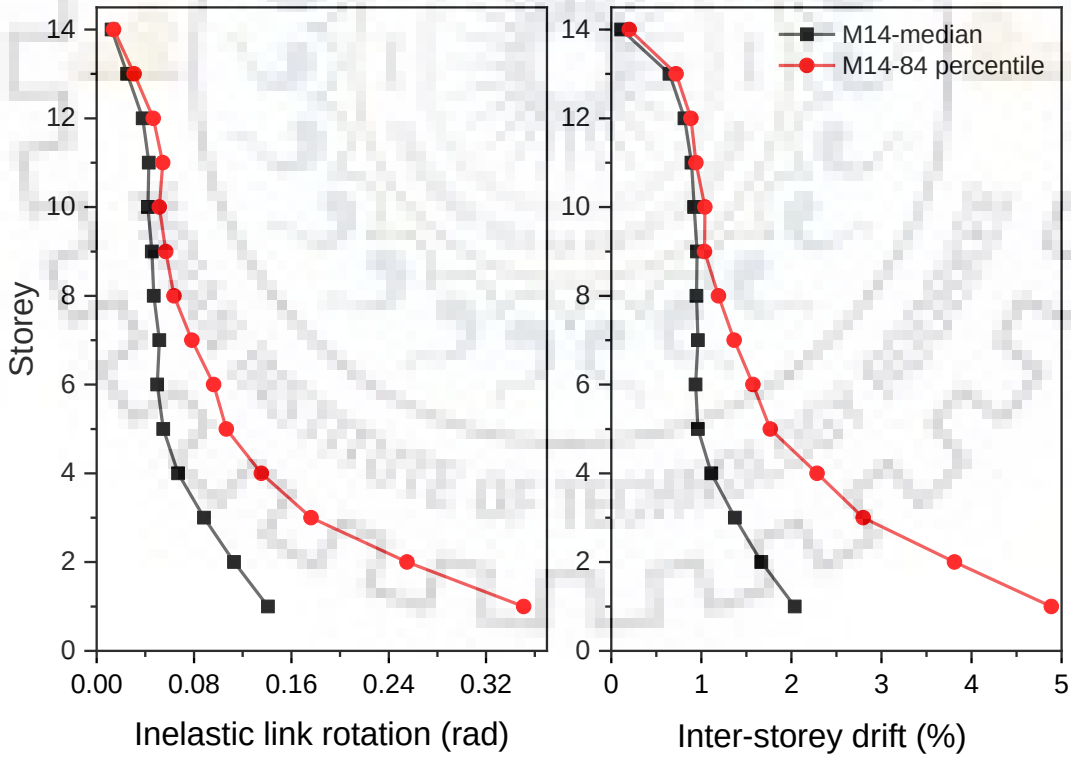


(b)

Fig 6.16 Inter-storey drift and inelastic link rotation envelopes for (a) 6 story and (b) 14 story archetypes

when subjected to Hector ground motion. The 84 percentile inelastic link rotation angle exceeded 0.15 rad for both models in the lower storeys.

# 7. PERFORMANCE BASED DESIGN OF EBFs

The eccentrically braced frames designed by current codes are expected to exhibit significant inelastic deformations during major seismic events. However, the design is based on elastic response of frames and the inelastic behavior is accounted for only implicitly. The design base shear is calculated based on elastic response and is reduced by Response Modification Factor, $R$, which is a function of structure ductility. Elastic and inelastic level deformations are correlated by the use of Displacement Amplification Factor, $C_d$. Various experimental studies have raised concerns over the use of single values for these modification factors for entire class of EBFs. The frames designed using such procedures exhibit deformations in an uncontrolled manner, often concentrating in few storey levels.

It is imperative to have a thorough knowledge of the yield mechanism of structure and non-linear force deformation relations in order to have a better prediction of global response during strong ground motions. This requires the selection of desirable yield mechanism and target strength and deformations and implementation of strength based hierarchy of the components in the design procedures very explicitly. This methodology considers structural inelasticity directly eliminating the need for any assessment after initial design and is referred to as Performance Based Plastic Design (PBPD).

The PBPD method uses yield mechanism and target level drift as key performance limit states. The design base shear is calculated by equating the work needed to push the structure up to the target drift monotonically to the energy required to push an equivalent elastic perfectly plastic single degree of freedom system to the same drift. The design lateral forces are distributed on the basis of disposition of story shears consistent with the inelastic dynamic response results. The frame members are designed and detailed using plastic design approach.

## 7.1 Design Procedure

This section presents the vertical distribution of design lateral forces, evaluation of design base shear and design of dissipative and non-dissipative members.

### 7.1.1 Desired Yield Mechanism

All the yielding is intended to be concentrated within the link sections only. The rest of the frame members are designed as non-dissipative members that behave elastically

regardless of the severity of seismic event. The rigid plastic collapse mechanism of the K-braced EBFs is shown in Fig 6.8.

### 7.1.2 Design Lateral Forces

The distribution of the lateral forces is based on the story shear observed in the non-linear dynamic analysis results (Chao et al. 2005). The forces are distributed as follows:

$$F_i = C'_{vi} V \tag{7.1}$$

where

$$C'_{vi} = \left(\beta_i - \beta_{i+1}\right)\left\{\frac{w_n h_n}{\sum_{j=1}^{n} w_j h_j}\right\}^{0.75T^{-0.2}} \qquad when\ i = n,\ \beta_{n+1} = 0 \tag{7.2}$$

$$\beta_i = \frac{V_i}{V_n} = \left\{\frac{\sum_{j=1}^{n} w_j h_j}{w_n h_n}\right\}^{0.75T^{-0.2}} \tag{7.3}$$

where, $\beta_i$ is the shear distribution factor at level $i$; $V_i$ and $V_n$ are story shears at level $i$ and roof level respectively, $W_j$ is the seismic weight at level $j$; $h_j$ is the height of level $j$ from base; $w_n$ is the weight of top storey, $h_n$ is the height of top level from base; $T$ is the fundamental time period of frame; $F_i$ is the design lateral force at level $i$; and $V$ is the design base shear.

The frames designed for this lateral load distribution reveal more uniform drifts along the height of structures compared to the code-specified force distributions. The distribution also takes higher modes of vibration into account.

### 7.1.3 Design Base Shear

The design base shear is calculated by equating the work needed to push the structure up to the target drift monotonically to the energy required to push an equivalent elastic perfectly plastic single degree of freedom system to the same drift as shown in Fig 7.1. The amount of work needed is taken as elastic input energy, $E$, multiplied by energy modification factor, $\gamma$.

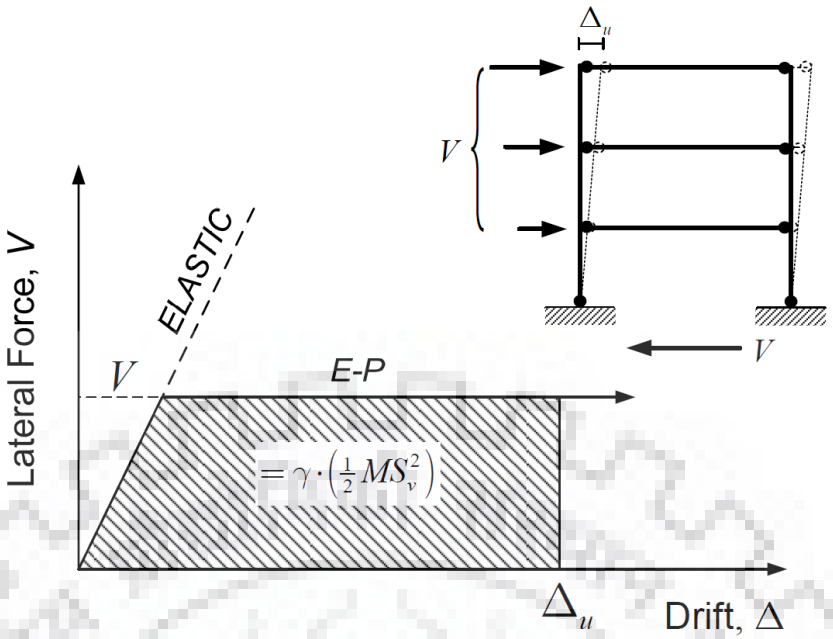


Fig 7.1 Equivalence of energy to evaluate design lateral force (adapted from Chao et al. 2005)

The energy equivalence is expressed as follows:

$$E_e + E_p = \gamma E = \gamma \frac{1}{2} M S_v^{\ 2} \tag{7.4}$$

where $E_e$ and $E_p$ are the elastic and plastic energy components required to push the building up to target drift respectively. $S_v$ is the design pseudo-spectral velocity and $M$ is the total mass of system. $\gamma$ is function of structural ductility factor, $\mu_s$, and ductility reduction factor, $R_\mu$, and is expressed as follows:

$$\gamma = \frac{2\mu_s - 1}{R_\mu^{\ 2}} \tag{7.5}$$

The elastic energy component is evaluated by converting the structure into an equivalent single degree of freedom system as follows:

$$E_e = \frac{1}{2} M \left\{ \frac{T}{2\pi} \times \frac{V}{W} \times G \right\}^2 \tag{7.6}$$

where $W$ is the total seismic weight of the building and $V$ is the desired base shear at yield.

The plastic energy component is evaluated by equating it to external work done by the design lateral forces in deforming the structure under a pre-selected yield mechanism as shown below:

$$E_p = \sum_{i=1}^{n} F_i h_i \theta_p \tag{7.7}$$

where $\theta_p$ is the global inelastic drift ratio of the frame.

The design base shear, $V$ is calculated using the following equation:

$$\frac{V}{W} = \frac{-\alpha + \sqrt{\alpha^2 + 4\gamma S_a{}^2}}{2} \tag{7.8}$$

where $\alpha$ is a dimension-less parameter. This parameter is a function of the structural stiffness, modal properties and design drift level and is calculated as follows:

$$\alpha = \left( \sum_{i=1}^{n} (\beta_i - \beta_{i+1}) h_i \right) \cdot \left\{ \frac{w_n h_n}{\sum_{j=1}^{n} w_j h_j} \right\}^{0.75T^{-0.2}} \cdot \left( \frac{\theta_p 8\pi^2}{T^2 g} \right) \tag{7.9}$$

The derivation of the design base shear is based on elastic perfectly plastic behavior of the structure. The drift control is implicit in the design PBPD procedure and need not be checked after the design. No iterations are required once the initial design is complete.

### 7.1.4 Design of Yielding Members

The distribution of lateral strength along the height of structure should be the same as distribution of design lateral forces to facilitate uniform yielding of links in EBF systems. The required strength of shear links at a level $i$, $\beta_i V_{pr}$, for K or D-braced EBFs is calculated is evaluated by equating the external work to internal work (Fig 7.2) as shown below:

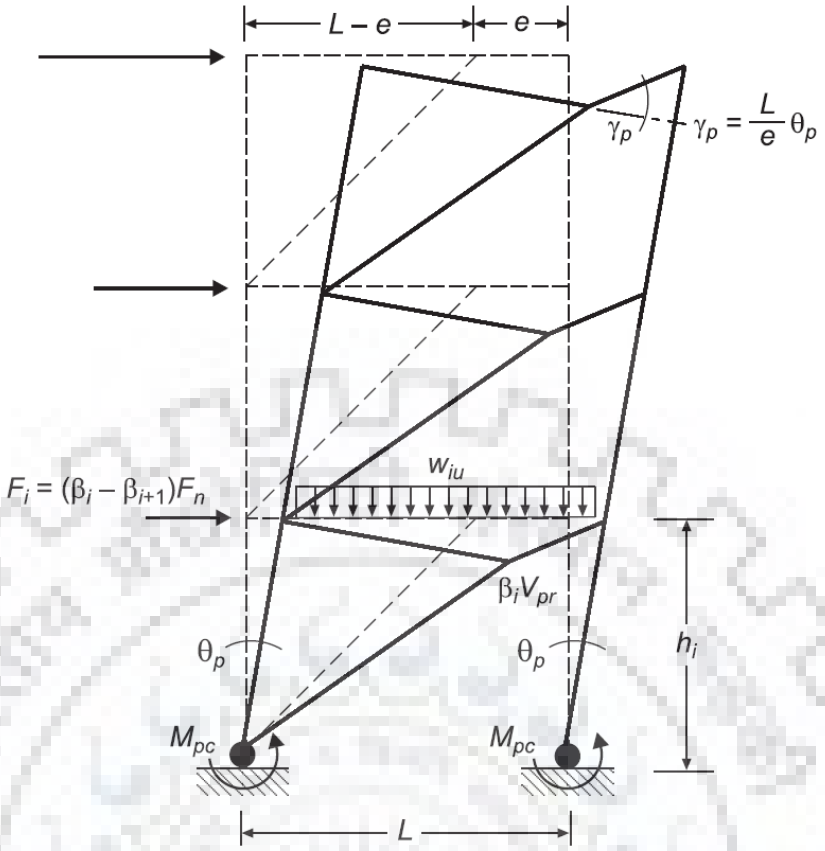


Fig 7.2 Yield mechanism for calculating the required shear strength of links (adapted form Chao et al. 2005)

$$\sum_{i=1}^{n} F_i h_i \theta_p + \frac{1}{2}\sum_{i=1}^{n} w_{iu} L\theta_p \left(L-e\right) = \sum_{i=1}^{n} \beta_i V_{pr} L\theta_p \tag{7.10}$$

$$\beta_i V_{pr} = \beta_i \frac{\sum_{i=1}^{n} F_i h_i + \frac{1}{2} L\left(L-e\right)\cdot \sum_{i=1}^{n} w_{iu}}{L\cdot \sum_{i=1}^{n} \beta_i} \tag{7.11}$$

where $V_{pr}$ is the required shear strength of roof level link. The equation is valid for columns pinned to base.

The design of non-dissipative members is done using the capacity design procedure.

## 7.2 Performance Based Design of 6 and 14 Storey EBFs

A set of two EBFs with 6 and 14 storeys were designed in accordance with Performance Based Plastic Design procedure mentioned in the preceding sections. The EBFs were similar to conventional EBFs designated as S6 and S14 designed in chapter 5 except for the difference in design procedure. These frames were modelled in SAP2000 in 2D. Similar modelling features were taken for conventional EBFs and those designed

conventionally to facilitate the comparison of analysis results between the two. The frames were analysed using non-linear static as well as dynamic analysis.

Performance of the frames was targeted based on two performance indices; desirable yield mechanism in which all the links exhibit uniform yielding and maximum inter-storey drift of 2% as recommended by Chao et al. [14]. However, target inter-storey drift of 2% could potentially increase the link rotation demands on the short links far exceeding their capacity limitation of 0.08 radians especially for mid and high-rise EBFs. Moreover, it was observed in the conventional design of S10 and S14 in chapter 5 that link rotation limitation on short links governs the design in lieu of inter-storey drift limitation. In this context, the frames were alternatively designed using PBPD procedure targeting performance criterion of maximum link rotation of 0.08 radians. The following equation that was established in chapter 5 was used to relate link rotation and inter-storey drift:

$$\gamma = \frac{L}{e}\left\{\frac{\delta}{h} - 0.0029\right\} \tag{7.12}$$

The 6 and 14 storey frames designed using performance criterion of 2% maximum inter-storey drift are designated as P6 and P14 respectively while those designed using the performance criterion of maximum link rotation of 0.08 radians are designated as Q6 and Q14 respectively.

### 7.2.1 Distribution of Design Lateral Loads

The distribution of lateral loads with reference to Equivalent Lateral Force distribution for the archetypes is shown in Fig. 7.3. Design base shear for the archetypes using PBPD procedure was comparatively higher than that calculated using the Equivalent Lateral Distribution procedure.

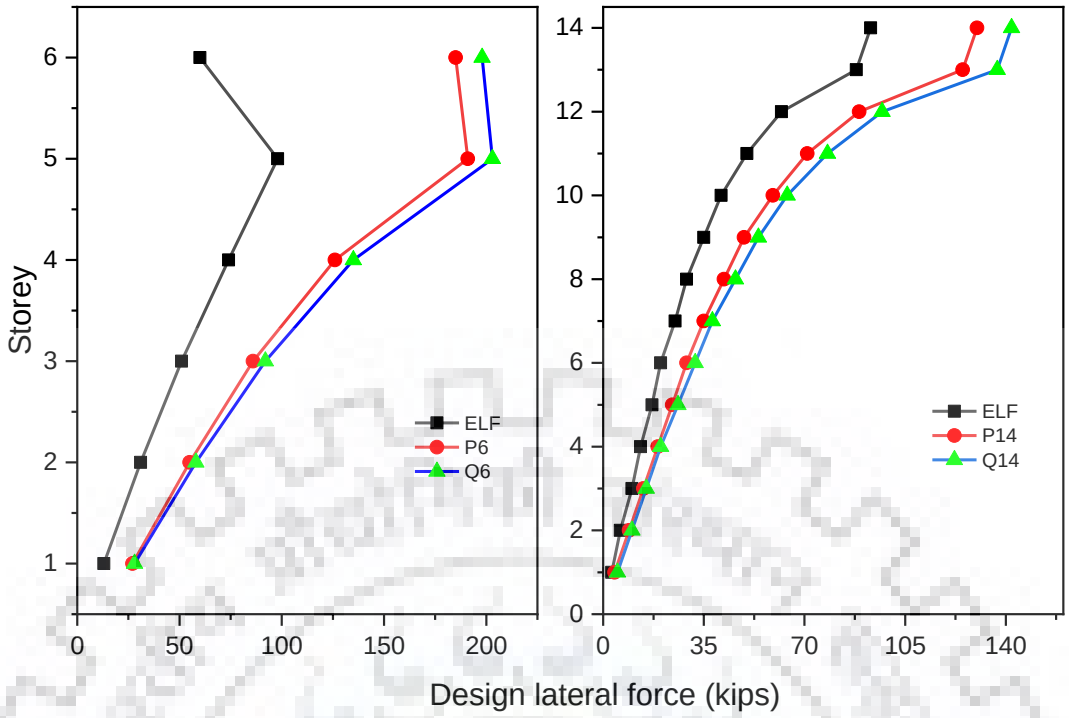


Fig 7.3 Comparison of design lateral forces between ELF and PBPD procedures

### 7.2.2 Distribution of Design Lateral Strength

The distribution of lateral strength along the height of structures was done vis-a-vis the distribution of design lateral forces to facilitate uniform yielding of links. The required strength of shear links at a level $i$, $\beta_i V_{pr}$, along with the link sections provided for archetypes are enlisted in Table 7.1 and Table 7.2. The non-dissipative frame members were designed using the capacity design approach.

Table 7-1 Distribution of design lateral strength and design link sections for P6 and Q6

| Level | P6 | | | Q6 | | |
|---|---|---|---|---|---|---|
| | $\beta_i V_{pr}$ (kips) | Design Link Section | $\phi V_P$ (kips) | $\beta_i V_{pr}$ (kips) | Design Link Section | $\phi V_P$ (kips) |
| 1 | 281 | W24×84 | 286 | 289 | W24×84 | 286 |
| 2 | 270 | W18×106 | 268 | 276 | W21×83 | 274 |
| 3 | 247 | W18×97 | 243 | 251 | W21×68 | 254 |
| 4 | 211 | W16×89 | 213 | 217 | W18×86 | 219 |
| 5 | 158 | W16×67 | 160 | 159 | W16×67 | 159 |
| 6 | 78 | W10×49 | 81 | 81 | W10×49 | 81 |

Table 7-2 Distribution of design lateral strength and design link sections for P14 and Q14

| Level | P14 | | | Q14 | | |
|---|---|---|---|---|---|---|
| | $\beta_i V_{pr}$ (kips) | Design Link Section | $\phi V_P$ (kips) | $\beta_i V_{pr}$ (kips) | Design Link Section | $\phi V_P$ (kips) |
| 1 | 292 | W24×84 | 285 | 319 | W24×103 | 333 |
| 2 | 290 | W24×84 | 285 | 317 | W24×103 | 333 |
| 3 | 287 | W24×84 | 285 | 313 | W24×103 | 333 |
| 4 | 281 | W24×84 | 285 | 307 | W18×119 | 300 |
| 5 | 273 | W21×83 | 273 | 298 | W18×119 | 300 |
| 6 | 263 | W18×106 | 267 | 288 | W24×84 | 285 |
| 7 | 251 | W24×68 | 251 | 274 | W21×83 | 274 |
| 8 | 236 | W16×100 | 236 | 258 | W24×68 | 252 |
| 9 | 219 | W18×86 | 218 | 239 | W21×73 | 241 |
| 10 | 198 | W18×76 | 193 | 217 | W18×86 | 218 |
| 11 | 174 | W14×82 | 173 | 190 | W18×76 | 192 |
| 12 | 144 | W14×68 | 141 | 157 | W16×67 | 159 |
| 13 | 107 | W15×58 | 106 | 117 | W12×65 | 115 |
| 14 | 54 | W10×49 | 65 | 59 | W10×49 | 81 |

## 7.3 Non-linear Analysis of Archetypes

The archetypes were analyzed using both non-linear static and dynamic analysis (non-linear static analysis was done for 6 story frames only). The analyses focused on yield pattern of frames, force and deformation demands and concentration of deformations at some storey levels or lack thereof. The performance of frames designed using PBPD procedure was compared against those that were designed conventionally.

### 7.3.1 Non-linear Static Analysis

The six story EBFs designed were subjected to a target displacement equal to 4% of the height of frames. Though this level of displacement is unlikely to be encountered during design earthquake, it was selected to determine the progressive yielding and collapse of the links and indicate the concentration or scatter of the inelastic action with respect to the height of archetypes. The pattern of yielding for archetypes is depicted with reference to the displacement level corresponding to first collapse of any component as shown in

Fig 7.4. Both Q6 exhibited more uniform link yielding compared to both S6 and Q6 in which the top storey link did not yield. However, the beam adjacent to link at second floor level yielded for both Q6.

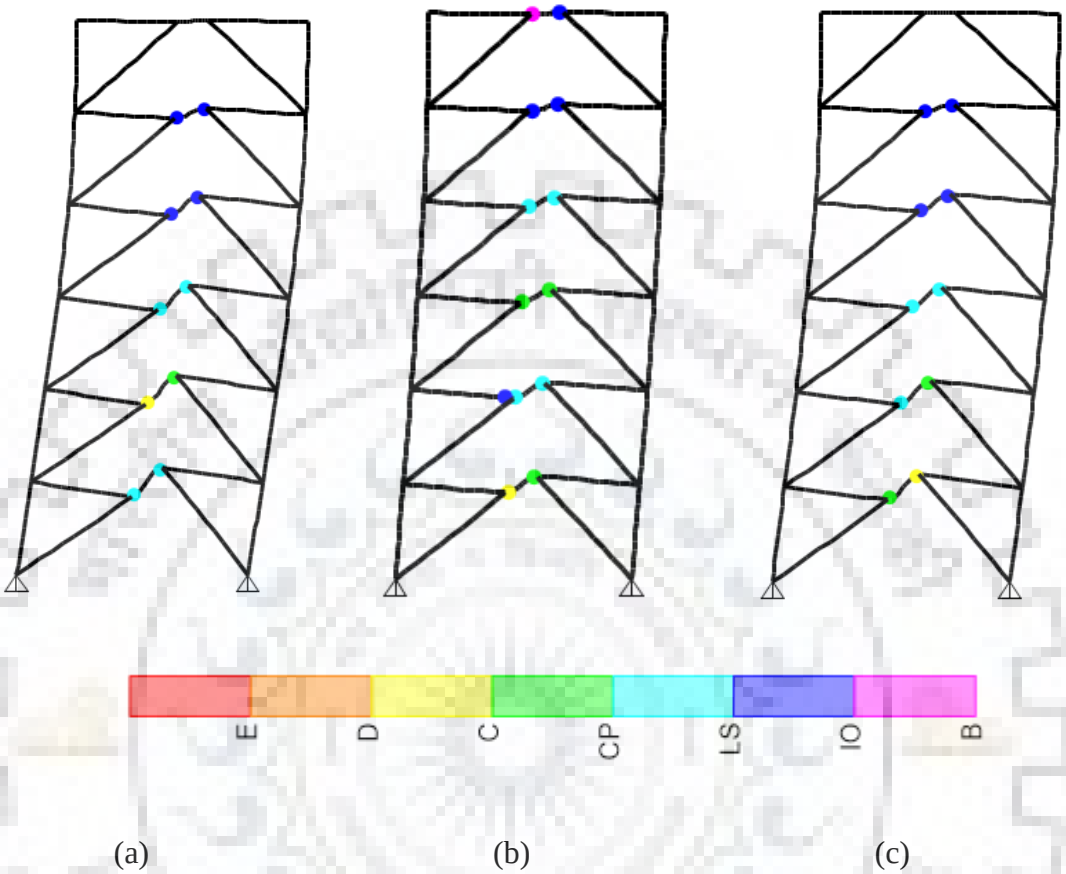


(a) (b) (c)

Fig 7.4 Yield mechanism corresponding to the first collapse of any component for (a) P6 (b) Q6 and (c) S6

The pushover curves are plotted in terms of base shear normalized to the design seismic horizontal shear, $\alpha$, versus the control node displacement expressed in percentage of

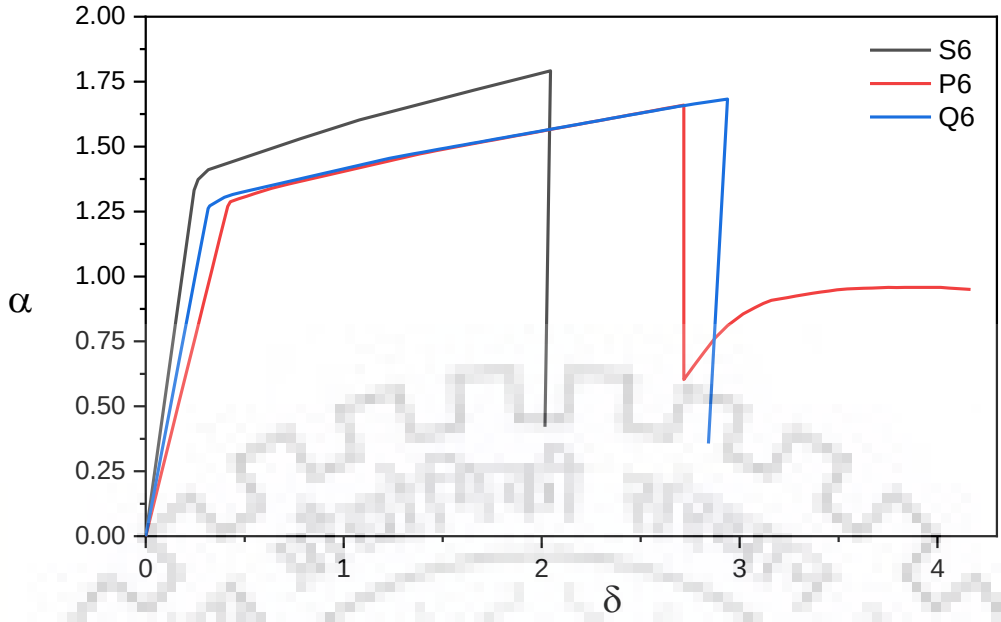


Fig 7.5 Normalized pushover curves for six story frames

height of the structures, $\delta$, as shown in Fig 7.5. All the models show almost equal ultimate lateral strength but the ductility of both the frames designed using PBPD procedure is higher compared to that of the conventionally designed frame.

The curves indicate very good strength as well as ductility characteristic of the archetypes. The sudden drop in lateral strength is characterized by the collapse of dissipative link elements starting from lower storeys and progressing towards upper ones with the monotonic increase in the control node displacement. Moreover, the non-linear static response of both the frames designed using PBPD procedure is similar.

### 7.3.2 Non-linear Dynamic Analysis

The same ground motion records used in the analysis of conventionally designed frames in chapter 5 were used for evaluating the dynamic response of performance design based frames. The results of analysis are presented in following sections.

#### 7.3.2.1 Yield Pattern

Both sets of performance design based archetypes; P6, Q6 and P14, Q14 exhibited more uniform link yielding compared to S6 and S14. The top storey links in performance design based archetypes, which seldom yielded in conventionally designed archetypes, yielded under most of the acceleration records. However, for former, the beams adjacent to the links yielded at various floor levels for multiple ground motion records but this did not

affect the overall frame behavior since the hinges did not rotate significantly on account of being spurious and hence did not partake in kinematics of collapse mechanism. The columns and braces did not yield in these archetypes for any of the acceleration records and a desirable yielding hierarchy was achieved since the beams adjacent to links yielded only if and when, the links had yielded.

#### 7.3.2.2 Drift and Inelastic Link Rotation Demands

One of the undesirable aspect of performance of the conventionally designed EBFs as analyzed was the exceedance of link rotation demands on some of the links beyond their capacities. This problem was eliminated in all of the archetypes designed using PBPD procedure. Both inter-storey drift and inelastic link rotation for the performance design based archetypes were within the code-specified limitations. The deformation demands were distributed much more uniformly in P6 and Q6 compared to S6 (Fig 7.6). Moreover, response of both P6 and Q6 frames was almost similar. However, the performance of Q14

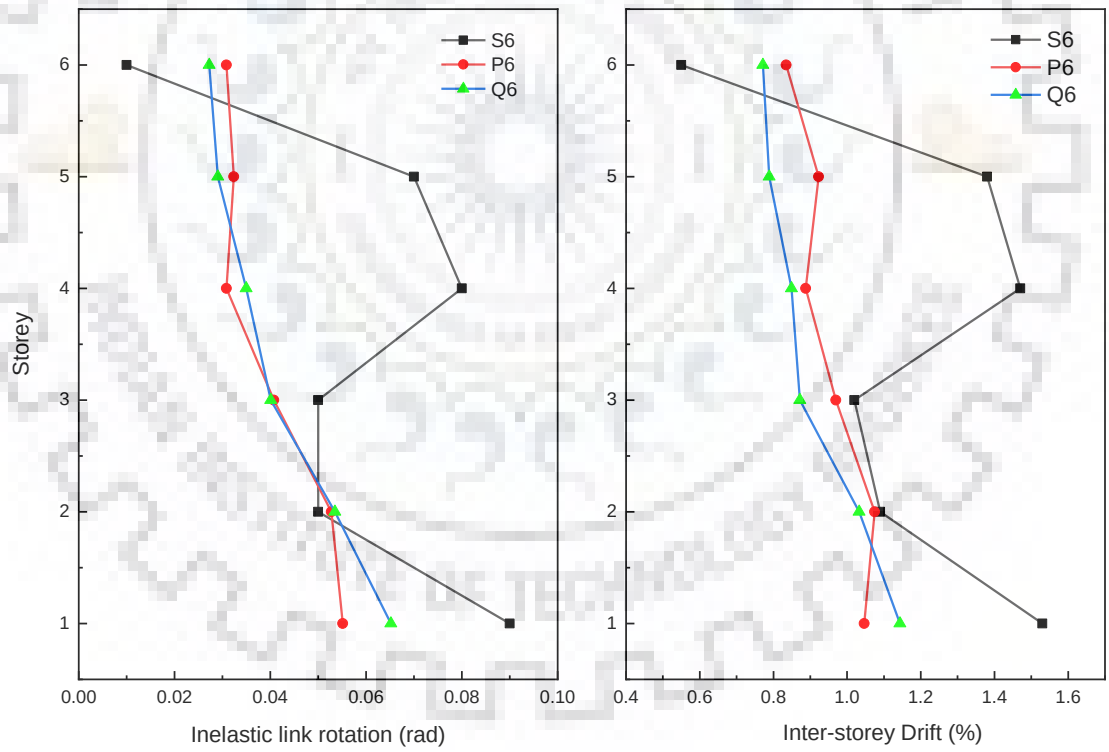


(a)

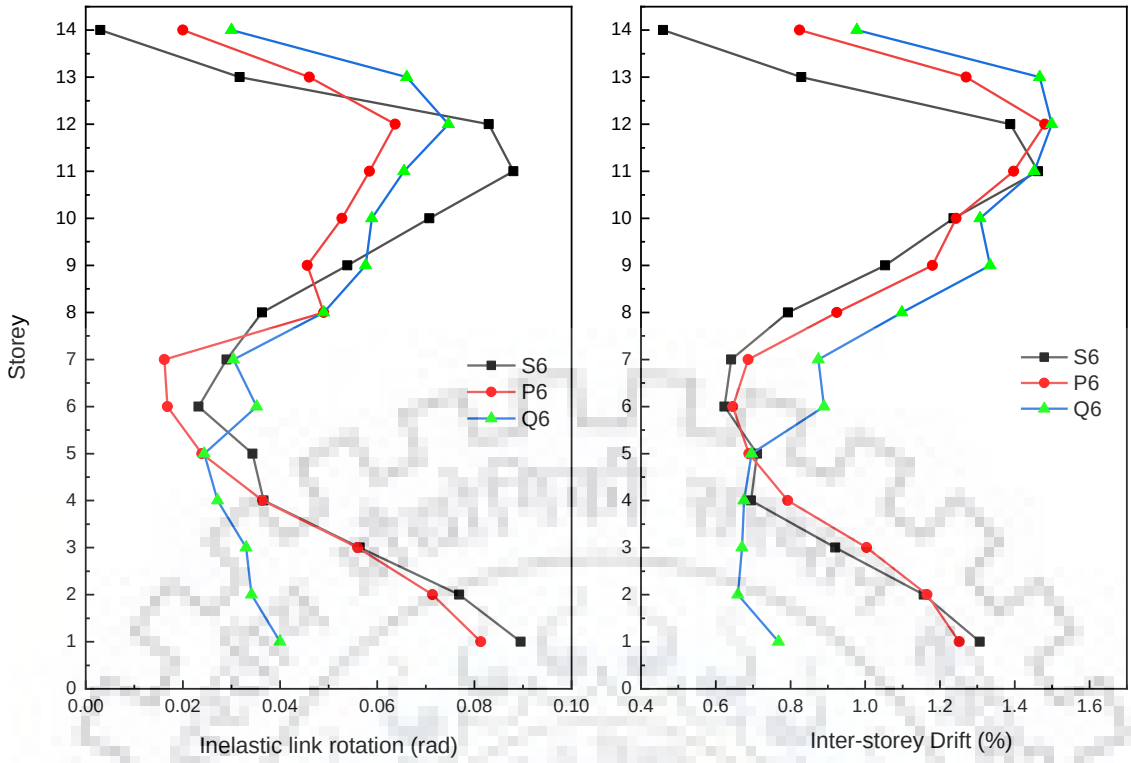


(b)

Fig 7.6 Comparison of peak inelastic link rotation and inter-storey drift envelopes for (a) 6 and (b) 14 storey archetypes

was better compared to both S14 and P14. The inelastic link rotation and inter-storey drift was more uniformly distributed in Q14 compared to P14. This is because the limitation on link rotation angle and not the inter-storey drift controlled the design for 14 storey archetypes when designed conventionally.

### 7.3.3 Energy Dissipation Results from PERFORM 3D

The two set of EBFs designed conventionally and using PBPD procedure were modelled in computer package PERFORM 3D [15] which is inherently a performance design based software. The modelling features used were the same as those that were implemented in modelling the archetypes in SAP2000.

The distribution of the energy dissipated by links over the height of archetypes is shown in Fig 7.7. For the six story frames, both P6 and Q6 show much more uniform distribution of energy dissipation by links compared to S6. But for the 14 story frames, this distribution is more uniform in Q14 compared to both S14 and Q14. This suggests that limiting maximum link rotation is a better performance index than the inter-storey drift, especially for high rise buildings.

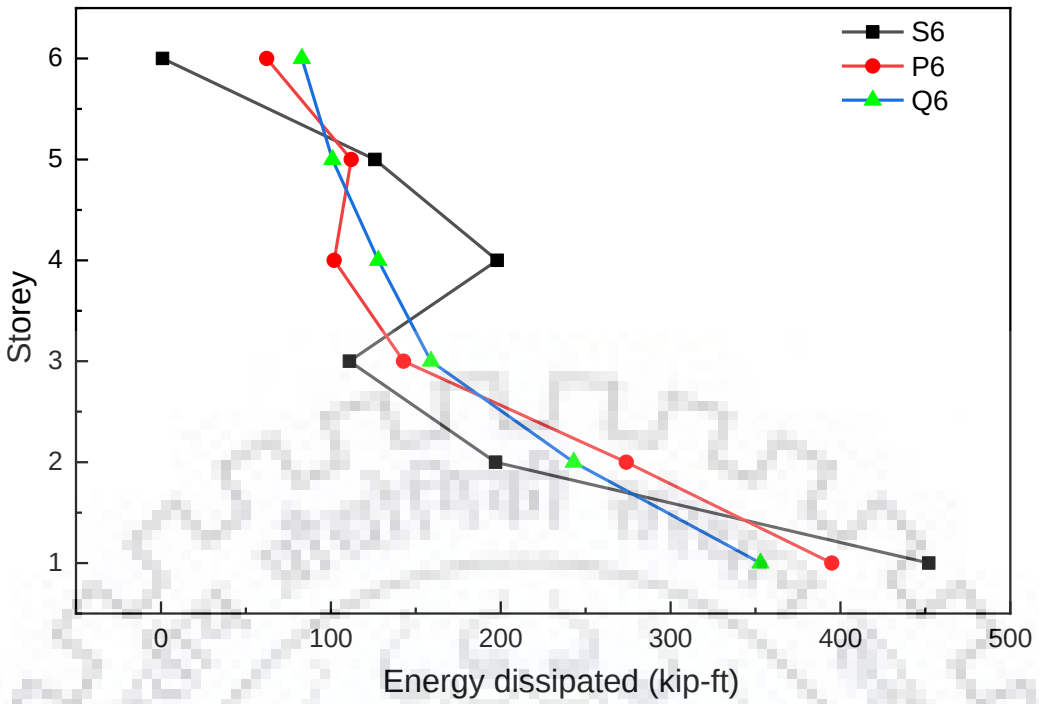


(a)

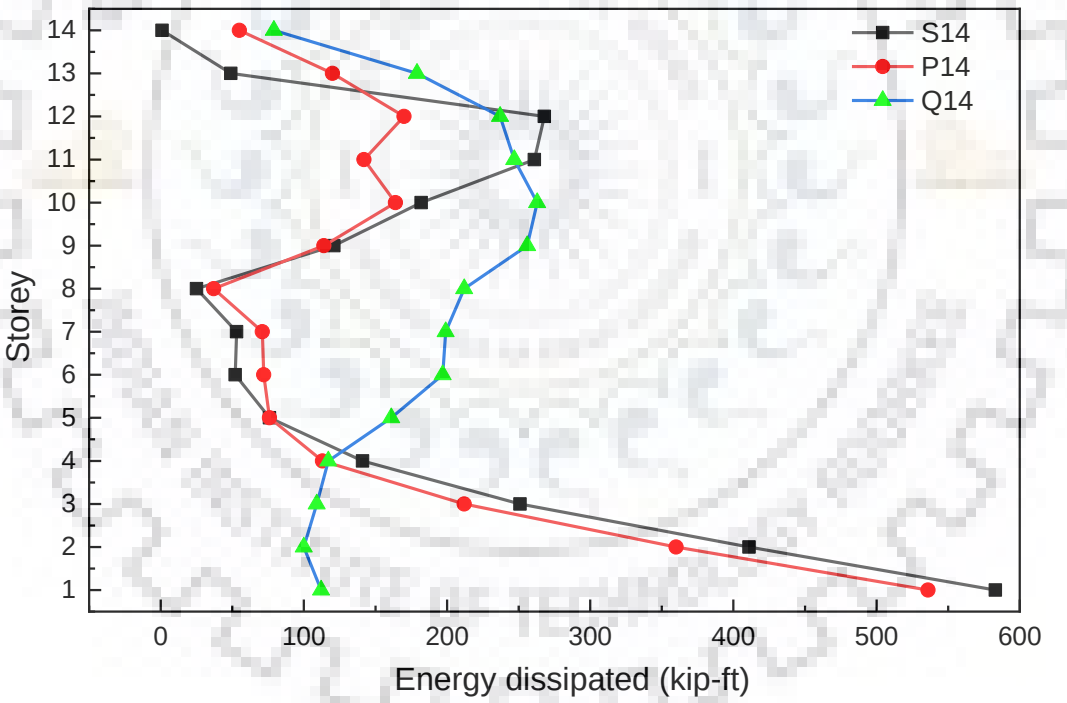


(b)

Fig 7.7 Distribution of energy dissipated by links along the height of archetypes

# 8. EBFS WITH REPLACEABLE SHEAR LINKS

In the conventional EBFs, the link is a part of the continuous beam section. The link is primarily designed for shear while the beam outside of link is designed to resist high axial force and moment induced due to fully yielded and strain hardened link. Balancing these two requirements is an iterative procedure often resulting in oversized link sections increasing the cost of entire structure in purview of the capacity design. The design of links is the critical factor in the context of optimizing the design of EBF systems. De-coupling the link segment from rest of the frame members by providing replaceable type links provides a viable solution to control the strength, ductility and stiffness of EBFs independently. The use of replaceable links facilitates a more direct design procedure and avoids the requirement of oversized links to suffice for the demands in the adjacent beams.

The repair of link sections in the conventional EBFs following a seismic event disrupts the operational use of building and is very time consuming and expensive. In contrast, the replaceable links ensure rapid removal and replacement of the links very conveniently. The structure can be re-centered to its un-deformed position by just disconnecting the distorted replaceable links. The use of replaceable links also facilitates the prefabrication

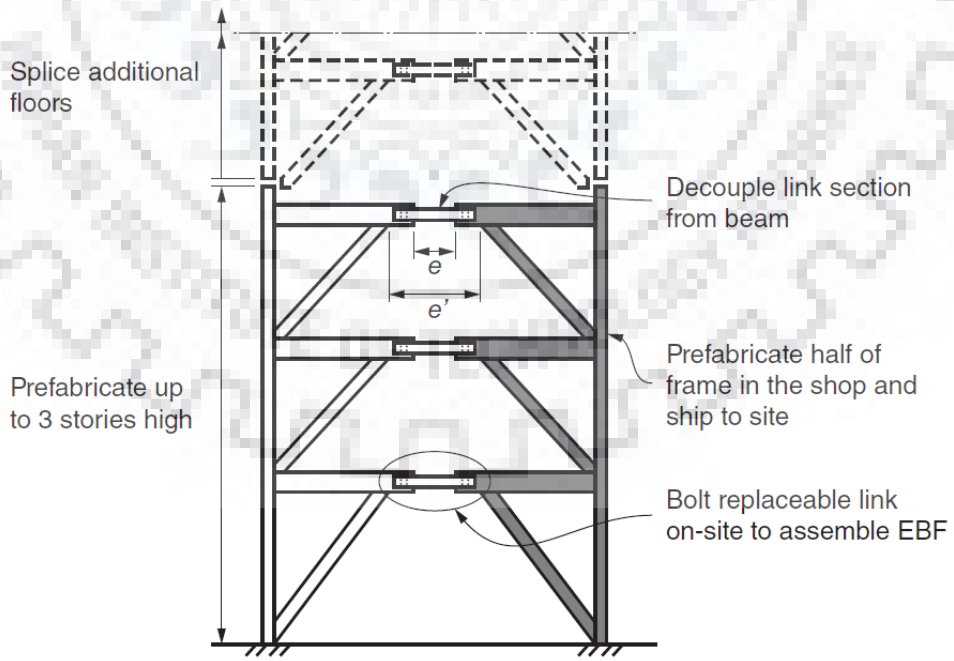


Fig 8.1 Replaceable links in EBF systems (adapted from Mansour et al. 2011)

of the multiple components within the workshop. Each half of the frame can be assembled in shop for multiple storeys and connected on-site with the replaceable link (Fig 8.1) thus reducing the erection time and cost. It also provides flexibility in using built-up link sections within webs and thick flanges so that the link sections provided do not supply exceedingly larger shear capacities than required hence optimizing the capacity design. Moreover, it is possible to concentrate the inelastic deformations within the replaceable link sections by providing lower grade steel (having higher deformation capacities) within the link sections only.

The use of replaceable links facilitates the decoupling of two link length parameters: the actual length of link, $e$, and center to center distance between the braces, $e'(e' > e)$. This enhances the architectural versatility of the EBF system allowing for larger openings while still achieving the desirable shear critical behavior.

## 8.1 Replaceable Link to Beam Connections

The connections are designed to resist the maximum forces generated by the fully yielded and strain hardened links. Generally, two types of replaceable shear links are provided as mentioned in the following sections.

### 8.1.1 Replaceable Link with End-plate Connection

The link section is a wide-flange beam section welded to end plates on either side. The link section – endplate assembly is connected through bolts to the floor beam. The end-plates are flush with floor beam to enable the placement of slab over it. The slab is not composite with the link section to enable easy replacement. The depth of the link could be smaller than that of the floor beam to provide space for bolts above and below the link (Fig 8.2 (a)) or both the floor beam and link segment could be of same depth (Fig 8.2 (b)). The floor beam to end-plate welded connection must not exhibit any rotation while limited yielding of the end-plates welded to link segments has not been found to be detrimental to its seismic performance [11]. The design of EBFs with replaceable links must incorporate the connection details like size of the bolts, thickness of end-plates and welding procedures since all these factors have significant effect on the stiffness of the connections.

Experimental results [11,12] have revealed that the replaceable links with extended end-plate connections perform the same as conventional links while those with the flush end-plates exhibit pinched hysteresis due to the deformation of connecting bolts.

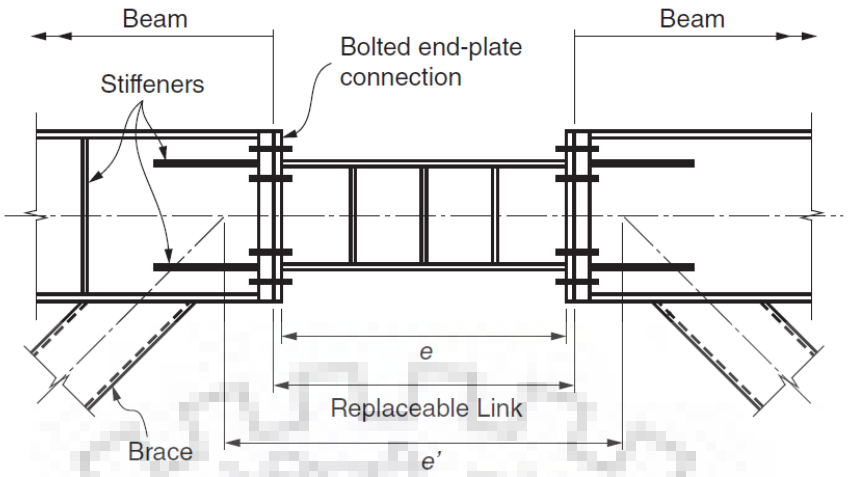


(a)

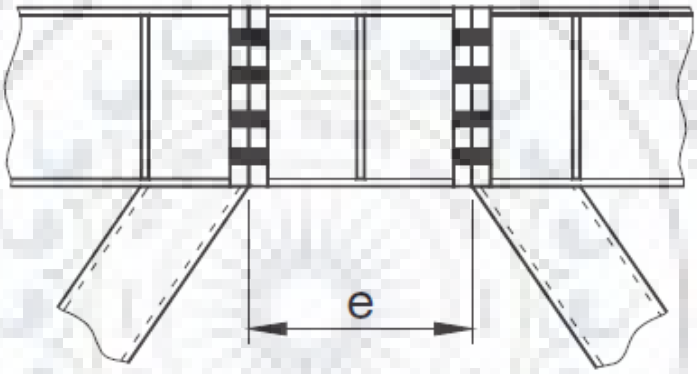


(b)

Fig 8.2 Replaceable link with bolted end-plate connection and (a) Floor beam deeper than the link section and (b) Floor beam and link section of the same depth (adapted from Dubina et al. 2008)

These type of replaceable links are expected to develop large residual plastic deformations often requiring hydraulic jacks or even flame cutting for removal and subsequent replacement.

### 8.1.2 Replaceable Link with Web-bolted Connection

The link segment is composed of two channel sections back to back connected to the floor beam through web-bolted connection (Fig 8.3). The two channel sections must be connected to ensure sufficient resistance to lateral torsional buckling. The depth of the channel sections is preferably smaller than that of the floor beam to avoid the interference with the deck slab. If required, cover plates are welded to the flanges to increase the link flexural resistance and induce shear dominant behavior. These type of replaceable links

are more convenient and quicker to handle. They are comparatively economical since the use of thick end-plates is eliminated. The bolts connecting the channel sections to the floor beams are easily accessible.

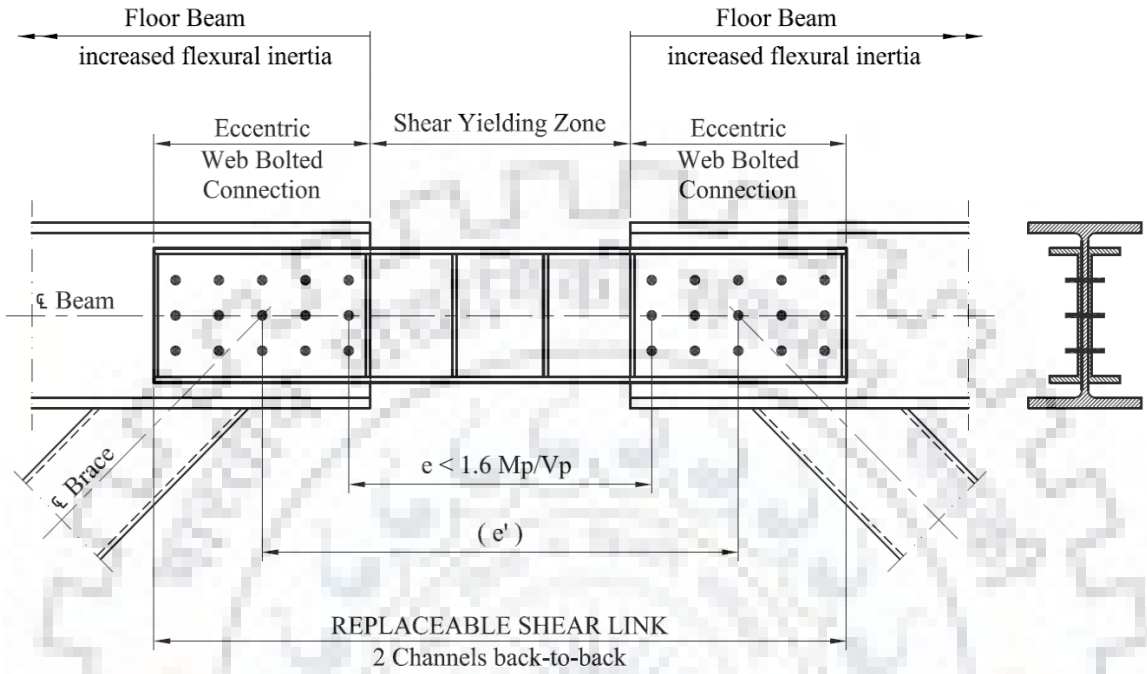


Fig 8.3 Replaceable link with web-bolted connection (adapted from Mansour et al. 2011)

Experimental studies [11,13] on replaceable links with web-bolted connections as well as the EBF sub-assemblages have revealed that these links exhibit pinched hysteresis due to the deformation of connections and the degree of pinching increases in direct correlation with these deformations.

## 8.2 Design and Analysis of EBFs with Replaceable Shear Links

A suite of 3, 6, 10 and 14 storey EBFs with replaceable shear links were designed and analyzed using non-linear static and dynamic analysis. The design was the same as used for conventional EBFs in accordance with AISC 341-16 with the exception that the link segment was de-coupled from the floor beam. In the conventional design, the beams adjacent to links are designed for forces generated by the fully yielded and strain hardened links and allowing for reduction of these forces by a factor of $\frac{1.1}{1.25}$ . The justification for the reduction in overstrength of links is that any overstrength that is available in the link sections will also be present in the beams outside links since both of these are a single continuous section. When using the replaceable type links, this overstrength in the beams

adjacent to links in not guaranteed. In this context, the beams were conservatively designed for unreduced forces.

Limited yielding in the beams adjacent to links is not detrimental to global frame behavior. However, it is desirable to concentrate all the yielding within the replaceable type links so that the repair of EBF systems following a damaging seismic event is facilitated by the removal and replacement of the distorted link segments only. This objective was aimed at by providing links of lower grade steel compared to the rest of members. All the links were composed of ASTM A36 steel with minimum yield strength of 36 ksi while the rest of members were ASTM A992 Grade 50 steel with minimum yield strength of 50 ksi.

### 8.2.1 Replaceable Link to Beam Connections

The replaceable links with end-plate bolted connections with both floor beams and link sections flush with the end-plates (Fig 8.2 (b)) were assumed in all the archetypes. These types of replaceable links undergo connection deformations like the rotation in end connections and slip in connections in addition to the shear distortion of link panel. The rotation angle of the conventional links is computed as the ratio of relative vertical link end displacement, $D_T$, to link length, $e$, as shown in Fig 8.4.

$$\gamma = \frac{D_T}{e} \tag{8.1}$$

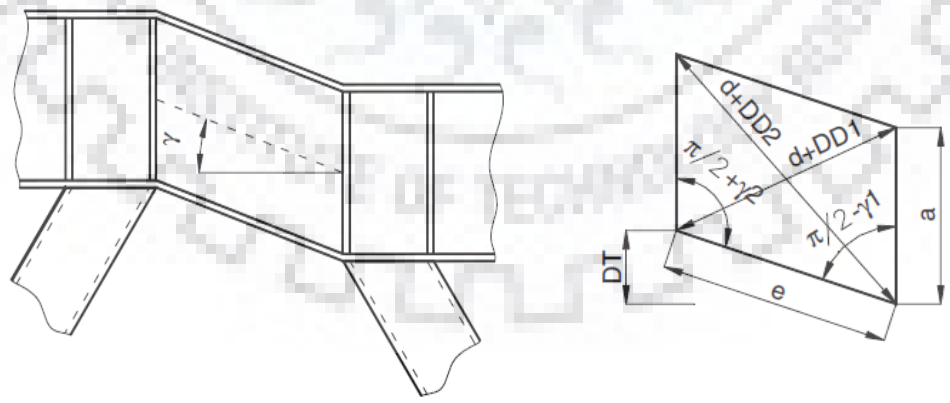


Fig 8.4 Deformation of conventional link (adapted from Dubina et al. 2008)

The total deformation of the replaceable links, $\gamma_T$, is given by the summation of shear distortion of web panel, $\gamma$, rotation of the end –plate connections, $\theta_M$ ,and rotation due to the slip of the connections, $\gamma_{AL}$, as expressed below:

$$\gamma_T = \gamma + \theta_M + \gamma_{AL} \tag{8.2}$$

$$\theta_M = \theta_S + \theta_J \tag{8.3}$$

$$\gamma_{AL} = \frac{D_{ALS} + D_{ALJ}}{e} \tag{8.4}$$

where $\theta_S$ and $\theta_J$ are end-plate rotations at the two ends of link and $D_{ALS}$ and $D_{ALJ}$ represent the vertical slip in the connection at either ends as shown in Fig 8.5.

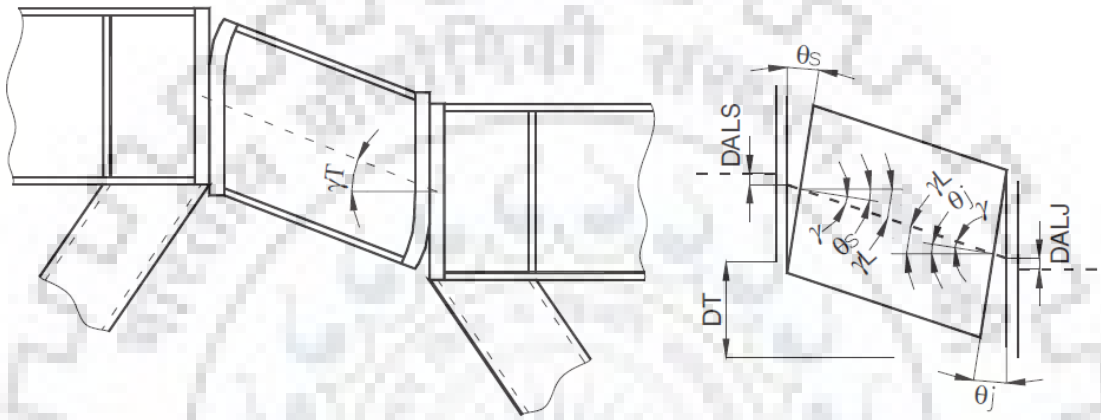


Fig 8.5 Deformation of replaceable link bolted to end-plates (adapted from Dubina et al. 2008)

The slip in connection and the semi-rigid nature of bolted end-plate connection reduces the stiffness of replaceable link. The flexibility of this connection needs to be explicitly modelled in the global analysis of EBF systems. Alternatively, this can be done by considering the equivalent link stiffness in which reductions are made to include the slip in the connection and end rotation effects. The latter procedure has been used in design and analysis of the archetypes. The replaceable links were assumed to have an equivalent stiffness of one fourth the theoretical stiffness of the continuous links based on the experiments conducted by Dubina et al (2008). It was further assumed that only the stiffness of the link section is affected by the flexibility of beam to link connections.

### 8.2.2 Modelling and Design of Archetypes

The 3, 6, 10 and 14 storey EBFs with bolted replaceable type links are designated as R3, R6, R10 and R14 respectively. These archetypes are geometrically similar to the analogous conventional EBFs S3, S6, S10 and S14. Both these set of archetypes were designed for the same site conditions, assembly weights, load combinations and using same design procedures. The design aspects unique to the replaceable type EBFs (like the

design of beams adjacent to links) were incorporated into the design. The modelling assumptions were also same between the two set of archetypes except for the use of equivalent link stiffness concept in replaceable link type EBFs.

The design frame sections of the replaceable link type archetypes are shown in Appendix C. The link sections in these archetypes were comparatively heavier than conventional EBFs (with reference to "S" designated models designed in chapter 6) on account of being lower grade steel composed sections. Since the semi-rigid nature of bolted end-plate connections between the floor beams and replaceable links decreased the overall stiffness of the archetypes and increased the deformations, heavier column and brace sections were required (especially in R10 and R14) to compensate for this loss of stiffness and limit the deformations within the codified values. It is important to note that although the stiffness of the replaceable links was only one fourth the shear stiffness of continuous links, global stiffness of the frames was reduced by only about 10%. This revealed that the axial stiffness of beams, columns and braces contributes significantly to the overall stiffness of EBF systems.

The fundamental time periods of the archetypes were calculated to be as follows:

| Model ID | R3 | R6 | R10 | R14 |
|---|---|---|---|---|
| Fundamental Time Period (sec) | 0.73 | 1.36 | 1.92 | 2.33 |

The comparison of frame weights of the conventional and replaceable link type EBFs is shown in Table 8.1. The replaceable link type EBFs are comparably heavier than conventional EBFs and the difference is significant for mid and high-rise archetypes in

Table 8-1 Comparison of frame weights for the conventional and replaceable link type EBFs

| No of storeys | Weight of frames (kips) | | $\frac{W_2}{W_1}$ |
|---|---|---|---|
| | Conventional EBFs, $W_1$ | Replaceable link type EBFs, $W_2$ | |
| 3 | 14.33 | 15.37 | 1.07 |
| 6 | 36.88 | 40.36 | 1.09 |
| 10 | 102.02 | 130.21 | 1.28 |
| 14 | 205.69 | 283.81 | 1.38 |

which limitation on the deformation demands controlled the design. Larger frame sections were needed to limit the deformations in these archetypes in order to compensate for the

loss of stiffness due to flexibility of the bolted end-plate connection of links to floor beams.

The archetypes were analyzed for non-linear static and dynamic responses. The procedure for analysis was the same as used for conventional EBFs. Same acceleration records were used for non-linear dynamic analysis.

### 8.2.3 Results of Non-linear Static Analysis

#### 8.2.3.1 Yield Pattern

The primary aim of non-linear static analysis was to predict the pattern of yielding. The pattern of yielding for the archetypes is depicted with reference to displacement level corresponding to the first collapse of any component as shown in Fig 8.6. The ground storey links were the first components to collapse except for S3 model in which case no component underwent collapse. The top storey links did not yield. Moreover, the links exhibited different levels of yielding along the height of archetypes indicated by color-coded designations, extensive yielding being mostly concentrated in the lower levels. The non-dissipative zones were not involved in yielding.

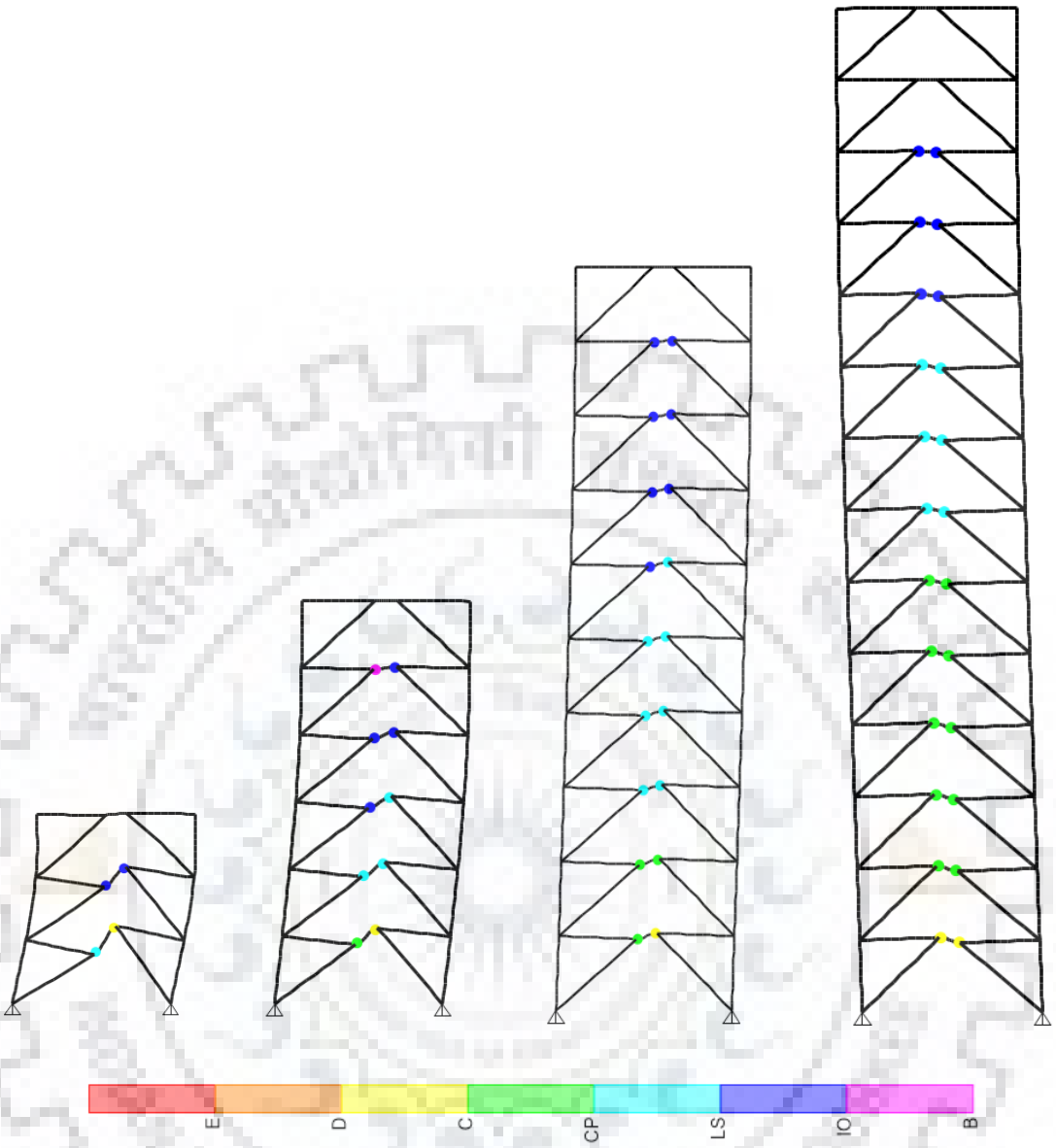


Fig 8.6 Yield pattern exhibited by the archetypes corresponding to first collapse of any component

### 8.2.3.2 Pushover Curves

The pushover curves are plotted in terms of base shear normalized to the design seismic horizontal shear, $\alpha$, versus the control node displacement expressed in percentage of height of the structures, $\delta$, as shown in Fig 8.7. Pushover curves of the conventional EBF archetypes (analyzed in previous chapter) are also plotted for reference. The comparison reveals the similarity in global lateral strength and ductility between the two set of EBFs. The sudden drop in lateral strength is characterized by the collapse of dissipative link elements starting from lower storeys and progressing towards upper ones with the monotonic increase in control node displacement. The base shear corresponding to the

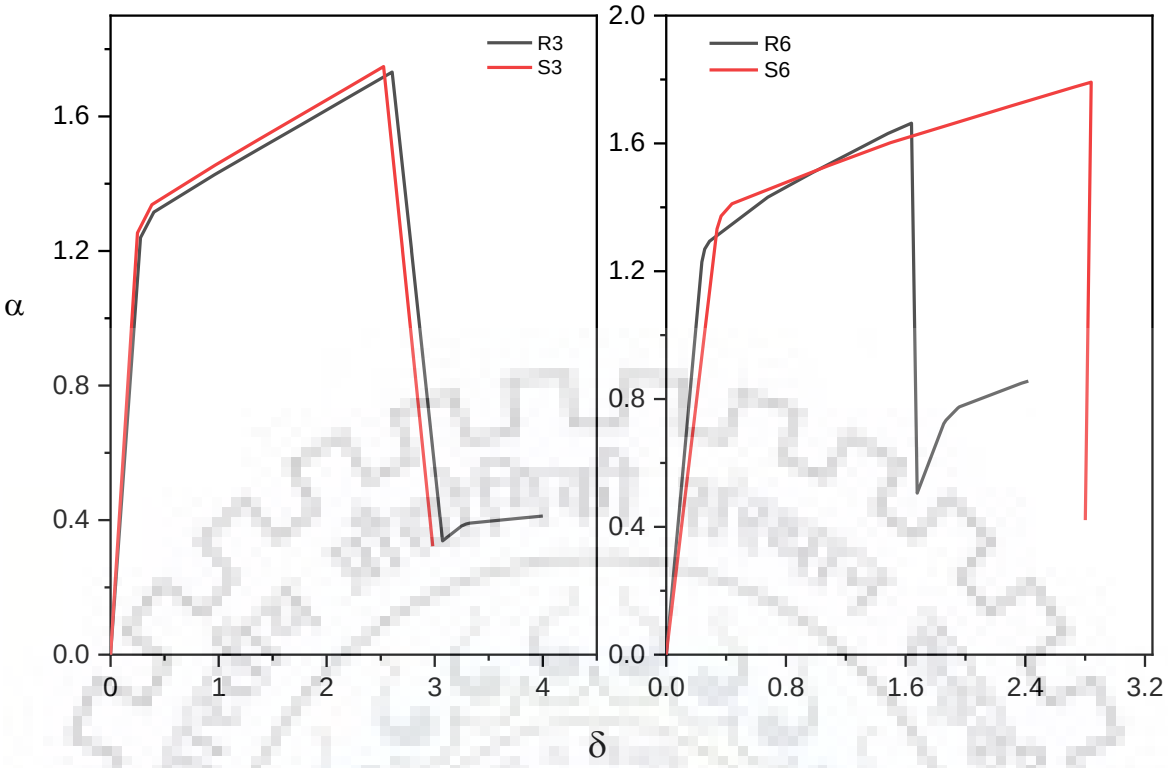


(a)

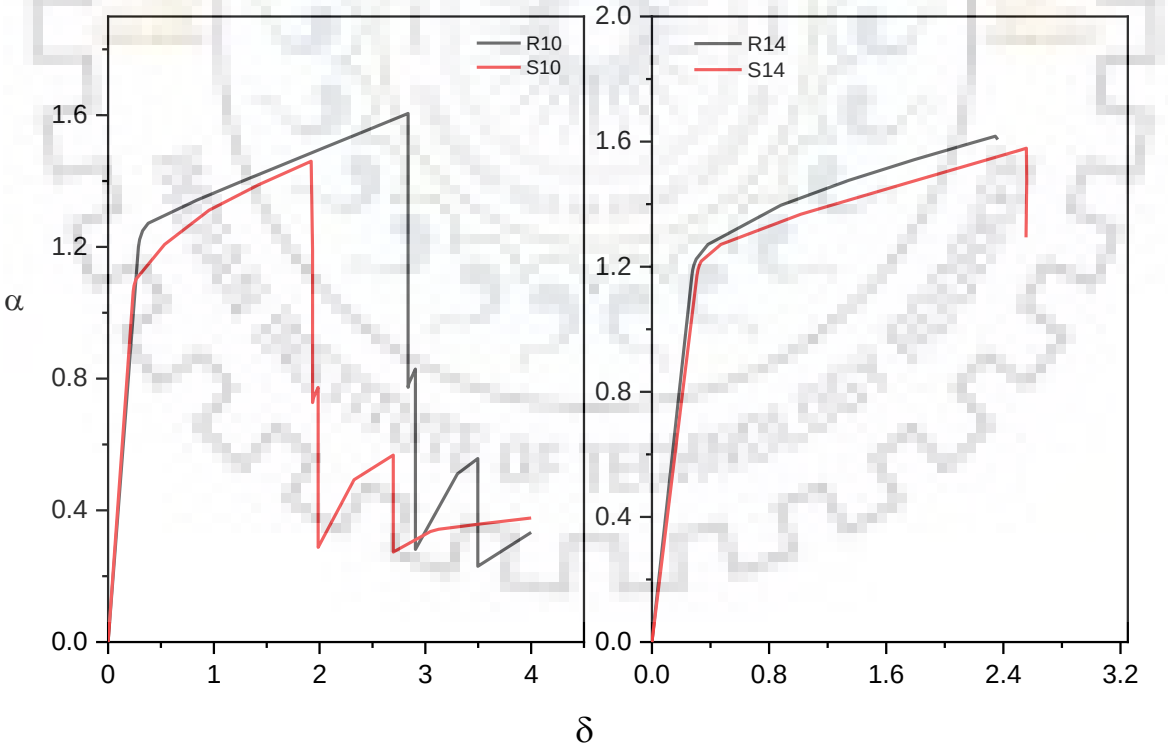


(b)

Fig 8.7 Comparison of pushover curves of replaceable link type EBFs with conventional EBFs for (a) 3 and 6 story and (b) 10 and 14 storey archetypes

first yield of link is almost same for the two systems implying their similar lateral design strengths.

### 8.2.4 Results of Non-linear Dynamic Analysis

The archetypes were analyzed for both global and component level responses. The progression and scatter of yielding and drift and link rotation angle demands were evaluated. Correlations between the various parameters were established. Comparison of the results obtained for replaceable type EBFs and conventional EBFs was done and the differences between the two are highlighted.

#### 8.2.4.1 Yield Pattern

All the archetypes were characterized by scattered pattern of yielding. Links at all the floors yielded for all acceleration records except for the top storey links in which case yielding occurred for only some of the records. However, the degree of yielding was not uniform over the height of structures, extensive yielding being mostly concentrated in lower levels as predicted by non-linear static analysis also. The links performed satisfactorily except for the first storey link in R14 which collapsed under Hector ground motion record although this did not alter the overall behaviour by causing soft-storey mechanism formation. The same link had also collapsed in S14 for the same ground motion record. The frame members in addition to link elements did not yield at any story level for any acceleration record. The yield pattern of replaceable type EBFs was found to be almost similar to that of conventional EBFs.

#### 8.2.4.2 Shear Demand in the Replaceable Links

The median of maximum shear forces, $V_{\max}$, induced by the ground motions in links normalized to their corresponding expected shear capacity, $R_y V_p$, were plotted (Fig 8.8). The maximum shear induced was found to be under-predicted for most links. However, the 84 percentile results exceeded 1.25 at few floor levels, mostly lower storeys and lower segment of the top storeys, while the median results were less than this value for all the archetypes.

The scatter in normalized maximum shear ratios at various floor levels of the replaceable type EBFs is smaller compared to that of the conventional EBFs. This is because the capacity to demand ratio of the links in replaceable type archetypes were comparatively smaller than those in the conventional EBFs as shown in Table 8.2. The use of links with

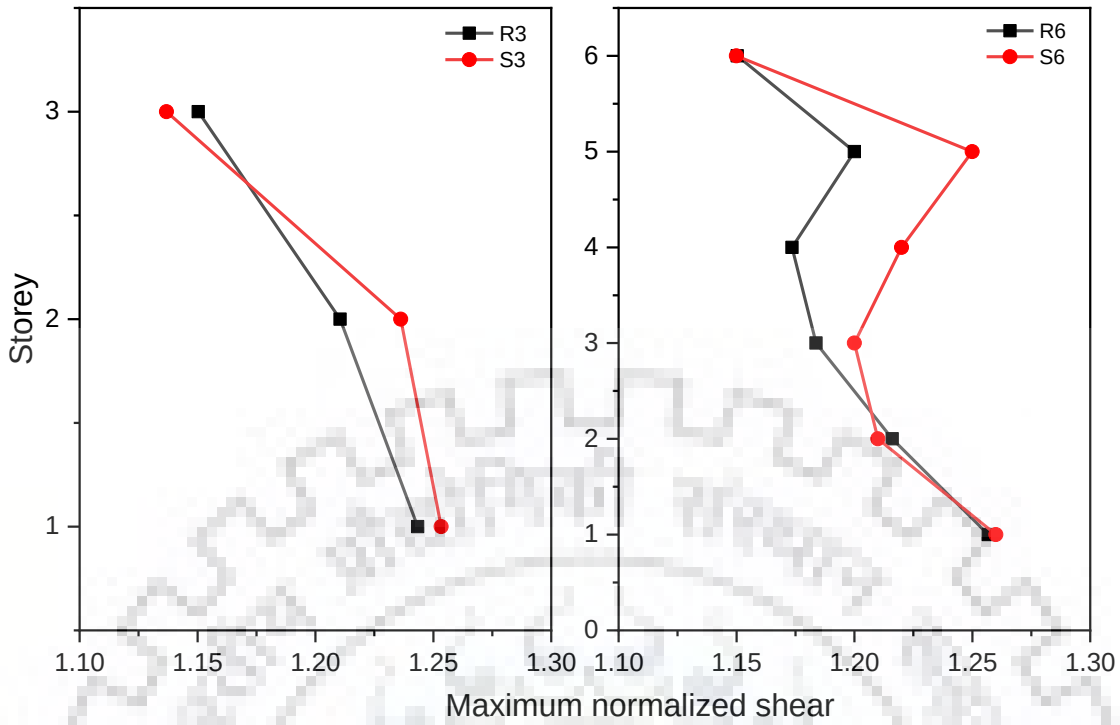


(a)

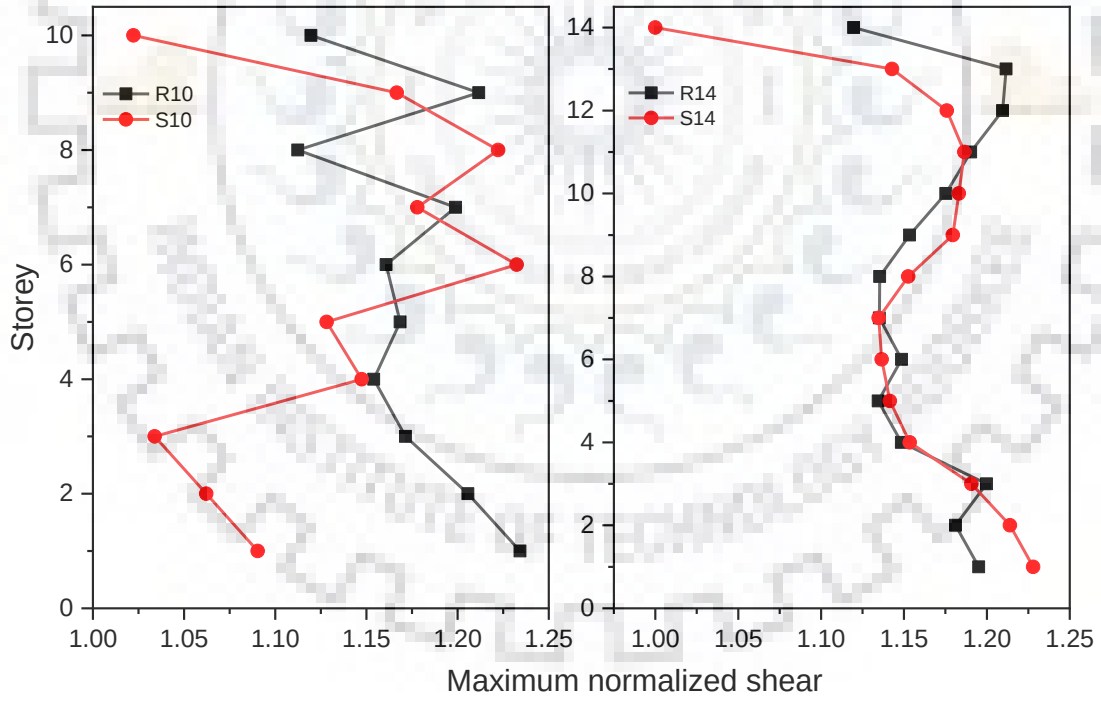


(b)

Fig 8.8 Comparison of maximum normalized shear envelopes in replaceable type and conventional links for (a) 3 and 6 storey and (b) 10 and 14 storey archetypes

smaller shear capacities while satisfying the section compactness requirements and still exhibiting shear behavior $(\rho < 1.6)$ was facilitated by the use of lower grade steel in the link sections.

Table 8-2 Comparison of the shear capacity to demand ratio of replaceable type and conventional links

| Storey | Capacity to Demand ratio of links | | | | | | | |
|---|---|---|---|---|---|---|---|---|
| | R3 | S3 | R6 | S6 | R10 | S10 | R14 | S14 |
| 1 | 1.15 | 1.59 | 1.11 | 1.18 | 1.11 | 1.15 | 1.10 | 1.10 |
| 2 | 1.21 | 1.64 | 1.15 | 1.18 | 1.13 | 1.15 | 1.10 | 1.10 |
| 3 | 1.92 | 3.66 | 1.15 | 1.25 | 1.15 | 1.15 | 1.10 | 1.10 |
| 4 | | | 1.27 | 1.19 | 1.17 | 1.14 | 1.11 | 1.12 |
| 5 | | | 1.47 | 1.48 | 1.08 | 1.14 | 1.14 | 1.10 |
| 6 | | | 2.60 | 3.61 | 1.14 | 1.17 | 1.12 | 1.14 |
| 7 | | | | | 1.10 | 1.15 | 1.13 | 1.12 |
| 8 | | | | | 1.13 | 1.26 | 1.14 | 1.10 |
| 9 | | | | | 1.23 | 2.34 | 1.17 | 1.10 |
| 10 | | | | | 3.26 | 4.21 | 1.15 | 1.11 |
| 11 | | | | | | | 1.19 | 1.15 |
| 12 | | | | | | | 1.14 | 1.19 |
| 13 | | | | | | | 1.25 | 1.75 |
| 14 | | | | | | | 3.26 | 4.54 |

#### 8.2.4.3 Drift and Inelastic Link Rotation Demands

The inter-storey drift and inelastic link rotation demands at various floor levels were plotted and compared against the deformation demands on the conventional archetypes (Fig 8.9). The deformation demands for the replaceable link type and conventional EBFs were more or less same, the difference being only marginal. IDR did not exceed the code limitation of 2%. However, the inelastic link rotation demand limitation of 0.08 radians was exceeded in the lowermost storeys of R6 and R10 models. The 84 percentile rotations exceeded this limit significantly (even by multi-folds in the lower storeys) at some floor levels implying sensitivity to a particular acceleration history in lieu of link shear. Maximum deformation demands in R3 and R6 models were restricted to lower storeys

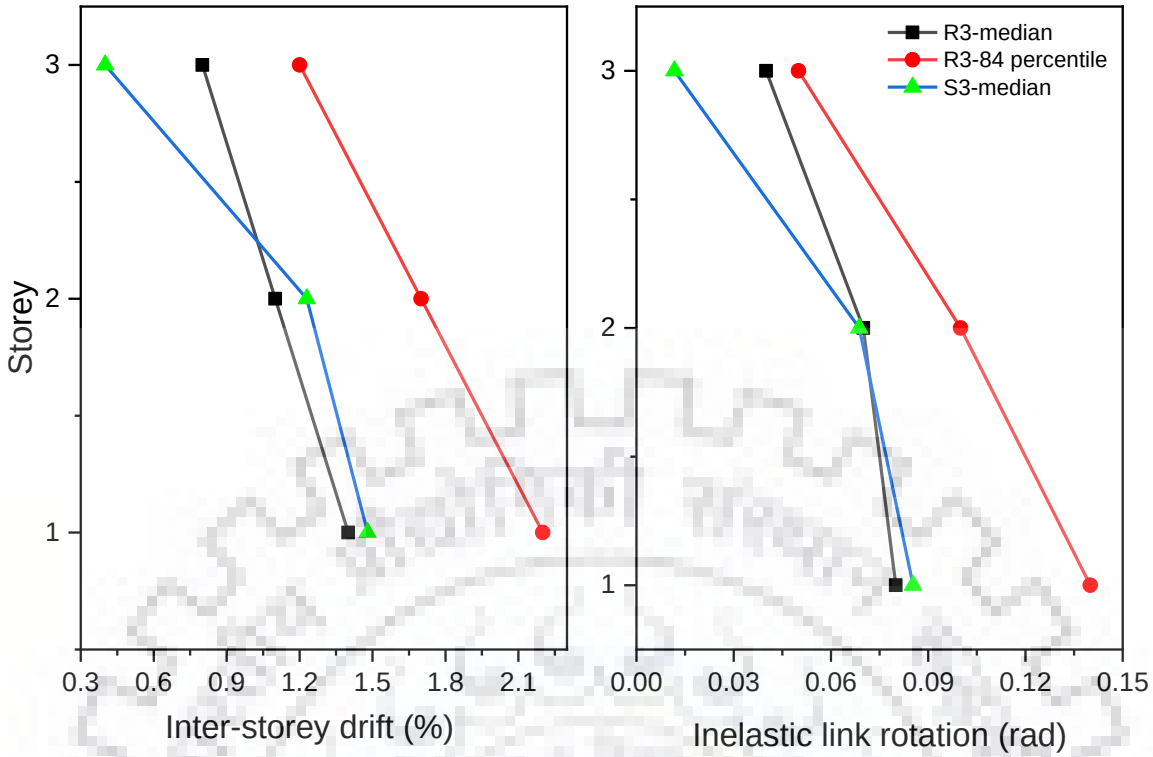
Storey
3
2
1
0.3
0.6
0.9
1.2
1.5
1.8
2.1
Inter-storey drift (%)
R3-median
R3-84 percentile
S3-median
0.00
0.03
0.06
0.09
0.12
0.15
Inelastic link rotation (rad)

(a)

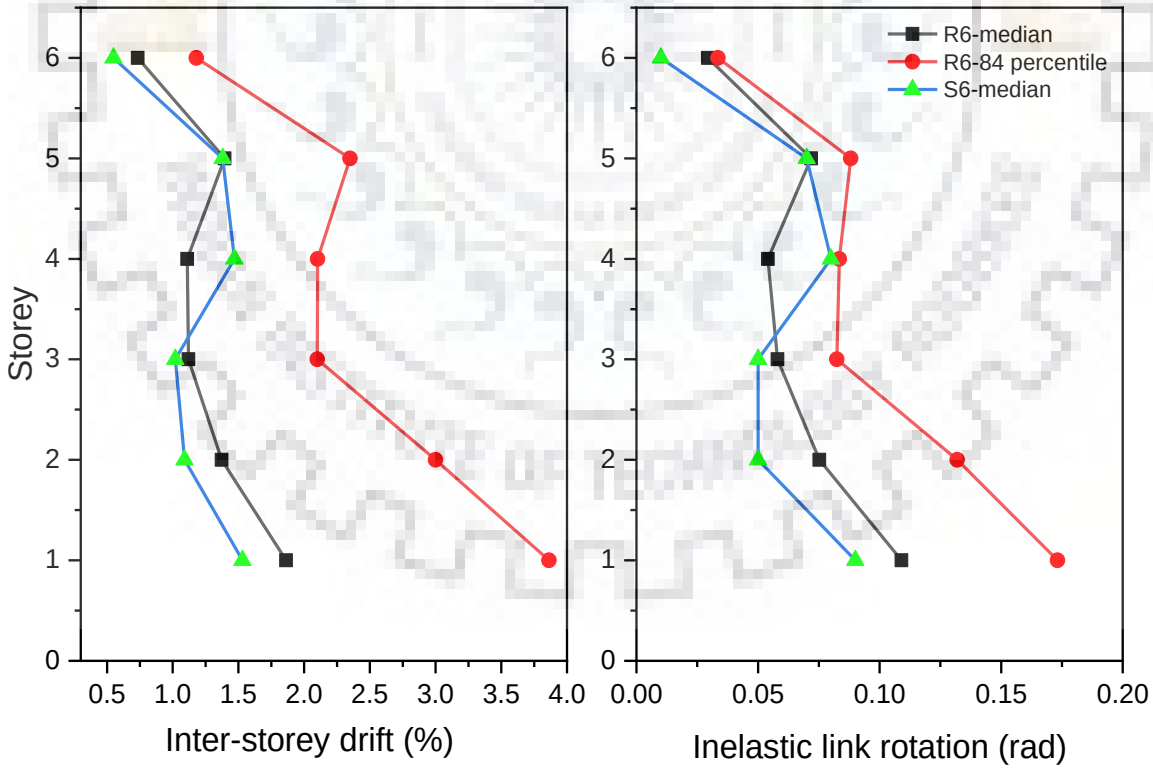
Storey
6
5
4
3
2
1
0
0.5
1.0
1.5
2.0
2.5
3.0
3.5
4.0
Inter-storey drift (%)
R6-median
R6-84 percentile
S6-median
0.00
0.05
0.10
0.15
0.20
Inelastic link rotation (rad)

(b)

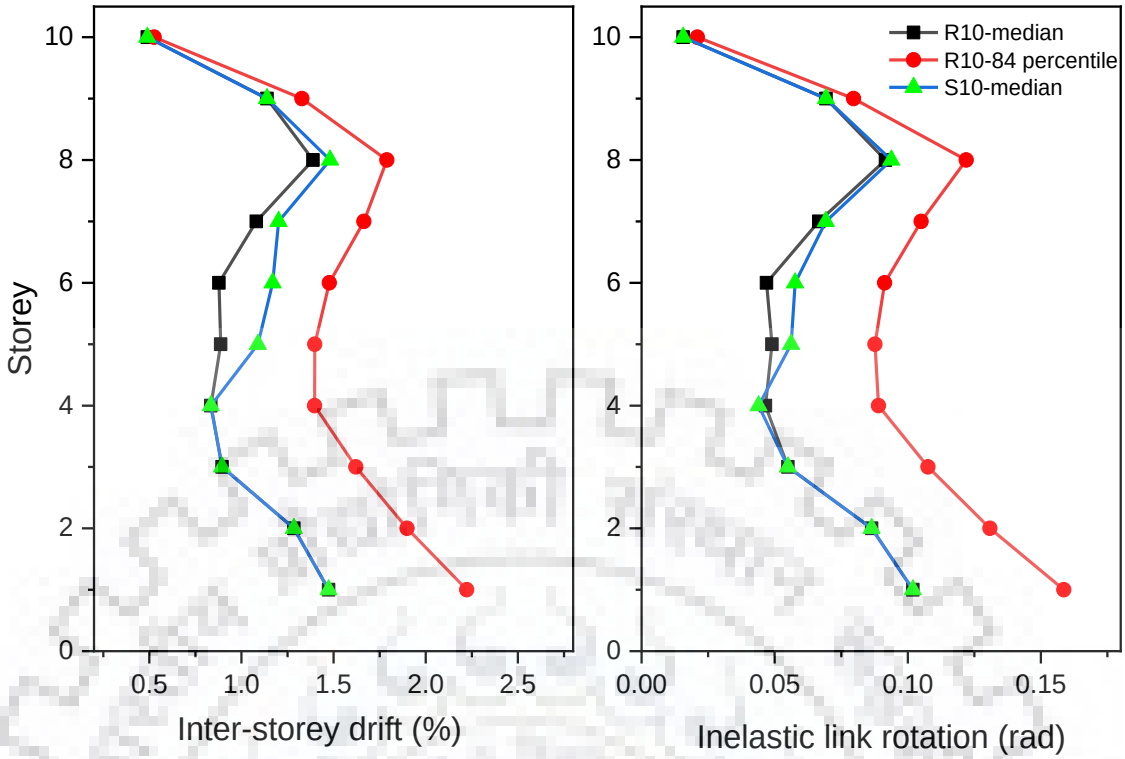


(c)

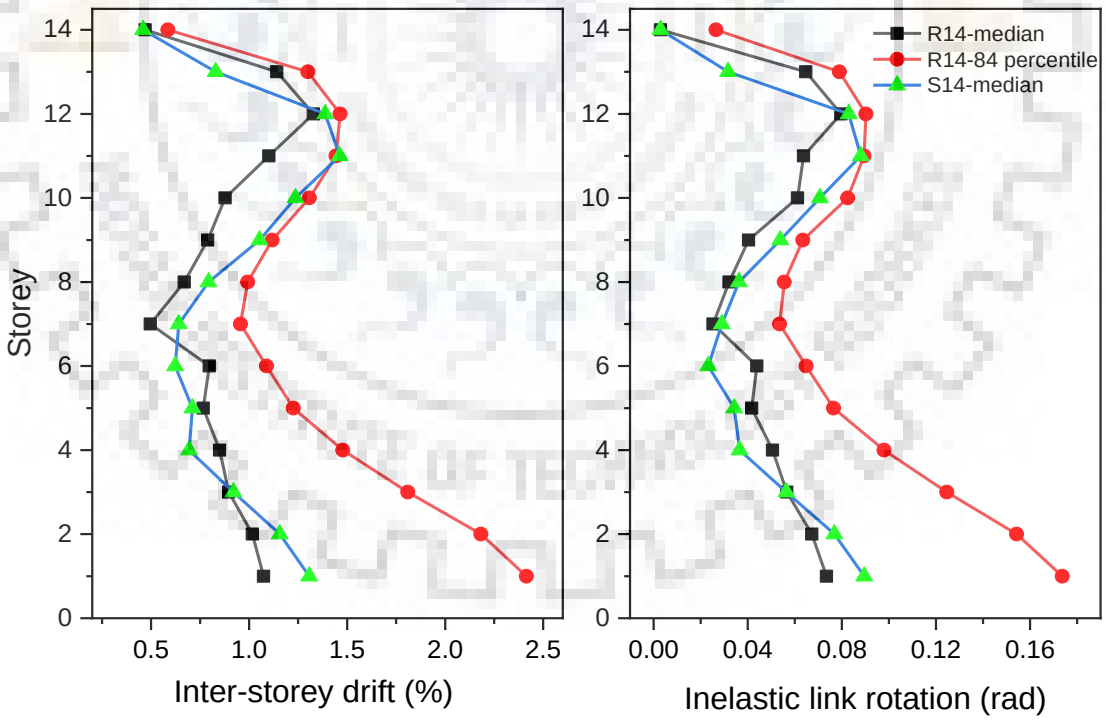


(d)

Fig 8.9 Comparison of peak inter-storey drift and inelastic link rotation envelopes of replaceable type and conventional links for (a) 3 (b) 6 (c) 10 and (d) 14 storey archetypes

and thus uniform dissipation of energy cannot be anticipated. Though the deformation demands in the top-most storeys of replaceable link type EBFs were marginally greater than those in the conventional archetypes, they were still insignificant to contribute to energy dissipation.

#### 8.2.4.4 Relation Between Drift and Inelastic Link Rotation

The peak drifts and link rotations computed for all the acceleration records at every storey level were plotted to evaluate the suitability of the assumed relationship between inelastic drift and link rotation based on rigid plastic behavior and investigate if the same relationship holds for replaceable link type EBF systems. The maximum values of these parameters occurred in same space-time domain for every acceleration record confirming the physical relationship between them. The pairs of results were plotted and linear relationships were established using regression analysis for each archetype separately. Data points corresponding to the top storey links were excluded in purview of very insignificant rotations. The plot is shown in Fig 8.10 for R14. The equation can be written as follows:

$$\frac{\delta}{h} = 0.129\gamma + 0.0029 \tag{8.5}$$

where $\delta$ is the inter-storey drift, $h$ is the story height and $\gamma$ is the inelastic link rotation. The intercept in the above equation is approximately equal to the ratio of link length, $e$, to the bay width, $L$, (0.133) and gives the following relation upon substitution.

$$\gamma = \frac{L}{e}\left\{\frac{\delta}{h} - 0.0022\right\} \tag{8.6}$$

The above equation predicts the relationship between the two parameters very precisely as can be seen from the plot and is consistent with the assumption of rigid plastic mechanism with the inter-storey drift index at a yield of 0.22%. Similar relation was established for R6 and R10 archetypes with inter-storey drift index at yield of 0.24% and 0.23% respectively. The inter-storey drift indices for the conventional archetypes were marginally greater than those for replaceable link type archetypes.

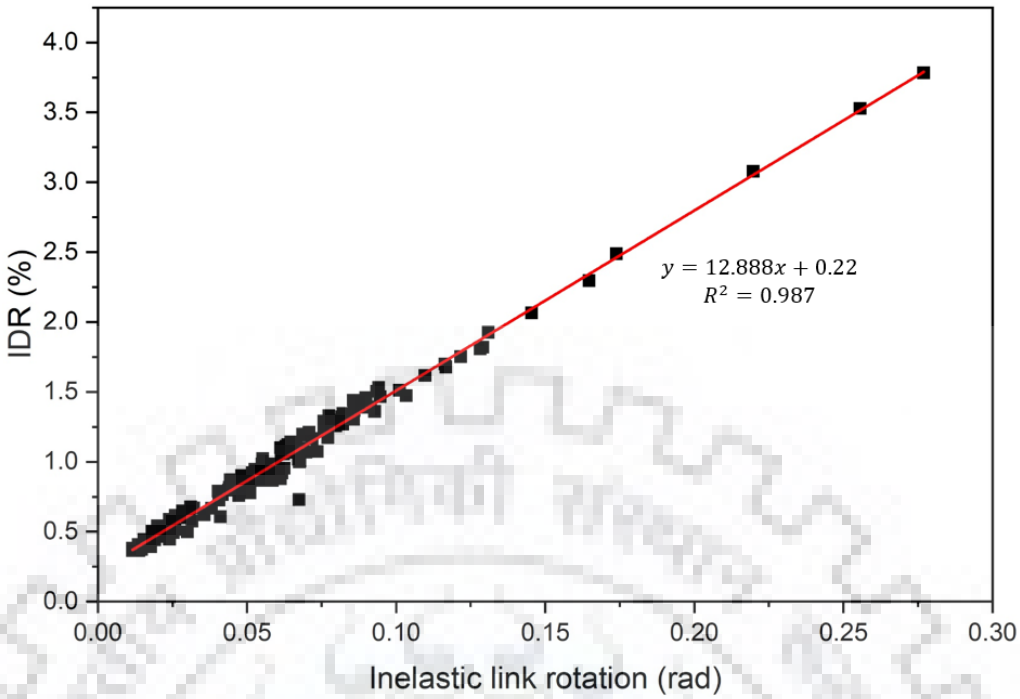


Fig 8.10 Relation between peak inter-storey drift and inelastic link rotation for R14

### 8.2.5 Overall Performance of the Replaceable Link Type EBFs

Based on the comparison of yield pattern, deformation demands, system ductility and lateral strength between the conventional EBFs and EBFs with replaceable links of lower grade steel connected through bolted end-plate connections to the floor beam, it can be concluded that the latter performed very much the same as former despite the flexibility of floor beam to link connections. The pattern of yielding was similar to what could be expected for the conventional EBF systems. The use of lower grade steel in the replaceable type link sections facilitates comparably more uniform distribution of the link shear capacity to demand ratios with height, including the top storey links in exhibiting greater plastic deformations and consequently the energy dissipation. The elements outside links of lower grade steel in these EBFs are expected to yield under comparably larger lateral displacements indicating greater resilience to earthquakes with damage concentrated in the replaceable links only. Additionally, these links exhibit lower permanent deformations and hence exhibit better re-centering characteristic, facilitating the convenient removal of links by eliminating the use of hydraulic jacks or flame cutting procedures.

# 9. CONCLUSIONS

The analysis of EBFs designed in accordance with AISC 341-16 demonstrated good lateral strength and ductility. The non-dissipative members did not participate in yielding under DBE level ground motions. However, the extensive deformations concentrated within few storeys even exceeding the codified limitations. The inelastic link rotation exceeded 0.08 radians in the lowermost storeys of 10 and 14 storey archetypes. The distribution of deformation demands with the height of archetypes was found to be the same as distribution of maximum normalized shear. The use of Displacement Amplification Factor of 4 did not predict the deformations expected under design level earthquake. The relationship between inter-storey drift and inelastic link rotation based on rigid-plastic mechanism was found to be valid (even though the use of Displacement Amplification Factor is implicit in it) with the inter-storey drift at index of 0.3% approximately.

The comparison of results between 2D and 3D archetypes demonstrated the contribution of non-LFRS members in resisting the lateral loads. The analysis of 6 and 14 storey EBFs demonstrated desirable yielding hierarchy under MCE level ground motions. The beams adjacent to links yielded only once the links had yielded. Whenever braces or columns exhibited some yielding, they did so only after the links and beams adjacent to links had yielded. The collapse of link at any particular floor level was followed by increased levels of yielding of the rest of members below this level. This could be explained by the drastic reduction in storey stiffness concentrating the deformations at that level potentially causing the collapse of frame members in addition to links. This was especially found to be dangerous if the yielding of columns occurred along with the link yielding. The probability of yielding of columns at any storey level was found to be maximum just before the collapse of links at or above the same level when the links develop full overstrength. Hence the collapse prevention of links could be a viable reference to avoid global collapse of the structure and could be used as acceptability criterion for performance evaluation of EBF systems at MCE level.

The uniform distribution of yielding of links was targeted by designing the frames using Performance Based Plastic Design (PBPD) procedure. The design was based on two key performance indices – a desirable yielding pattern and maximum target inter-storey drift of 2% (Chao et al. 2004). The conventional design of EBFs demonstrated that inelastic

link rotation and not inter-storey drift controlled the design when capacity design did not. Based on this, the archetypes were also designed based on maximum target inelastic link rotation of 0.08 rad. The archetypes designed using PBPD procedure demonstrated much uniform distribution of deformations along the height compared to those that were conventionally designed. Moreover, the deformations did not exceed the codified limitations in the former archetypes. The energy dissipated by link sections was more uniformly distributed in the same. The 6 story frames designed using maximum target inelastic link rotation of 0.08 rad and maximum inter-storey drift of 2% was almost similar. However, the performance of 14 story EBF was comparatively better when designed using maximum target inelastic link rotation of 0.08 rad since it exhibited uniform distribution of deformations and link energy dissipation with height.

The EBFs with replaceable shear links of lower grade steel connected through bolted end-plate connections to the floor beams demonstrated performance much similar to the conventional EBFs despite the flexibility of link to beam connections. The use of lower grade steel in link sections increased the resilience of EBF systems to larger ground motion intensities with yielding concentrated within the link sections only.

# REFERENCES


1. AISC 341-16 (2016), Seismic provisions for structural steel buildings, *American Institute of Steel Construction, Chicago, Illinois 60601-6204.*
2. Azad S & Topkaya C (2017), "A review of research on steel eccentrically braced frames", *Journal of constructional steel research, 128, 53-73*.
3. Kasai K & Popov E (1986), "Cyclic web buckling control for shear link beams", *Journal of Structural Engineering, 112*(3), 505-523.
4. CSI, SAP2000 Integrated Software for Structural Analysis and Design, *Computers and Structures Inc., Berkeley, California.*
5. SEAOC (2012), IBC structural/seismic design manual, Vol. 4: Example for steel-framed buildings, *Structural Engineers Association of California, Sacramento, CA.*
6. ASCE (2016), Minimum Design Loads for Buildings and Other Structures, Standard ASCE/SEI 7–16, *Reston, VA, American Society of Civil Engineers, 2016.*
7. FEMA (2000), Commentary for the seismic rehabilitation of buildings, FEMA-356, *Federal Emergency Management Agency, Washington, DC*.
8. Ricles M, & Egor P (1987), "Dynamic analysis of seismically resistant eccentrically braced frames", *University of California, Earthquake Engineering Research Center, 1987.*
9. PEER, NGA West2 strong ground motion database, *Pacific Earthquake Engineering Research Center, University of California, Berkeley, CA 94720-1792.*
10. FEMA P695 (2009), Quantification of building seismic performance factors, *Federal Emergency Management Agency, Washington, D.C.*
11. Mansour N (2011), Development of the design of eccentrically braced frames with replaceable shear links, *University of Toronto, PhD dissertation, 2010.*
12. Dubina D, Stratan A & Dinu F (2008), "Dual high-strength steel eccentrically braced frames with removable links", *Earthquake Engineering & Structural Dynamics 2008, 37(15):1703–1720.*
13. Mansour N, Christopoulos C & Tremblay R (2011), "Experimental validation of replaceable shear links for eccentrically braced steel frames", *Journal of Structural Engineering, ASCE 2011, 137(10):1141–1152.*

14. Chao S & Goel S C, (2005), “Performance-based seismic design of EBF using target drift and yield mechanism as performance criteria”, *Ann Arbor 1001 (2005): 48109-2125.*
15. CSI, PERFORM 3D, Structural and Earthquake Engineering Software, *Computers and Structures Inc., Berkeley, California*.

# APPENDICES

## APPENDIX A: Sample Design (S14)

This appendix presents the design of 14-storey EBF designated as S14. The design of the rest of archetypes was done using the same procedure. The base shear calculations, design forces in the members, selection of frame sections and drift and link rotation analyses are presented in subsequent sections.

### Calculation of Base Shear

The base shear was calculated in accordance with ASCE 7-16. The approximate fundamental time period, $T_a$, is computed as follows:

$$T_a = C_t h^x \tag{A.1}$$

where $C_t$ and $x$ are coefficients depending upon the structure type. For an eccentrically braced frame:

$$C_t = 0.03 \text{ and } x = 0.75$$

$$T_a = 0.03 \times 168^{0.75}$$

$$T_{max} = 1.39\ sec$$

The fundamental time period of structure, $T$, can be calculated from a properly substantiated frame analysis, or alternatively the approximate building period, $T_a$, could be used. The fundamental time period should not exceed maximum time period, $T_{\max}$, which is the product of coefficient of upper limit on the calculated period, $C_u$, and approximate fundamental time period, $T_a$.

$$T_{\max} = C_u T_a \tag{A.2}$$

For $S_{D1} > 0.4, C_u = 1.0$.

$$T_{max} = 1.4 \times 1.39$$

$$T_{max} = 1.95\ sec$$

For this building, the fundamental period as determined from elastic frame analysis exceeded the maximum fundamental period. Therefore $T_{\max}$ was used in calculating the seismic response coefficient, $C_s$.

The seismic response coefficient, $C_s$, is determined as follows:

$$C_s = \frac{S_{DS}}{\frac{R}{I}} \tag{A.3}$$

$$\Rightarrow C_s = \frac{1.0}{\frac{8.0}{1.0}} = 0.125$$

$C_s$ need not exceed the following:

$$C_s = \frac{S_{D1}}{T\frac{R}{I}} \tag{A.4}$$

$$\Rightarrow C_s = \frac{0.6}{1.95 \times \frac{8.0}{1.0}} = 0.038 \prec 0.044$$

$$\Rightarrow C_s = 0.044$$

The effective seismic weight, $W$, of the building was calculated on the basis of assembly weights mentioned in chapter 5 as shown in Table A.1.

Table A.1 Calculation of the floor weights

| Storey | Assembly | Unit weight (psf) | Area ($ft^2$) | Weight (kips) | Floor Weight (kips) |
|---|---|---|---|---|---|
| Typical Floor | Floor | 78 | 18819 | 1467 | 1590 |
| | External Wall | 19 | 6480 | 123 | |
| Roof | Roof | 36 | 18819 | 677 | 770 |
| | Parapet Wall | 19 | 4860 | 93 | |

$$\Rightarrow W = (13 \times 1590) + 770 = 21{,}440\ kips$$

The seismic base shear, $V$, is calculated as follows:

$$V = C_s W = 0.044 \times 21{,}440$$

$$V = 944\ kips$$

## Design of 14-storey EBF

The single-bay EBF was modelled in SAP2000. The mass corresponding to effective seismic weight, $W$, of half the building was lumped at the column nodes at each storey level since it was assumed that the lateral loads are resisted entirely by the Lateral Force Resisting System (LFRS) and since there are two EBFs (LFRS) in the building to resist the lateral load in a particular direction. The seismic mass attributed to a single EBF was further distributed equally between the two EBF column nodes at each storey level. So

seismic mass of 397.5 kips was lumped at all the EBF column nodes except at the top-storey column nodes in which case it was 192.5 kips. The base shear was distributed vertically in accordance with the Equivalent Lateral Force (ELF) procedure. Since there are two EBFs provided in the building to resist the lateral loads in a particular orientation, only half of the total story shear was applied on the model. The center of stiffness was assumed to be at an offset of 5% from the center of mass of the floors to account for accidental torsion. The Equivalent Lateral Force applied to the frame and the link design shear at each storey level is shown in Table A.2

Table A.2 Equivalent Lateral Force distribution and link design shear

| Storey | Equivalent Lateral Force (kips) | Design frame shear (kips) | Link design shear, $V_L$ (kips) |
|---|---|---|---|
| 1 | 2 | 1 | 197 |
| 2 | 7 | 4 | 196 |
| 3 | 13 | 7 | 195 |
| 4 | 21 | 11 | 192 |
| 5 | 31 | 16 | 187 |
| 6 | 43 | 22 | 181 |
| 7 | 56 | 29 | 172 |
| 8 | 70 | 36 | 161 |
| 9 | 86 | 45 | 146 |
| 10 | 103 | 53 | 128 |
| 11 | 122 | 63 | 107 |
| 12 | 142 | 74 | 81 |
| 13 | 162 | 84 | 52 |
| 14 | 89 | 46 | 20 |

Having calculated the link design shear, suitable link sections were selected. Link length ratio of less than 1.6 was targeted to make the links critical for shear. The link sections selected for design are enlisted in Table A.3 along with the section capacities and demand to capacity (D/C) ratios.

The section capacities were calculated using the same expressions as mentioned for model HF-6 in chapter 3. The link length ratio was kept more or less uniform throughout the building height. Links of length 42 inches were provided in all the storeys of S14.

Table A.3 Link sections provided and their shear capacities

| Storey | Link Design Shear (kips) | Section | Plastic Shear Capacity, $V_P$ (kips) | Adjusted Shear Capacity, $V_m$ (kips) | Link Length Ratio, $\rho$ | D/C Ratio |
|---|---|---|---|---|---|---|
| 1 | 197 | W18×76 | 215 | 295 | 1.11 | 0.92 |
| 2 | 196 | W18×76 | 215 | 295 | 1.11 | 0.91 |
| 3 | 195 | W18×76 | 215 | 295 | 1.11 | 0.91 |
| 4 | 192 | W18×76 | 215 | 295 | 1.11 | 0.89 |
| 5 | 187 | W16×77 | 205 | 281 | 1.14 | 0.91 |
| 6 | 181 | W16×77 | 205 | 281 | 1.14 | 0.88 |
| 7 | 172 | W14×82 | 193 | 265 | 1.16 | 0.89 |
| 8 | 161 | W16×67 | 177 | 244 | 1.15 | 0.91 |
| 9 | 146 | W14×68 | 156 | 215 | 1.14 | 0.94 |
| 10 | 128 | W14×61 | 142 | 195 | 1.17 | 0.90 |
| 11 | 107 | W12×58 | 118 | 162 | 1.15 | 0.91 |
| 12 | 81 | W10×49 | 91 | 125 | 1.26 | 0.89 |
| 13 | 52 | W10×49 | 91 | 125 | 1.26 | 0.57 |
| 14 | 20 | W10×49 | 91 | 125 | 1.26 | 0.22 |

Uniform demand to capacity ratio was also targeted for the links in all storeys. This condition could not be satisfied for the top-storey links due to the link length ratio limitation and section compactness requirements.

A half-frame model similar to the one explained in chapter 3 was used to design the columns and braces and to check the adequacy of the link sections provided for the forces

Table A.4 Column and brace sections provided

| Columns | | Braces | |
|---|---|---|---|
| Storey | Section | Storey | Section |
| 1-3 | W14×500 | 1-4 | W18158 |
| 4-6 | W14×426 | 5-8 | W12×152 |
| 7-9 | W14×283 | 9-11 | W12×136 |
| 10-12 | W14×193 | 12-14 | W12×120 |
| 13-14 | W10×100 | | |

in the beam segments outside the links. The column and brace sections provided are enlisted in Table A.4.

## Check on Inter-storey Drift and Link Rotation Angle

The inter-storey drift was checked in accordance with ASCE 7-16 which limits it at 2% of the storey height. The link rotation angle for short shear links should be less than 0.08 rad and was calculated assuming the frame to collapse under rigid-plastic mechanism. From the analysis of model, the elastic displacement, $\delta_{xe}$, between ground level and the first storey level was 0.015 feet. The corresponding displacement at inelastic level, $\Delta$, is evaluated by multiplying this displacement with Displacement Amplification Factor, $C_d$, and further dividing by Importance factor, $I$, of the building as follows:

$$\Delta = \frac{C_d \delta_{xe}}{I} \tag{A.5}$$

$$\Rightarrow \Delta_1 = 0$$

$$\Rightarrow \Delta_2 = \frac{4 \times 0.015}{1} = 0.06\ feet$$

The story drift, $\delta_x$, is calculated as follows:

$$\delta_x = \Delta_x - \Delta_{(x-1)}$$

$$\Rightarrow \delta_2 = \Delta_2 - \Delta_1 = 0.06\ feet$$

Inter-storey Drift Ratio (IDR) is calculated as follows:

$$IDR = \frac{\delta_x}{h} 100$$

$$\Rightarrow IDR_1 = \frac{0.06}{12} 100 = 0.50\ \%$$

The link rotation angle, $\gamma_p$, is calculated as follows:

$$\gamma_p = \frac{L}{e} \theta_p \tag{A.6}$$

where, $\theta_p$ is the plastic storey drift angle and is calculated as follows:

$$\theta_p = \frac{\Delta_p}{h} \tag{A.7}$$

where, $\Delta_p$ is the inelastic portion of design storey drift and is computed as follows:

$$\Delta_p = \delta_x - \delta_{xe} \tag{A.8}$$

$$\Rightarrow \Delta_{p_1} = 0.06 - 0.015 = 0.45\ feet$$

$$\Rightarrow \theta_{p_1} = \frac{0.045}{12} = 0.0038\, rad$$

$$\Rightarrow \gamma_p = \frac{30}{4} 0.0038 = 0.028\, rad < 0.08\, rad$$

The IDR and link rotation angle calculated for all the storeys are enlisted in Table A.5.

Table A.5 Inter-storey drift and link rotation angle from elastic analysis of the frame

| Storey | IDR (%) | Link rotation angle (rad) |
|---|---|---|
| 1 | 0.50 | 0.028 |
| 2 | 0.62 | 0.040 |
| 3 | 0.74 | 0.047 |
| 4 | 0.84 | 0.054 |
| 5 | 0.98 | 0.063 |
| 6 | 1.06 | 0.068 |
| 7 | 1.11 | 0.071 |
| 8 | 1.17 | 0.075 |
| 9 | 1.22 | 0.079 |
| 10 | 1.22 | 0.078 |
| 11 | 1.21 | 0.078 |
| 12 | 1.18 | 0.076 |
| 13 | 1.10 | 0.070 |
| 14 | 0.99 | 0.064 |

IDR and link rotation angle at all the floors were found to be less than 2% and 0.08 rad respectively.

## Check on Stability of the Frame

The stability of structures in linear analysis was evaluated using the stability coefficient, $\theta$, which is the ratio of secondary moments to primary moments. The lesser the stability coefficient, greater is the stability of structure. The use of this factor helps in including the P-Δ effects into elastic design procedures. The stability coefficient is calculated in accordance with FEMA 356 as follows:

$$\theta_i = \frac{P_i \delta_i}{V_i h_i} \tag{A.9}$$

where:

$P_i$ = vertical design load for storey *i* under consideration

$V_i$ = Shear at storey *i* under consideration due to design earthquake shaking

$h_i$ = height of the storey *i*

$\delta_i$ = lateral drift in storey *i* in the direction under consideration

The calculations involved to evaluate the coefficient at first storey level are shown below:

$$P_1 = 21440 + \{(13 \times 0.033) + 0.010\} \times 18819 = 29701\ kips$$

$$\delta_1 = 0.0149 - 0 = 0.0149\ feet$$

$$V_1 = 944\ kips \qquad h_1 = 12\ feet$$

The design vertical loads were calculated as $1.0D + 0.50L$ load effects.

The stability coefficients calculated for all the storeys are tabulated in Table A.6.

**Table A.6 Calculation of stability coefficient**

| Storey | $P_i$ (kips) | $\Delta_i$ (feet) | $V_i$ (kips) | $h_i$ (feet) | $\theta$ |
|---|---|---|---|---|---|
| 1 | 29701 | 0.0149 | 944 | 12 | 0.039 |
| 2 | 27980 | 0.018 | 942 | 12 | 0.046 |
| 3 | 25732 | 0.022 | 935 | 12 | 0.050 |
| 4 | 23484 | 0.025 | 922 | 12 | 0.053 |
| 5 | 21236 | 0.029 | 901 | 12 | 0.057 |
| 6 | 18988 | 0.031 | 870 | 12 | 0.057 |
| 7 | 16740 | 0.033 | 827 | 12 | 0.056 |
| 8 | 14492 | 0.035 | 771 | 12 | 0.055 |
| 9 | 12244 | 0.036 | 701 | 12 | 0.053 |
| 10 | 9996 | 0.036 | 615 | 12 | 0.049 |
| 11 | 7748 | 0.036 | 512 | 12 | 0.045 |
| 12 | 5500 | 0.035 | 390 | 12 | 0.041 |
| 13 | 3252 | 0.032 | 248 | 12 | 0.035 |
| 14 | 1004 | 0.029 | 86 | 12 | 0.028 |

The stability coefficient at all the storey levels was found to be less than 0.33 implying that the structure was stable. Further, the stability coefficient did not exceed 0.1 at any storey level. Hence, the P-Δ effects were not considered in the linear design procedure.

# APPENDIX B: Scaled and Unscaled Response Spectra of Selected Ground Motions

The non-linear dynamic analysis was carried for an ensemble of eleven ground motions. The source-to-site distance was greater than 10 km for all selected ground motions and hence these qualify as far-field ground motions. Each ground motion was scaled to be compatible with the design target spectrum. The scale factors used lie within the range of 0.82 – 2.62. Period range of $0.2T - 2T$ was targeted for scaling in accordance with ASCE 7. The ground motion records were scaled such that the average of response spectra of the selected ground motions closely match the design target spectrum and does not fall below 90% of the latter within the specified period range. This appendix shows the plots of scaled and unscaled response spectra of the Design Basis Earthquake (DBE) level ground motions. For reference, the design target spectrum is also plotted. The ground motions were taken from PEER NGA-West2 ground motion database.

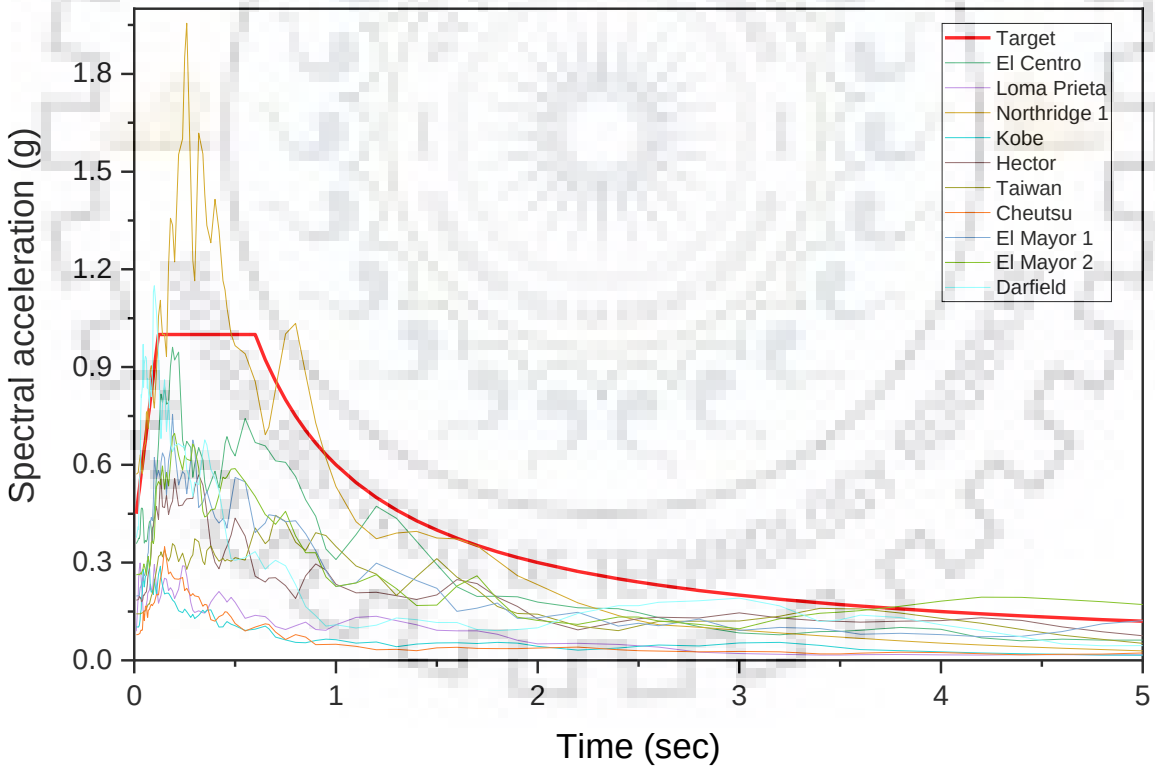


Fig B.1 Unscaled response spectra of the ground motions

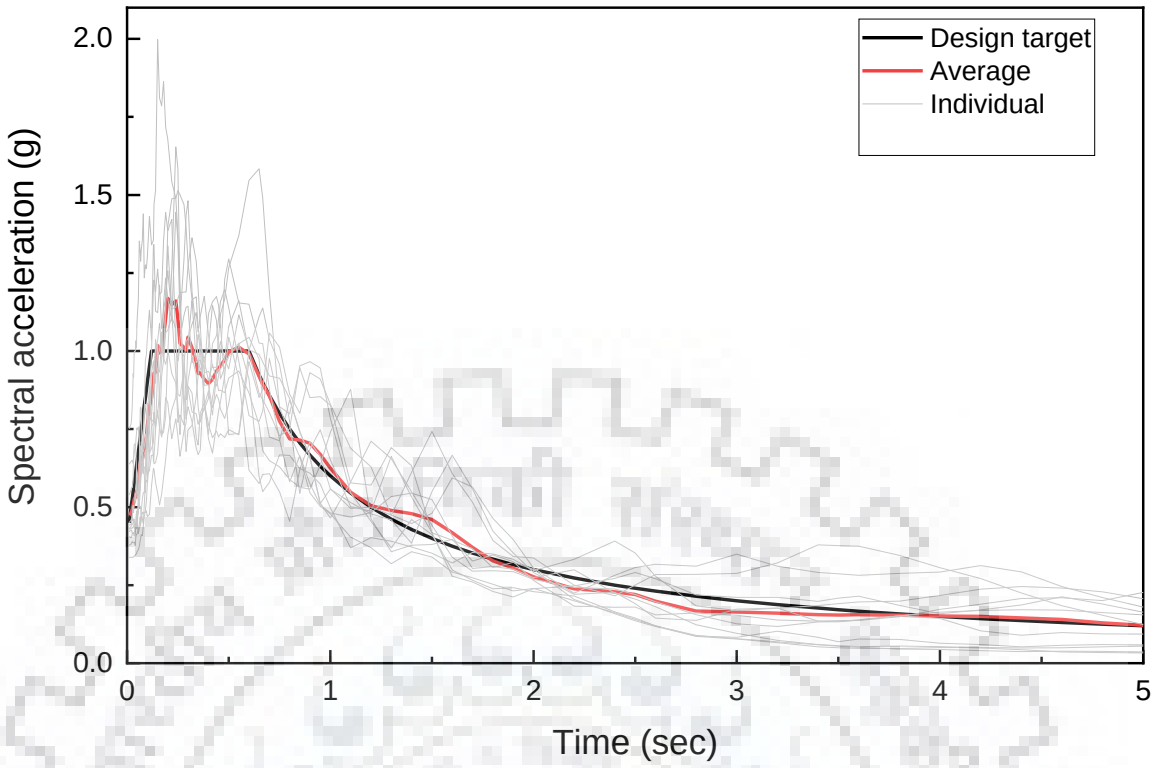


Fig B.2 Scaled response spectra of the ground motions

The scaled and unscaled response spectra for the individual 11 ground motions are shown below.

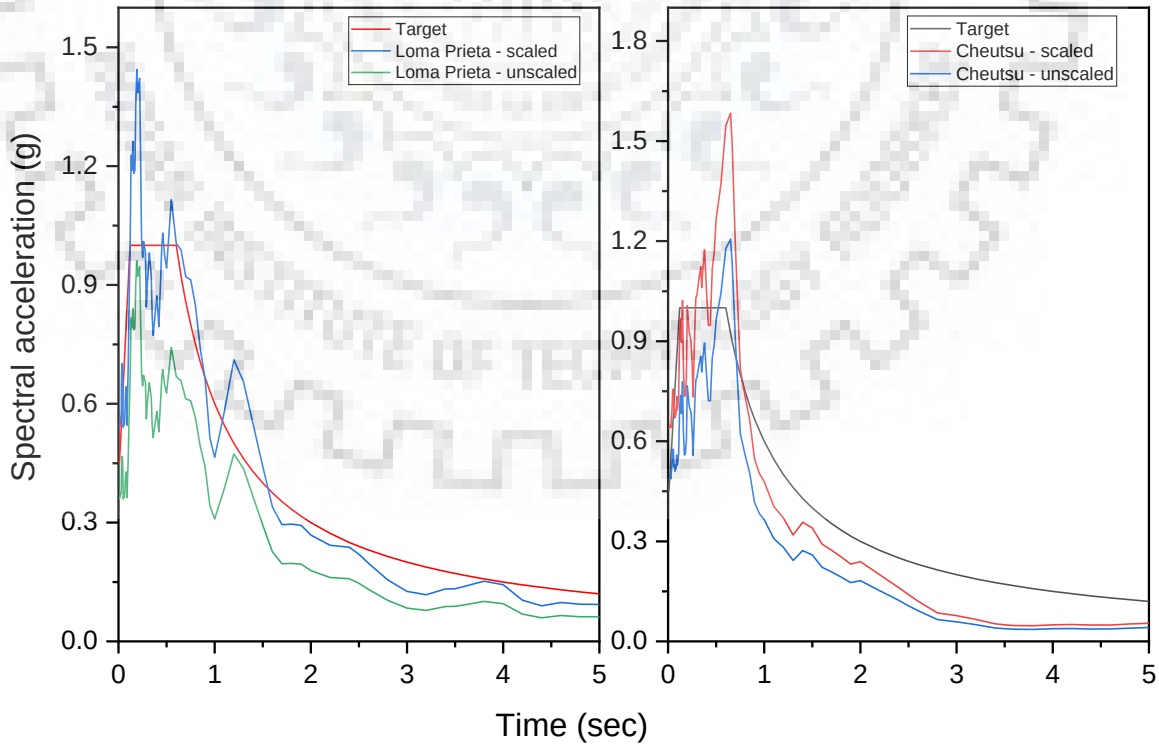

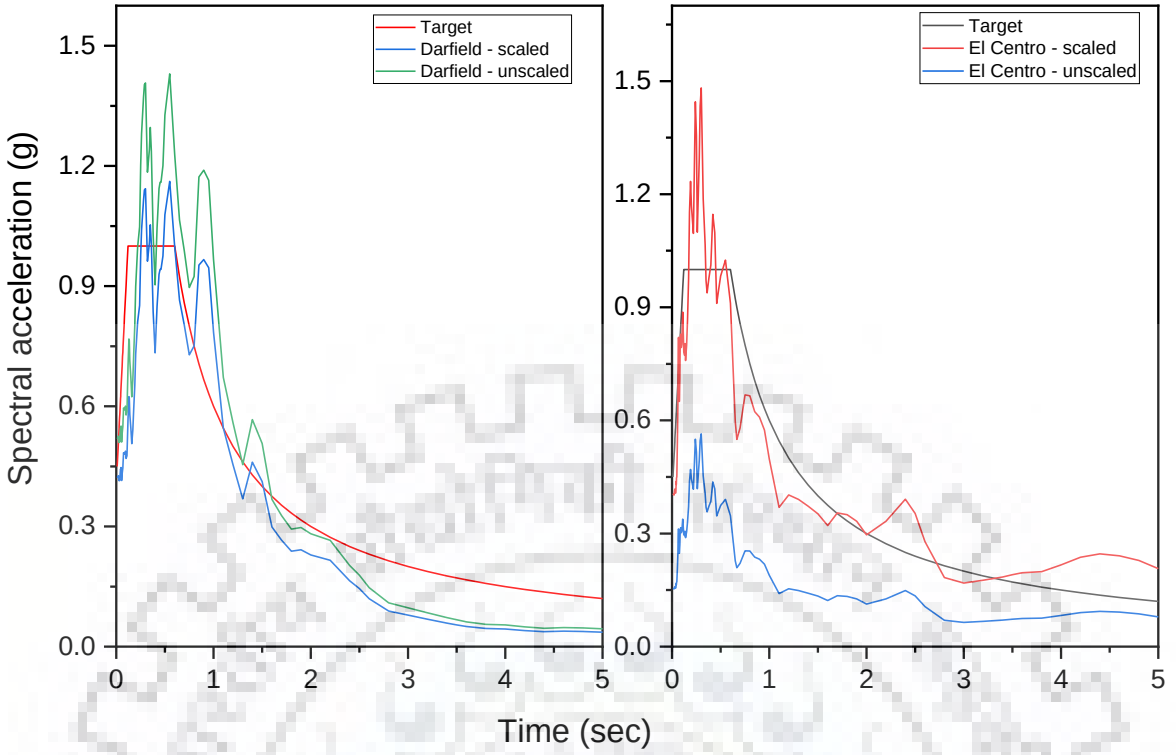
Target
Darfield - scaled
Darfield - unscaled
Target
El Centro - scaled
El Centro - unscaled
Spectral acceleration (g)
Time (sec)

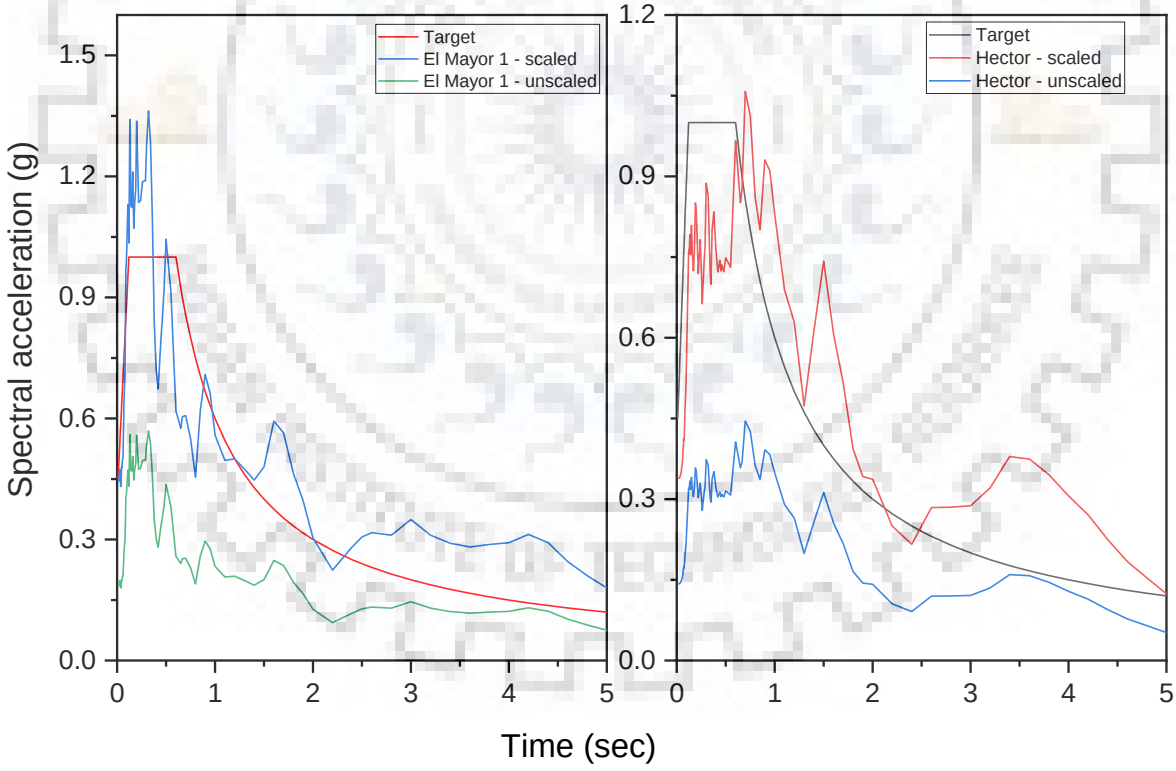
Target
El Mayor 1 - scaled
El Mayor 1 - unscaled
Target
Hector - scaled
Hector - unscaled
Spectral acceleration (g)
Time (sec)

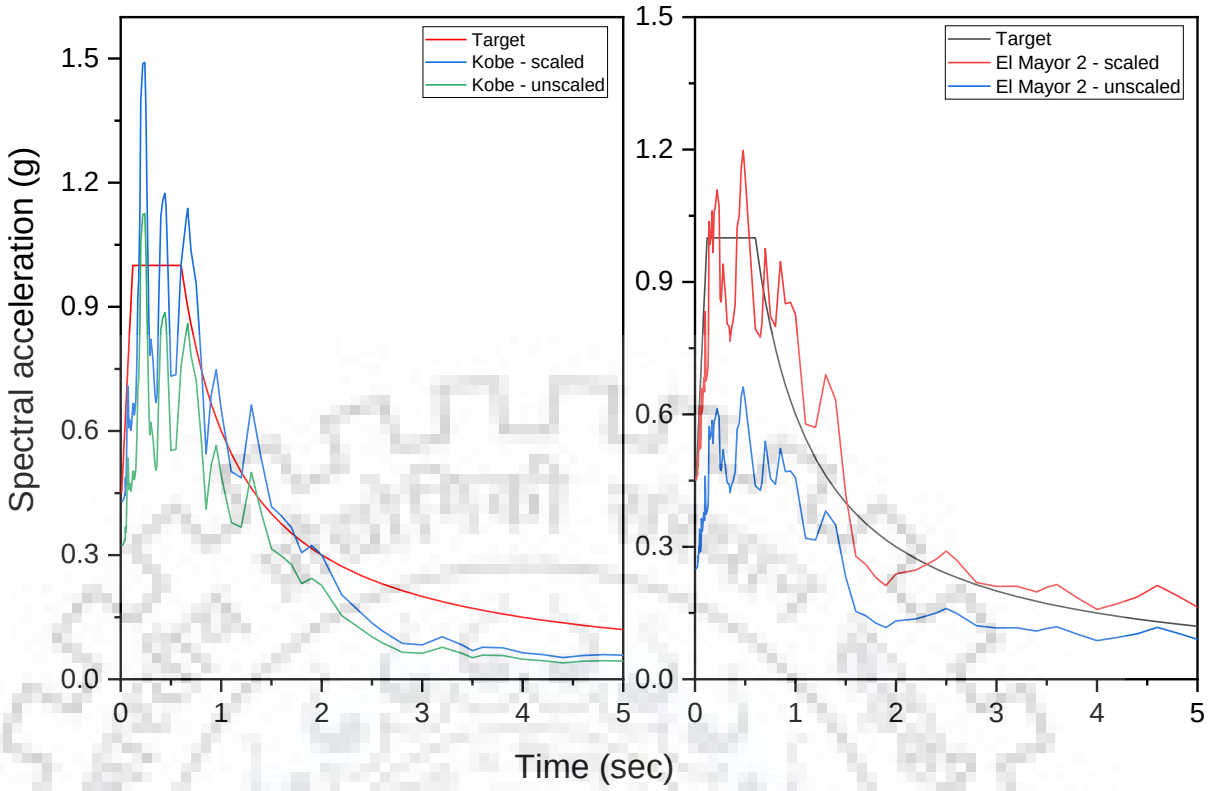
Target
Kobe - scaled
Kobe - unscaled
Target
El Mayor 2 - scaled
El Mayor 2 - unscaled
Spectral acceleration (g)
Time (sec)

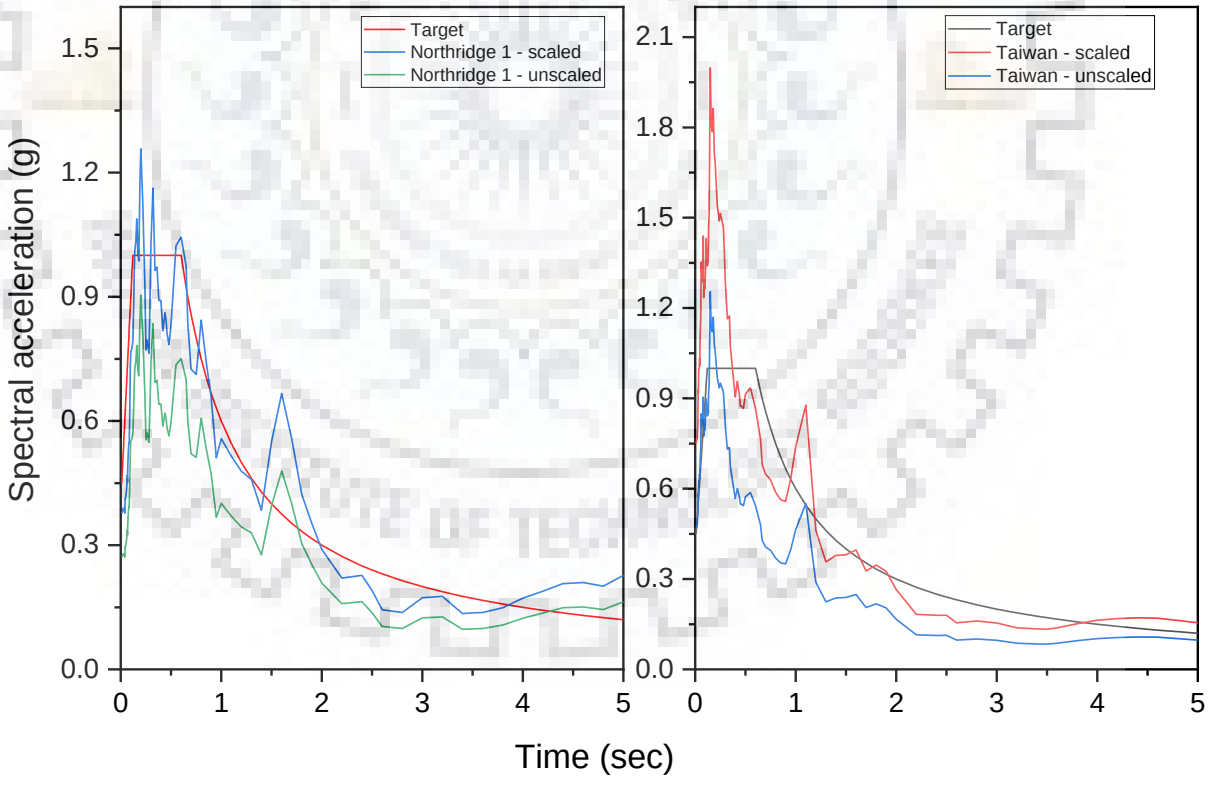
Target
Northridge 1 - scaled
Northridge 1 - unscaled
Target
Taiwan - scaled
Taiwan - unscaled
Spectral acceleration (g)
Time (sec)

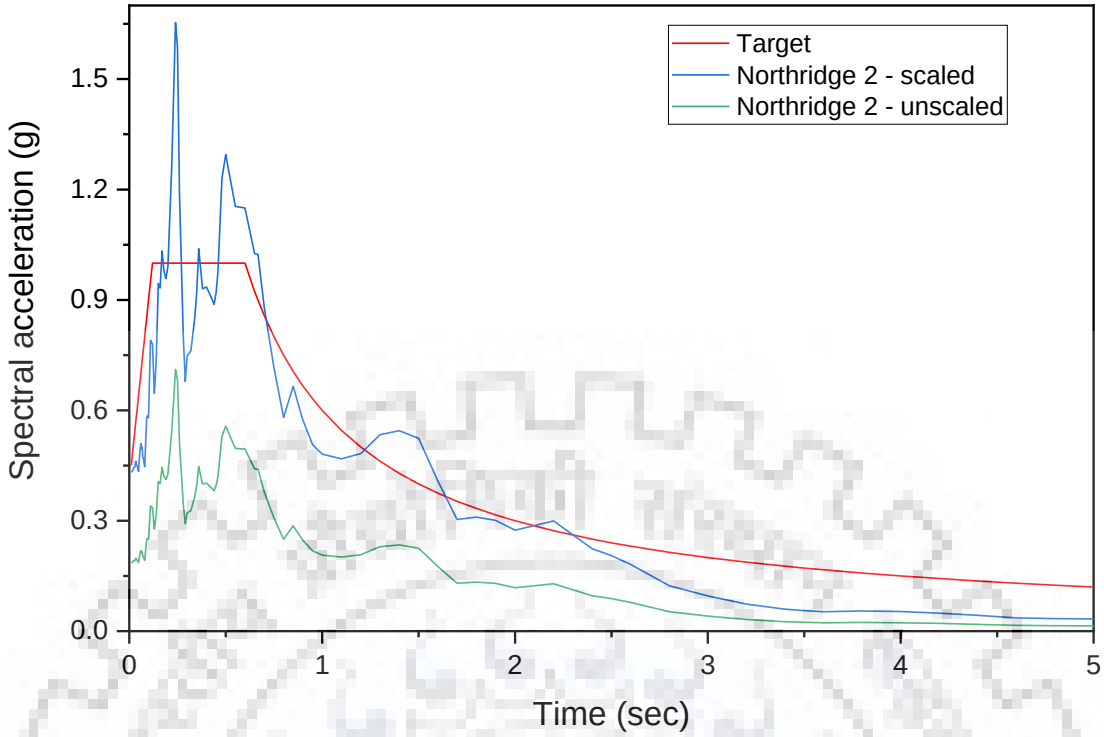


Fig B.3 Unscaled and scaled response spectra of the individual ground motions

# APPENDIX C: Design Frame Sections

## Design Frame Sections for Conventional Archetypes

The design frame sections of S3 and S6 are enlisted in Table C.1.

Table C.1 Design frame sections of S3 and S6

| Storey | S3 | | | S6 | | |
|---|---|---|---|---|---|---|
| | Beams | Columns | Braces | Beams | Columns | Braces |
| 1 | W12×53 | W12×96 | W14×61 | W14×68 | W14×132 | W12×72 |
| 2 | W10×49 | W10×45 | W12×53 | W14×68 | W14×132 | W12×72 |
| 3 | W10×49 | W8×21 | W12×53 | W12×72 | W12×96 | W12×72 |
| 4 | | | | W12×53 | W12×96 | W12×53 |
| 5 | | | | W10×49 | W8×40 | W12×53 |
| 6 | | | | W10×49 | W8×40 | W12×53 |

The design frame sections of S10 and S14 are enlisted in Table C.2.

Table C.2 Design frame sections of S10 and S14

| Storey | S10 | | | S14 | | |
|---|---|---|---|---|---|---|
| | Beams | Columns | Braces | Beams | Columns | Braces |
| 1 | W16×67 | W14×257 | W12×136 | W18×76 | W14×500 | W18×158 |
| 2 | W16×67 | W14×257 | W12×136 | W18×76 | W14×500 | W18×158 |
| 3 | W14×68 | W14×211 | W12×136 | W18×76 | W14×500 | W18×158 |
| 4 | W14×68 | W14×211 | W12×120 | W18×76 | W14×426 | W18×158 |
| 5 | W14×61 | W14×176 | W12×120 | W16×77 | W14×426 | W12×152 |
| 6 | W12×58 | W14×176 | W12×120 | W16×77 | W14×426 | W12×152 |
| 7 | W10×49 | W12×120 | W12×106 | W14×82 | W14×283 | W12×152 |
| 8 | W10×49 | W12×120 | W12×106 | W16×67 | W14×283 | W12×152 |
| 9 | W10×49 | W12×96 | W12×106 | W14×68 | W14×283 | W12×136 |
| 10 | W10×49 | W12×96 | W12×106 | W14×61 | W14×193 | W12×136 |
| 11 | | | | W12×58 | W14×193 | W12×136 |
| 12 | | | | W10×49 | W10×100 | W12×120 |
| 13 | | | | W10×49 | W10×100 | W12×120 |
| 14 | | | | W10×49 | W10×100 | W12×120 |

## Design Frame Sections for Replaceable Link Type EBFs

The design frame sections of R3 are enlisted in Table C.3.

Table C.3 Design frame sections of R3

| Storey | Links (ASTM A36) | Floor Beams (ASTM A992) | Columns | Braces |
|---|---|---|---|---|
| 1 | W14×68 | W14×68 | W12×96 | W12×58 |
| 2 | W12×65 | W12×65 | W8×40 | W12×58 |
| 3 | W10×49 | W10×49 | W8×40 | W10×45 |

The design frame sections of R6 are enlisted in Table C.4

Table C.4 Design frame sections of R6

| Storey | Links (ASTM A36) | Floor Beams (ASTM A992) | Columns | Braces |
|---|---|---|---|---|
| 1 | W16×77 | W16×77 | W14×132 | W12×72 |
| 2 | W16×77 | W16×77 | W14×132 | W12×72 |
| 3 | W10×100 | W10×100 | W12×96 | W12×72 |
| 4 | W12×87 | W12×87 | W12×96 | W12×58 |
| 5 | W10×68 | W10×68 | W8×40 | W12×58 |
| 6 | W10×49 | W10×49 | W8×40 | W12×58 |

The design frame sections of R10 are enlisted in Table C.5

Table C.5 Design frame sections of R10

| Storey | Links (ASTM A36) | Floor Beams (ASTM A992) | Columns | Braces |
|---|---|---|---|---|
| 1 | W18×86 | W18×86 | W14×370 | W12×152 |
| 2 | W18×86 | W18×86 | W14×370 | W12×152 |
| 3 | W18×86 | W18×86 | W14×311 | W12×152 |
| 4 | W16×89 | W16×89 | W14×311 | W12×152 |
| 5 | W16×77 | W16×77 | W14×257 | W12×136 |
| 6 | W14×82 | W14×82 | W14×257 | W12×136 |
| 7 | W14×68 | W14×68 | W12×152 | W12×136 |
| 8 | W12×65 | W12×65 | W12×152 | W12×120 |
| 9 | W10×49 | W10×49 | W12×136 | W12×120 |
| 10 | W1×049 | W10×49 | W12×136 | W12×120 |

The design frame sections of R14 are enlisted in Table C.6

Table C.6 Design frame sections of R14

| Storey | Links (ASTM A36) | Floor Beams (ASTM A992) | Columns | Braces |
|---|---|---|---|---|
| 1 | W24×76 | W24×76 | W14×730 | W18×192 |
| 2 | W24×76 | W24×76 | W14×730 | W18×192 |
| 3 | W24×76 | W24×76 | W14×730 | W18×192 |
| 4 | W24×76 | W24×76 | W14×665 | W18×192 |
| 5 | W24×76 | W24×76 | W14×665 | W12×210 |
| 6 | W24×68 | W24×68 | W14×665 | W12×210 |
| 7 | W21×73 | W21×73 | W14×398 | W12×210 |
| 8 | W21×68 | W21×68 | W14×398 | W12×210 |
| 9 | W21×62 | W21×62 | W14×398 | W12×190 |
| 10 | W16×77 | W16×77 | W14×311 | W12×190 |
| 11 | W16×67 | W16×67 | W14×311 | W12×190 |
| 12 | W14×48 | W14×48 | W14×311 | W12×170 |
| 13 | W10×49 | W10×49 | W14×159 | W12×170 |
| 14 | W10×49 | W10×49 | W14×159 | W12×170 |